# Theory of Phase Behavior of Weakly Charged Polyelectrolytes

# THEORY OF PHASE BEHAVIOR OF WEAKLY CHARGED POLYELECTROLYTES

BY

YOUHAI SUN, M.Sc.

A THESIS
SUBMITTED TO THE DEPARTMENT OF PHYSICS & ASTRONOMY
AND THE SCHOOL OF GRADUATE STUDIES
OF MCMASTER UNIVERSITY
IN PARTIAL FULFILMENT OF THE REQUIREMENTS
FOR THE DEGREE OF
DOCTOR OF PHILOSOPHY

Doctor of Philosophy (2013) McMaster University
(Department of Physics & Astronomy) Hamilton, Ontario, Canada

| | |
|---|---|
| TITLE: | Theory of Phase Behavior of Weakly Charged Polyelectrolytes |
| AUTHOR: | Youhai Sun<br>M.Sc., (Physics)<br>McMaster, Hamilton, Canada |
| SUPERVISOR: | Dr. An-Chang Shi |
| NUMBER OF PAGES: | xii, 117 |

# Abstract

A self-consistent field theory is developed for weakly charged polymeric systems composed of charged-neutral diblock copolymers and homopolymers. This generic model can be used to describe the phase behavior of a number of different charged polymeric systems, including charged polymer/homopolymer blends and ionic liquid/homopolymer mixtures. It is found that the miscibility of the system is increased by the increase of the charge fraction and the anion volume. Random phase approximation has also been used to calculate the spinodal lines for polyelectrolyte/homopolymer blends and polyelectrolyte solutions. Both systems exhibit micro- and macro- phase separated regions. It is also shown that an increase of the charge fraction stabilizes the homogeneous phase over the inhomogeneous ones and a decrease of the Bjerrum length stabilizes the microphase separated state over the macrophase separated state. Finally, the reciprocal-space method is used to solve the self-consistent field equations for the polyelectrolyte/homopolymer blends. Full phase diagrams showing microphase separated structures of lamellae, hexogonal and body-centered cubic lattice, as well as 2-phase region of coexistence of lamellae and homogeneous are obtained.

# Acknowledgements

I would like to take this opportunity to thank the amazing people who helped me during my graduate study. I couldn't have done this work without the help of my supervisor, Dr An-Chang Shi. His patience, understanding and comprehensive guidance helped me a lot in the past few years. I appreciate all the useful things he taught me and thank him for being such a great mentor. I also would like to thank my committee, Dr Cecile Fradin, Dr Paul Higgs and Dr Nikolas Provatas for their valuable suggestions to my research.

I would like to thank my officemate Ashkan Dehghan for his collaboration on section 5.3 of this thesis, many helpful comments and editing of this thesis. Also, thanks to Kyle Pastor for useful discussions and helping me with the language mistakes of this thesis. I would also like to thank many people who have been worked in our group, Jiajia, Jianfeng, Weiquan, Weihua, Issei, Dave, Lily and Rui for helping me in my study and daily life.

Last but not least, I would like to thank my parents, my parents-in-law, my husband and my daughter for their loving support.

# Contents

# List of Figures

# Chapter 1

# Introduction

A polymer is a macromolecule consisting of a large number of repeating units covalently joined together to form a long chain [1] [2]. A macromolecule is usually termed a polymer if the number of repeating units exceeds 100. It is possible to have polymers containing over tens of thousands of repeating units [3]. Examples of polymers include synthetic polymers such as polystyrene and biological polymers such as DNA. A polyethylene chain consists of repeating units of $CH_2$ groups, which can be considered as the simplest polymer chain. There is a tremendous variety of polymeric materials. Different polymers are distinguished by different compositions of monomer units and chain architecture. For example, polymer chains may be linear or branched according to the way they are synthesized. Polymers can be homopolymers if the molecule is formed from a single type of repeating unit and copolymers if the molecule is composed of more than one type of repeating units. Polymers can also be classified into neutral polymers and charged polymers according to their ability to carry charges.

Charged polymers are polymers with ionizable groups [4]. These ionizable groups tend to dissociate under certain conditions, such as in polar solvents, leaving the polymers with net charges. This dissociation can affect a wealth of structural, functional, and dynamical properties of polymer systems [5]. Charged polymers are of fundamental importance in biology and biochemistry and are widely used in industry. As building blocks of living matter, most proteins and biopolymers are charged in aqueous environment [6]. Industrial applications of charged polymers range from waterwaste treatment to paper making [7]. According to the type of charges, charged polymers can be classified into two classes, polyampholytes and polyelectrolytes.

Polyampholytes are macromolecules carrying both positively and negatively ionizable groups [8]. Under appropriate conditions, these groups dissociate, leaving both positively and negatively charged groups on the polymer chain . Examples of polyampholytes include certain kinds of proteins such as gelatin. Copolymers synthesized from monomers with acidic and basic groups are polyampholytes as well [9]. The properties of polyampholyte chains depend on many factors, such as the fraction of positively and negatively charged monomers and the distribution of charged monomers along the polymer backbone. Experiments as well as molecular dynamics simulations have been carried out to understand the properties of polyampholytes [10] [11].

In the current study, we will focus on the phase behavior of polymeric systems containing polyelectrolytes. Polyelectrolytes are polymers having many positively or negatively ionizable groups, which can be dissociated leaving charged polymer chains and small counterions in solution [12] [13] [14]. Polyacrylic acids (PAA) and polymethacrylic acids (PMAA) can be considered as the simplest polyelectrolytes. These polymers become negatively charged when dissolved in water with the addition of alkali [15]. Other examples include natural polyelectrolytes such as proteins, nucleic acids and synthetic polyelectrolytes such as polyvinyl sulfonic acid (PVSA) and polyethyleneimine (PEI). Some typical examples of negatively charged polyelectrolytes are shown in Fig. 1.1 [16]. The polystyrene sulfonate (PSS) molecules become negatively charged due to the dissociation of the $Na^+$ ion, the polymethacrylic acid (PMAA) molecules become negatively charged due to the releasing of the $H^+$ ion, and the DNA molecules become negatively charged due to the dissociation of the phosphate groups.

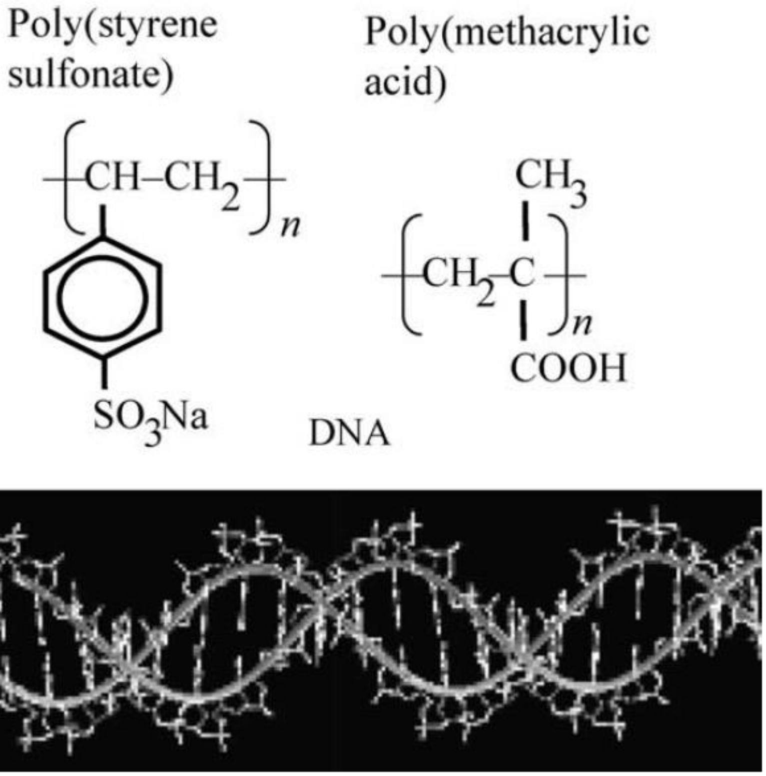

Figure 1.1: Examples of negatively charged polyelectrolytes [16].

The properties of polyelectrolyte systems depend on many factors such as the fraction of ionizable groups, the degree of dissociation, solvent quality for the polymer backbone, salt concentration, and the solution dielectric constant, etc. For example, the degree of dissociation varies significantly depending on the specifics of the system. Polyvinyl sulfonic acid (PVSA) usually dissociates completely when dissolved in water while the degree of dissociation for polyacrylic acid (PAA) is small in pure water [12]. Different from those of uncharged polymers, electrostatic interactions between charges in polyelectrolyte systems can lead to rich behavior. The polyelectrolyte nature of biopolymers are expected to form the basis of various biological phenomena. For example, the process of polymer translocation that occurs in many biological phenomena is highly related to the electrostatic interactions in the system [17]

Because of their unique properties and technological importance, polyelectrolytes have been studied extensively by experimental and theoretical approaches since the early days of polymer science [18] [19] [20] [21] [22]. The existence of both long-range Coulombic interactions and short-range interactions results in specific properties to polyelectrolytes that are absent in neutral polymers. The study of a single-chain properties of polyelectrolytes has been performed by theoretical approaches in early years [23] [24] [25], as well as computer simulations in recent years [26] [27] [28]. The overall shape of a single polyelectrolyte chain is determined by the balance of the electrostatic interaction and the surface tension. In infinite dilute solutions, a polyelectrolyte chain can be in a Gaussian coil state if the solvent is close to the $\theta$-temperature and the electrostatic repulsion between charges are weak. In poor solvent and at low charge density, a polyelectrolyte chain exhibts spherical globule state. When charge density increases, a necklace type configuration with different numbers of beads has also been predicted using scaling arguments [29]. Later theoretical approaches also support the existence of a necklace conformation for strongly charged polyelectrolytes and finite concentrations when counterion condensation occurs [30] [31]. Molecular dynamic simulation also showed that, depending on the interaction parameter and charge fraction, the strongly charged polyelectrolyte chain can be in different conformation states: collapsed globule, sausage-like aggregate, fully stretched chain, and pearl-necklace globule [32] [33].

Polyelectrolyte solutions have also attracted much attention [34] [35]. It is well known that, dilute and semidilute solutions of neutral polymer chains readily segregate into polymer rich and solvent rich phases due to the low translational entropy of polymer chains [36]. The macrophase separation will be limited if we introduce charges on the polymer chains. This is due to the significant losses of translational entropy of the counterions if the system undergoes macrophase separation as the counterions must follow the corresponding polymer co-ions. It was discovered that microphase separation phenomenon, which is common in block-copolymer systems, can take place in systems containing weakly charged polyelectrolytes [37]. For example, Shibayama et al. [38] have detected microphase separation for polyelectrolyte gels in poor solvents. There is a common feature of the physical reasons which lead to the formation of microdomain structures: both system have the stabilizing factor which prevents the macroscopic demixing, the connectivity of the blocks in one chain for block-copolymers and the contribution of mobile counterions to the entropy of mixing for polyelectrolytes. Theoretically, the possibility of microphase separation in weakly charged semidilute solutions of polyelectrolytes was first considered by Borue and Erukhimovich [39]. Later on, they developed a microscopic statistical theory of polyelectrolyte solutions using random phase approximation (RPA) and restricting the contribution of entropy of solvent molecules to second-order terms [40]. They presented the phase diagram with lamelar structure, hexagonal lattice, BCC lattice, as well as the two phase region.

In the case of polymer blends, it is well known that polymer blends involving two neutral polymer components A and B usually phase separate into A-rich and B-rich phases if the interaction of A-B is energetically unfavorable [1]. The presence of charges enhances the compatibility effectively due to the significant losses of translational entropy of the counterions if the system undergoes macrophase sepration [41] [42]. Further theoretical studies for polymer blends with one weakly charged component also led to the conclusion that microdomain structures may appear under certain conditions [43]. In 1992, Khokhlov and Nyrkova [44] performed a detailed study for the case of mixture of an arbitrary number of polyelectrolyte components with a low molecular weight solvent. Their theory is in the framework of the lattice Flory-Huggins model in the self-consistent field approximation. As a result, the condition for stability of a homogeneous phase was found. The aforementioned RPA-type analysis has also been applied to studies for block polyelectrolytes where the order-disorder transition has been examined by solving the generalized spinodal equations [45] [46] [47].

In order to address the problem of phase boundaries or binodals, Dobrynin and Erukhimovich [48] made the first attempt to study the problem for the mixture of weakly charged and neutral polymers. They performed a study using the weak segregation theory which was first developed by Leibler [49]. They also discussed the method of accounting for the fluctuation corrections in polyelectrolyte systems. The phase diagram and the final equilibrium microdomain structures valid near the critical point were obtained. In 1994, microphase separation in poor-solvent weakly charged polyelectrolyte solutions was also studied by Dormidontova et al. [50] in the weak segregation limit within the framework of the mean field approximation. The possibility of macrophase separate to coexistence of phases having different crystal symmetries in the system was taken into account. A complete phase diagram of the solution system near the critical point was obtained. Later, Gritsevich [51] also studied the fluctuation effects and their influence on the phase diagram for the same polyelectrolyte solution system.

In order to obtain the full form of the phase diagram (not only near the critical point), Nyrkova, Khokhlov and Doi [52] calculated the phase diagram by direct minimization of a Landau-type free energy where the polymer conformations were described using a square gradient approximation. They performed the analysis for two polyelectrolyte systems, a mixture of weakly charged polyelectrolyte/neutral homopolymer and a system of weakly charged polyelectrolytes in poor solvent. It was shown that the final phase diagram has the feature of coexistence of macro- and microphase separation.

The self-consistent field theory (SCFT) for polymer systems, which was initially developed by Edwards [53], Helfand [54] [55], has been successfully applied for neutral polymer systems to study the interfaces of polymer blends, microphase separation of block copolymers, etc [56] [57] [58] [59] [37]. Shi and Noolandi [60] extended the SCFT to systems containing weakly charged polymers. They started from the Edwards Hamiltonian for the polymers and included electrostatic interactions in the partition function. The partition function was then transformed using the Hubbard-Stratonovich transformation into a functional integral over the polymer concentrations, the ion concentrations, the electrostatic potential and the corresponding field variables. A set of self-consistent equations was then obtained by using the mean-field approximation. They studied the interface of a phase-separated poor solvent solution of polyelectrolyte as a simple example, and also derived the asymptotic forms of the theory at weak and strong segregation limits. Later, Wang et al. [61] considered the position-dependency of the dielectric constant and applied the SCFT to inhomogeneous polyelectrolyte systems with both smeared and annealed charge distributions. They studied the interface of a phase-separated polyelectrolyte solution in a poor solvent, as well as the lamellar structures of symmetric diblock polyelectrolytes A-B where A and B carry opposite charges. The phase behavior of polyelectrolyte blends was also examined by them, showing both macroscopic phase separation and microphase separation.

The above mentioned RPA and SCFT analysis have also been applied to other charged polymer systems. Kumar and Muthukumar [62] studied the microphase separation for charged-neutral diblock copolymer melts by using the RPA and SCFT. It was shown that the stability limits calculated using the RPA aggreed with the SCFT calculations. They found lamellar, cylindrical and spherical morphologies in the ordered phase. Recently, Yang et al. [63] also obtained the phase diagram of charged triblock copolymer melt and solution using the SCFT.

Although there have been extensive studies on the polyelectrolyte/homopolymer blends and polyelectrolyte solutions, a comprehensive SCFT study of the phase behavior of these systems and complete phase diagram is still lacking. The current study fills in this gap by developing a SCFT for a generic model containing weakly charged polyelectrolytes, and applying the theory to the phase behavior of the system.

As shown by previous theoretical and experimental studies, charged polymer systems can be in homogeneous state, marcophase separated state, and microphase separated state. The physical properties of charged polymer system vary drastically in different states. A good understanding of the phase behavior of charged polymer systems is crucial. Because charged polymer systems are usually composed of more than one element, their phase behavior is controlled by a large number of parameters, such as chain lengths, charge fraction, monomer interactions, electrostatic interactions. More accurate theoretical study is crucially important to understand the phase behavior in these complex systems.

The systems we are interested in include charged-neutral diblock copolymer/homopolymer blends, polyelectrolyte/homopolymer blends and polyelectrolyte solutions. As the self-consistent field theory for weakly charged polyelectrolyte systems originated by Shi and Noolandi [60] has been successful, we will use the self-consistent field theory as the main tool to study the phase behavior of the multi-component charged polymer systems. We restrict our discussion to the equilibirium statistical properties of the system and exclude the phenomena of dynamical fluctuation.

The structure of this thesis is organized as follows: The theoretical framework and the derivation of the mean-field equations are given in Chapter 2. We developed the theory for a system composed of charged-neutral diblock copolymers and neutral homopolymers in this chapter. The stability of the homogeneous phase with respect to macrophase separation is studied in Chapter 3 for different charged systems. In

Chapter 4, we use the random phase approximation to study the stability of homogeneous phase, leading to both macrophase and microphase separation transition for the polyelectrolyte/homopolymer blends and the polyelectrolyte solutions. In Chapter 5, we use the reciprocal-space method to solve the self-consistent field equations. The microphase structures are resolved for the case of polyelectrolyte/homopolymer blends. In Chapter 6, we summarize the key results of this work and make some comments on the theory and the results.

# Chapter 2

# Theoretical Framework

The system of interest consists of charged and neutral polymers, as well as counterions. For simplicity, we assume that the polyelectrolytes are weakly charged so that their conformations can be described using the Gaussian chain model or Edwards model of polymers [64]. Furthermore, there are short-range interactions between all the species and long-range Coulombic interactions between charged species. The mean field theory replace this many-body problem for polymer chains and counterions with an ideal chain in an effective mean field potential $\omega_P^{eff}(\mathbf{r})$ and a couterion in an effective mean field potential $\omega_I^{eff}(\mathbf{r})$, respectively. These mean field potentials can be solved from a closed set of equations self-consistently. In this chapter, we construct this set of self-consistent equations for a generic system consisting charged-neutral diblock copolymers, neutral homopolymers, and counterions. The theoretical development follows closely to the work of Shi and Noolandi [60].

## 2.1 The Model

For a canonical ensemble of a volume $V$, we consider $n_0$ AB diblock copolymers, with A block being charged, $n_I$ counterions, and $n_C$ C homoplymers. We associate each block with a Kuhn statistical length $b_\alpha$ ($\alpha = A, B, C$) and a bulk density $\rho_{0\alpha}$. The bulk density of the counterions is denoted by $\rho_I$. We also set a reference density $\rho_0$ to be the same order of the monomer density. The degrees of polymerization of the blocks are $N_A = fZ_0$, $N_B = (1-f)Z_0$, and $N_C = Z_C$, where $Z_0$ is the total number of monomers in the AB diblock copolymer and $Z_C$ is the total number of monomers in the C homopolymer. We denote the valence number of the A-monomers to be $z_A$ and the valence number of the counterions to be $z_I$. We assume that the $t$-th A-monomer of the $i$th diblock chain is able to acquire charges $c_{i,A}(t)z_Ae$, where the variable $c_{i,A}(t)$ is the charge distribution along the $i$-th polymer chain determined by the nature of the charge distribution. We can denote the probability of a particular charge distribution by $P(\{c_{i,A}(t)\})$. Furthermore, the charge distribution can be written in the form $P(\{c_{i,A}(t)\}) = \prod_t p(c_{i,A}(t), t)$. There are two possible charge distributions if we assume charge occurs uniformly along the A-blocks: (1) the semeared charge distribution, $p(c_{i,A}(t)) = \delta(c_{i,A} - p_A)$, under this distribution, each A-monomer carries the fractional charge $p_A$; and (2) the annealed case, where each A-monomer carries charges $z_Ae$ with a probability $p_A$ [65].

Let $\mathbf{R}_i^0(t)$ denote the position of the $t$-th monomer of the $i$-th AB chain, $\mathbf{r}_i^I$ denote the posititon of the $i$-th counterion and $\mathbf{R}_i^C(t)$ denote the position of the $t$-th monomer of the $i$-th C chain. For a given configuration of the system, the inhomogeneous monomer densities of the polymers are given by

$$\begin{aligned}
\hat{\rho}_A(\mathbf{r}) &= \sum_{i=1}^{n_0} \int_0^{fZ_0} dt\delta(\mathbf{r} - \mathbf{R}_i^0(t)), && (2.1)\\
\hat{\rho}_B(\mathbf{r}) &= \sum_{i=1}^{n_0} \int_{fZ_0}^{Z_0} dt\delta(\mathbf{r} - \mathbf{R}_i^0(t)), && (2.2)\\
\hat{\rho}_C(\mathbf{r}) &= \sum_{i=1}^{n_C} \int_0^{Z_C} dt\delta(\mathbf{r} - \mathbf{R}_i^C(t)). && (2.3)
\end{aligned}$$

The number densities of the counterions are given by

$$\hat{\rho}_I(\mathbf{r}) = \sum_{i=1}^{n_I} \delta(\mathbf{r} - \mathbf{r}_i^I). \tag{2.4}$$

The total charge density at position **r** is the summation of the charge density from the polymers and the charge density from the counterions,

$$\hat{\rho}_e(\mathbf{r}) = \hat{\rho}_{A,e}(\mathbf{r}) + \hat{\rho}_{I,e}(\mathbf{r}), \tag{2.5}$$

where the contribution from the polymers are

$$\hat{\rho}_{A,e}(\mathbf{r}) = \sum_{i=1}^{n_0} \int_0^{fZ_0} dtc_{i,A}(t)z_A e\delta(\mathbf{r} - \mathbf{R}_i^0(t)), \tag{2.6}$$

and the contributions from the counterions are

$$\hat{\rho}_{I,e}(\mathbf{r}) = \sum_{i=1}^{n_I} z_I e\delta(\mathbf{r} - \mathbf{r}_i^I). \tag{2.7}$$

The system is neutral, so that

$$\int d\mathbf{r}\hat{\rho}_e(\mathbf{r}) = 0. \tag{2.8}$$

We also assume that the polymeric system is incompressible,

$$\sum_j \frac{\hat{\rho}_j(\mathbf{r})}{\rho_{j0}} = \sum_j \hat{\phi}_j(\mathbf{r}) = 1, \tag{2.9}$$

where the index $j$ runs over all the species in the system ($j = A, B, C, I$).

The thermodynamics of the system is described by the partition function, which can be written in terms of a functional integral over all the chain conformations and counterion positions,

$$\begin{aligned} \mathcal{Z} &= \prod_k (\frac{\zeta_k^{n_k}}{n_k!}) \int \prod_\beta [\prod_{i=1}^{n_\beta} (D\mathbf{R}_i^\beta(t) P_\beta(\{\mathbf{R}_i^\beta(t)\}))] \int \prod_{i=1}^{n_I} d\mathbf{r}_i^I \int D\psi(\mathbf{r}) \\ & \prod_{i=1}^{n_0} [\sum_{\{c_{i,A}(t)\}} P(\{c_{i,A}(t)\})] \exp[-\frac{E(\{\hat{\rho}\},\{\psi\})}{k_B T}] \prod_{\mathbf{r}} \delta[\sum_j \hat{\phi}_j(\mathbf{r}) - 1], \end{aligned} \tag{2.10}$$

where $k = 0, C, I$ and $\beta = 0, C$. $\zeta_0$ is the partition function of a $AB$-polymer chain due to the kinetic energy, $\zeta_C$ is the partition function of a $C$-polymer chain due to the kinetic energy and $\zeta_I$ is the partition function of a counterion due to the kinetic energy, the summation $\sum_{\{c_{i,A}(t)\}}$ is over the charge distributions for the $i$-th chain, and $\psi(\mathbf{r})$ is the electrostatic potential of the system. The single-chain probability density functional $P_\beta(\{\mathbf{R}_i^\alpha(t)\})$ has the standard form according to Edwards model,

$$P_\beta(\{\mathbf{R}_i^\beta(t)\}) \propto \exp[-\int_0^{Z_\beta} dt \frac{3}{2b_\beta^2(t)} (\frac{d\mathbf{R}_i^\beta(t)}{dt})^2]. \tag{2.11}$$

We have also introduced a $\delta$ function to ensure the incompressibility constraint for the system. The energy of the system consisits of two parts,

$$E(\{\hat{\rho}\},\{\psi\}) = W(\{\hat{\rho}_j\}) + U_e(\{\hat{\rho}_e\},\{\psi\}), \tag{2.12}$$

where $W(\{\hat{\rho}_j\})$ is the interaction potential between the monomers and ionic molecules, and $U_e$ is the electrostatic energy of the system. The interaction potential $W(\{\hat{\rho}_j\})$ is assumed to have the two-body form,

$$W(\{\hat{\rho}_j\}) = \frac{1}{2}\sum_{j,j'}\int d\mathbf{r}d\mathbf{r}'\hat{\rho}_j(\mathbf{r})W_{j,j'}(\mathbf{r}-\mathbf{r}')\hat{\rho}_{j'}(\mathbf{r}'). \tag{2.13}$$

The electrostatic energy of the system has the form (see Appendix A for details)

$$U_e(\{\hat{\rho}_e\},\{\psi\}) = \int d\mathbf{r}[\hat{\rho}_e(\mathbf{r})\psi(\mathbf{r}) - \frac{\epsilon}{8\pi}|\nabla\psi(\mathbf{r})|^2], \tag{2.14}$$

where $\epsilon$ is the dielectric constant of the medium.

The partition function of the system can be written in the form of a functional integral by carrying out a Hubbard-Stratonovich transformation (see Appendix B for detalis),

$$\mathcal{Z} = \int\prod_j\{D\rho_j D\omega_j\}\int D\rho_e D\omega_e\int D\psi\prod_{\mathbf{r}}\delta[\sum_j\phi_j(\mathbf{r})-1]\exp[-\frac{F(\{\rho\},\{\omega\},\{\psi\})}{k_BT}], \tag{2.15}$$

where the free energy functional has the form

$$\begin{aligned}
\frac{F}{\rho_0 k_B T} &= \int d\mathbf{r}\{\sum_j \mu_{0j}\phi_j(\mathbf{r}) + \chi_{AB}\phi_A(\mathbf{r})\phi_B(\mathbf{r}) + \chi_{AI}\phi_A(\mathbf{r})\phi_I(\mathbf{r}) + \chi_{AC}\phi_A(\mathbf{r})\phi_C(\mathbf{r}) \\
&\quad +\chi_{BI}\phi_B(\mathbf{r})\phi_I(\mathbf{r}) + \chi_{BC}\phi_B(\mathbf{r})\phi_C(\mathbf{r}) + \chi_{CI}\phi_C(\mathbf{r})\phi_I(\mathbf{r})\} \\
&\quad -\int d\mathbf{r}\{\sum_j \frac{\rho_{0j}}{\rho_0}\omega_j(\mathbf{r})\phi_j(\mathbf{r}) + \omega_e(\mathbf{r})\phi_e(\mathbf{r})\} \\
&\quad +\int d\mathbf{r}\{\phi_e(\mathbf{r})\varphi(\mathbf{r}) - \frac{\kappa^2}{2}|\nabla\varphi(\mathbf{r})|^2\} \\
&\quad -V\frac{\rho_{0A}}{\rho_0}\frac{\bar{\phi}_A}{fZ_0}\ln(\frac{Q_0}{\bar{\phi}_A}) - V\frac{\rho_{0C}}{\rho_0}\frac{\bar{\phi}_C}{Z_C}\ln(\frac{Q_C}{\bar{\phi}_C}) - V\frac{\rho_{0I}}{\rho_0}\frac{\bar{\phi}_I}{1}\ln(\frac{Q_I}{\bar{\phi}_I}), \qquad (2.16)
\end{aligned}$$

where the parameters $\chi_{jj'}$ are defined in Appendix B. The charge volume fraction is given by $e\phi_e(\mathbf{r}) = \rho_e(\mathbf{r})/\rho_0$, and the field $\omega_e(\mathbf{r})$ is rescaled by a factor of $e$. The dimensionless electrostatic potential $\varphi(\mathbf{r})$ is defined as $\varphi(\mathbf{r}) = \frac{e}{k_B T}\psi(\mathbf{r})$. The characteristic length $\kappa$ is given by $\kappa^2 = \frac{\epsilon k_B T}{4\pi e^2 \rho_0}$, and the constants $\mu_{0j}$ are given by

$$\mu_{0j} = \frac{\rho_{0j}}{k_B T \rho_0}[\frac{1}{2}W_{jj}\rho_{0j} - k_B T\frac{1}{Z_j}\ln(\frac{\zeta_j e Z_j}{\rho_{0j}})]. \qquad (2.17)$$

The chain conformation contribution to the partition function is contained in the single chain partition function, which can be carried out using the propagators,

$$Q_0 = \frac{1}{V}\int d\mathbf{r} q_0(\mathbf{r}, Z_0, \omega_0), \qquad (2.18)$$

$$Q_C = \frac{1}{V}\int d\mathbf{r} q_C(\mathbf{r}, Z_C, \omega_C), \qquad (2.19)$$

where the integrated propagators are the solution of the modified diffusion equations,

$$\begin{aligned}\frac{\partial}{\partial t}q_0(\mathbf{r},t;\omega_0) &= \frac{[b(t)]^2}{6}\nabla^2 q_0(\mathbf{r},t;\omega_0) - \omega_0(\mathbf{r},t)q_0(\mathbf{r},t;\omega_0), & (2.20)\\ \frac{\partial}{\partial t}q_C(\mathbf{r},t;\omega_C) &= \frac{b_C^2}{6}\nabla^2 q_C(\mathbf{r},t;\omega_C) - \omega_C(\mathbf{r})q_C(\mathbf{r},t;\omega_C), & (2.21)\end{aligned}$$

with the initial conditions $q_0(\mathbf{r},0;[\omega_A^{eff},\omega_B]) = 1$, $q_C(\mathbf{r},0;\omega_C) = 1$, and

$$b(t) = \begin{cases} b_A & \text{if } 0 \leqslant t \leqslant fZ_0, \\ b_B & \text{if } fZ_0 < t \leq Z_0, \end{cases}$$

$$\omega_0(\mathbf{r},t) = \begin{cases} \omega_A^{eff}(\mathbf{r},t) & \text{if } 0 \leqslant t \leqslant fZ_0, \\ \omega_B(\mathbf{r}) & \text{if } fZ_0 < t \leq Z_0. \end{cases}$$

## 2.2 Mean-Field Approximation

The partition function eqn (2.15) is exact. What we have achieved is writing the partition function in terms of a functional intergral. In general, the functional integral is too complicated to be evaluated directly. A variety of approximation methods can be developed on the basis of this formalism. The mean field approximation amounts to evaluate the functional integral by using the saddle-function method. It is realized by replacing the sum over the canonical ensemble with a Gaussian integral around the most probable state that minimizes the argument of the exponential function. The free energy of the system with this approximation is given by the minimization of the free energy functional $F(\{\phi\},\{\omega\},\{\varphi\})$ with respect to $\phi_j(\mathbf{r}), \omega_j(\mathbf{r}), \phi_e(\mathbf{r}), \omega_e(\mathbf{r})$, and

$\varphi(\mathbf{r})$, subject to the constraints of incompressibility,

$$\frac{\delta F}{\delta \phi_j} = 0, \tag{2.22}$$

$$\frac{\delta F}{\delta \omega_j} = 0, \tag{2.23}$$

$$\frac{\delta F}{\delta \phi_e} = 0, \tag{2.24}$$

$$\frac{\delta F}{\delta \omega_e} = 0, \tag{2.25}$$

$$\frac{\delta F}{\delta \varphi} = 0. \tag{2.26}$$

Denoting the Lagrangian multipliers corresponding to the constraints by $\eta(\mathbf{r})$, and evaluating theses functional derivatives, we obtain the following variational equations,

$$\frac{\delta F}{\delta \phi_A(\mathbf{r})} = \mu_{0A} + \chi_{AB}\phi_B(\mathbf{r}) + \chi_{AC}\phi_C(\mathbf{r}) + \chi_{AI}\phi_I(\mathbf{r}) - \frac{\rho_{0A}}{\rho_0}\omega_A(\mathbf{r}) + \eta(\mathbf{r}) = 0, \tag{2.27}$$

$$\frac{\delta F}{\delta \phi_B(\mathbf{r})} = \mu_{0B} + \chi_{AB}\phi_A(\mathbf{r}) + \chi_{BC}\phi_C(\mathbf{r}) + \chi_{BI}\phi_I(\mathbf{r}) - \frac{\rho_{0B}}{\rho_0}\omega_B(\mathbf{r}) + \eta(\mathbf{r}) = 0, \tag{2.28}$$

$$\frac{\delta F}{\delta \phi_C(\mathbf{r})} = \mu_{0C} + \chi_{AC}\phi_A(\mathbf{r}) + \chi_{BC}\phi_B(\mathbf{r}) + \chi_{CI}\phi_I(\mathbf{r}) - \frac{\rho_{0C}}{\rho_0}\omega_C(\mathbf{r}) + \eta(\mathbf{r}) = 0, \tag{2.29}$$

$$\frac{\delta F}{\delta \phi_I(\mathbf{r})} = \mu_{0I} + \chi_{AI}\phi_A(\mathbf{r}) + \chi_{BI}\phi_B(\mathbf{r}) + \chi_{CI}\phi_C(\mathbf{r}) - \frac{\rho_{0I}}{\rho_0}\omega_I(\mathbf{r}) + \eta(\mathbf{r}) = 0, \tag{2.30}$$

$$\frac{\delta F}{\delta \phi_e(\mathbf{r})} = -\omega_e(\mathbf{r}) + \varphi(\mathbf{r}) = 0, \tag{2.31}$$

$$\frac{\delta F}{\delta \omega_A(\mathbf{r})} = -\frac{\rho_{0A}}{\rho_0}[\phi_A(\mathbf{r}) + \frac{\bar{\phi}_A V}{Q_0 f Z_0}\frac{\partial \omega_A^{eff}(\mathbf{r})}{\partial \omega_A(\mathbf{r})}\frac{\delta Q_0}{\delta \omega_A^{eff}(\mathbf{r})}] = 0, \tag{2.32}$$

$$\frac{\delta F}{\delta \omega_B(\mathbf{r})} = -\frac{\rho_{0B}}{\rho_0}[\phi_B(\mathbf{r}) + \frac{\bar{\phi}_B V}{Q_0 (1-f) Z_0}\frac{\partial \omega_B^{eff}(\mathbf{r})}{\partial \omega_B(\mathbf{r})}\frac{\delta Q_0}{\delta \omega_B^{eff}(\mathbf{r})}] = 0, \tag{2.33}$$

$$\frac{\delta F}{\delta \omega_C(\mathbf{r})} = -\frac{\rho_{0C}}{\rho_0}[\phi_C(\mathbf{r}) + \frac{\bar{\phi}_C V}{Q_C Z_C}\frac{\partial \omega_C^{eff}(\mathbf{r})}{\partial \omega_C(\mathbf{r})}\frac{\delta Q_C}{\delta \omega_C^{eff}(\mathbf{r})}] = 0, \tag{2.34}$$

$$\frac{\delta F}{\delta \omega_I(\mathbf{r})} = -\frac{\rho_{0I}}{\rho_0}[\phi_I(\mathbf{r}) + \frac{\bar{\phi}_I V}{Q_I}\frac{\partial \omega_I^{eff}(\mathbf{r})}{\partial \omega_I(\mathbf{r})}\frac{\delta Q_I}{\delta \omega_I^{eff}(\mathbf{r})}] = 0, \tag{2.35}$$

$$\frac{\delta F}{\delta \omega_e(\mathbf{r})} = -[\phi_e(\mathbf{r}) + \frac{\rho_{0A}}{\rho_0}\frac{\bar{\phi}_A V}{Q_0 f Z_0}\frac{\partial \omega_A^{eff}(\mathbf{r})}{\partial \omega_e(\mathbf{r})}\frac{\delta Q_0}{\delta \omega_A^{eff}(\mathbf{r})} + \frac{\rho_{0I}}{\rho_0}\frac{\bar{\phi}_I V}{Q_I}\frac{\partial \omega_I^{eff}(\mathbf{r})}{\partial \omega_e(\mathbf{r})}\frac{\delta Q_I}{\delta \omega_I^{eff}(\mathbf{r})}] = 0, \tag{2.36}$$

$$\frac{\delta F}{\delta \psi(\mathbf{r})} = \phi_e(\mathbf{r}) + \kappa^2 \nabla^2 \varphi(\mathbf{r}) = 0. \tag{2.37}$$

The functional derivatives in the above expressions can be obtained for the single molecular partition functions and the effective fields. The mean-field equations are obtained from the minimization conditions given above. In particular, the mean-field equilibrium concentrations for the polymers are given by

$$\phi_A(\mathbf{r}) = \frac{\bar{\phi}_A}{Q_0 f Z_0}\int_0^{fZ_0} dt q_{0c}(\mathbf{r}, Z_0 - t; [\omega_A^{eff}, \omega_B]) q_0(\mathbf{r}, t; [\omega_A^{eff}, \omega_B]), \tag{2.38}$$

$$\phi_B(\mathbf{r}) = \frac{\bar{\phi}_B}{Q_0 (1-f) Z_0}\int_{fZ_0}^{Z_0} dt q_{0c}(\mathbf{r}, Z_0 - t; [\omega_A^{eff}, \omega_B]) q_0(\mathbf{r}, t; [\omega_A^{eff}, \omega_B]), \tag{2.39}$$

$$\phi_C(\mathbf{r}) = \frac{\bar{\phi}_C}{Q_C Z_C}\int_0^{Z_C} dt q_C(\mathbf{r}, Z_C - t; [\omega_C]) q_C(\mathbf{r}, t; [\omega_C]). \tag{2.40}$$

The ionic densities can be obtained in a simple form due to the simplicity of the single particle partition function,

$$\phi_I(\mathbf{r}) = \frac{\bar{\phi}_I}{Q_I} q_I(\mathbf{r}), \tag{2.41}$$

where the propagator has the form

$$q_I(\mathbf{r}) = \exp[-\omega_I^{eff}(\mathbf{r})]. \tag{2.42}$$

The mean-field equation for the charge density depends on the charge distributions. For the smeared distribution $p(c_A(t)) = \delta(c_A(t) - p_A)$, each monomer carries $p_A z_A e$ charge. We have

$$\phi_e(\mathbf{r}) = \frac{\rho_{0A}}{\rho_0} p_A z_A \phi_A(\mathbf{r}) + \frac{\rho_{0I}}{\rho_0} z_I \phi_I(\mathbf{r}). \tag{2.43}$$

The effective fields with semeared charge distribution are defined by

$$\begin{aligned} \omega_A^{eff}(\mathbf{r}) &= \omega_A(\mathbf{r}) + z_A p_A \omega_e(\mathbf{r}), & (2.44)\\ \omega_I^{eff}(\mathbf{r}) &= \omega_I(\mathbf{r}) + z_I \omega_e(\mathbf{r}). & (2.45) \end{aligned}$$

The mean fields are to be obtained self-consistently from the minimization conditions. Since the mean-fields are defined up to an additive constant, we can adsorb the constants $\mu_{0j}$ into them and obtain

$$\begin{aligned} \omega_A(\mathbf{r}) &= \frac{\rho_0}{\rho_{0A}}[\chi_{AB}\phi_B(\mathbf{r}) + \chi_{AC}\phi_C(\mathbf{r}) + \chi_{AI}\phi_I(\mathbf{r}) + \eta(\mathbf{r})], & (2.46)\\ \omega_B(\mathbf{r}) &= \frac{\rho_0}{\rho_{0B}}[\chi_{AB}\phi_A(\mathbf{r}) + \chi_{BC}\phi_C(\mathbf{r}) + \chi_{BI}\phi_I(\mathbf{r}) + \eta(\mathbf{r})], & (2.47)\\ \omega_C(\mathbf{r}) &= \frac{\rho_0}{\rho_{0C}}[\chi_{AC}\phi_A(\mathbf{r}) + \chi_{BC}\phi_B(\mathbf{r}) + \chi_{CI}\phi_I(\mathbf{r}) + \eta(\mathbf{r})], & (2.48)\\ \omega_I(\mathbf{r}) &= \frac{\rho_0}{\rho_{0I}}[\chi_{AI}\phi_A(\mathbf{r}) + \chi_{BI}\phi_B(\mathbf{r}) + \chi_{CI}\phi_C(\mathbf{r}) + \eta(\mathbf{r})], & (2.49)\\ \omega_e(\mathbf{r}) &= \varphi(\mathbf{r}). & (2.50) \end{aligned}$$

The electrostatic potential is obtained from the minimization with respect to the electrostatic potential,

$$\nabla^2 \varphi(\mathbf{r}) = -\frac{1}{\kappa^2}\phi_e(\mathbf{r}), \tag{2.51}$$

which is the Poisson-Boltzmann equation in electrostatics.

The function $\eta(\mathbf{r})$ is to be adjusted to ensure the incompressibility condition,

$$\phi_A(\mathbf{r}) + \phi_B(\mathbf{r}) + \phi_C(\mathbf{r}) + \phi_I(\mathbf{r}) = 1. \tag{2.52}$$

The charge neutrality condition requires that the total charge of the system is zero,

$$\int d\mathbf{r}\phi_e(\mathbf{r}) = 0. \tag{2.53}$$

The above set of equations forms the basis of the mean-field theory of weakly charged multicomponent polyelectrolyte system. It should be noted that the mean-field equations are a set of self-consistent equations for the densities $\phi_j(\mathbf{r})$, the mean-fields $\omega_j(\mathbf{r})$, and the electrostatic potential $\varphi(\mathbf{r})$. For a given set of input parameters, these equations can be solved to obtain the equilibrium concentrations and fields. In general, the mean-field equations have to be solved numerically.

The free energy of the system can be computed after solving the mean-field equations. The terms linear in the concentrations can be neglected as they contribute a constant to the chemical potential. Denoting the average volume fraction for A monomer to be $\bar{\phi}_A$, C monomer to be $\bar{\phi}_C$ and I counterion to be $\bar{\phi}_I$, the free energy functional can be cast as

$$\begin{aligned}
\frac{F}{\rho_0 k_B T} &= \int d\mathbf{r}\{\chi_{AB}\phi_A(\mathbf{r})\phi_B(\mathbf{r}) + \chi_{AC}\phi_A(\mathbf{r})\phi_C(\mathbf{r}) + \chi_{BC}\phi_B(\mathbf{r})\phi_C(\mathbf{r})\} \\
&\quad + \int d\mathbf{r}\{\chi_{AI}\phi_A(\mathbf{r})\phi_I(\mathbf{r}) + \chi_{BI}\phi_B(\mathbf{r})\phi_I(\mathbf{r}) + \chi_{CI}\phi_C(\mathbf{r})\phi_I(\mathbf{r})\} \\
&\quad + V(\frac{1}{fZ_0}\frac{\rho_{0A}}{\rho_0}\bar{\phi}_A \ln\bar{\phi}_A + \frac{1}{Z_c}\frac{\rho_{0C}}{\rho_0}\bar{\phi}_C \ln\bar{\phi}_C + \frac{\rho_{0I}}{\rho_0}\bar{\phi}_I \ln\bar{\phi}_I) \\
&\quad - \int d\mathbf{r}\{\sum_j \frac{\rho_{0j}}{\rho_0}\omega_j(\mathbf{r})\phi_j(\mathbf{r}) \\
&\quad + \frac{1}{fZ_0}\frac{\rho_{0A}}{\rho_0}\phi_A(\mathbf{r})\ln Q_0 + \frac{1}{Z_C}\frac{\rho_{0C}}{\rho_0}\phi_C(\mathbf{r})\ln Q_C + \frac{\rho_{0I}}{\rho_0}\phi_I(\mathbf{r})\ln Q_I\} \\
&\quad + \int d\mathbf{r}\{[\frac{\rho_{0A}}{\rho_0}p_A z_A \phi_A(\mathbf{r}) + \frac{\rho_{0I}}{\rho_0}z_I\phi_I(\mathbf{r})]\varphi(\mathbf{r}) - \frac{\kappa^2}{2}|\nabla\varphi(\mathbf{r})|^2\}, \quad (2.54)
\end{aligned}$$

where we have neglected the superscript in the effective fields $\omega_j^{eff}$. We have also eliminated the variables $\phi_e(\mathbf{r})$ and $\omega_e(\mathbf{r})$ by expressing them in terms of $\phi_j(\mathbf{r})$ and $\varphi(\mathbf{r})$. This final expression of free energy contains contribution to free energy from different factors. The terms in the first and second lines describe the energy of nonelectrostatic interaction of the components. The entropy of the system comes from the third, forth and the fifth line. The last line describes the free energy of the Coulombic interactions. The calculated free energy can be used to obtain the phase diagrams of the system.

The mean-field theory derived above is very similar to the mean-field theory for neutral polymer systems. We only have one extra equation, the Poisson-Boltzmann equation. The chemical potential becomes the effective chemical potential containing the electrostatic contribution. The procedure for solving the mean-field equations in neutral polymer systems should be able to apply to the charged polymer systems.

Before getting into detailed examples, it is worthwhile to notice that the theory derived above is based on the following essential assumptions:

(a) The polyelectrolytes are weakly charged so that they can be described Gaussian chains;

(b) The dielectric constant $\epsilon$ does not depend on $\mathbf{r}$;

(c) The molecular interactions are short-ranged so that the Flory-Huggins $\chi$-parameter description is valid, and the hard core interactions can be modeled by the incompressibility condition;

(d) The mean-field approximation is valid.

Throughout this work, we will assume that the above conditions are fullfilled.

In summary, the mean-field theory of weakly charged polyelectrolytes developed above is a coupled theory of the polymer mean-field theory and the electrostatic theory. The coupling between the densities and the electrostatic potential is through the self-consistent field equations. This mean-field theory provides a general theoretical framework for the study of systems containing weakly charged polyelectrolytes. It can be applied to a variety of problems containing weakly charged polyelectrolytes, as demonstrated in the following chapters.

# Chapter 3

# Homogeneous Phases: Phase Diagrams

As a simple application, the free energy density functional derived in the previous chapter can be used to study the phase behavior of homogeneous phases. Knowledge of the stability and phase diagram of homogeneous phases can be used to study the miscibility of the system [44]. Furthermore, it is always useful to analyze the homogeneous phase free energy first before we turn to complicated applications of the self-consistent field theory.

For a homogeneous phase, the densities and conjugate fields become constants. In this case, the solutions of the modified diffusion equations can be obtained exactly,

$$q_0(\mathbf{r},t) = \begin{cases} \exp[-\omega_A t] & 0 < t \leq fZ_0, \\ \exp[-\omega_A f Z_0] \cdot \exp[-\omega_B (t - fZ_0)] & fZ_0 < t \leq Z_0, \end{cases}$$

$$q_{0c}(\mathbf{r},t) = \begin{cases} \exp[-\omega_B t] & 0 < t \leq (1-f)Z_0, \\ \exp[-\omega_B(1-f)Z_0] \cdot \exp[-\omega_A(t - Z_0 + fZ_0)] & (1-f)Z_0 < t \leq Z_0. \end{cases}$$

The concentrations are obtained as $\phi_A(\mathbf{r}) = \bar{\phi}_A$, $\phi_B(\mathbf{r}) = \bar{\phi}_B$. The other concentrations can be obtained easily $\phi_C(\mathbf{r}) = \bar{\phi}_C$, $\phi_I(\mathbf{r}) = \bar{\phi}_I$. Let $v_j = \frac{\rho_0}{\rho_{0j}}$ be the parameters characterize the different volumes of the monomers and counterions, the free energy of the homogeneous phase is then given by

$$\begin{aligned} \frac{F_H}{\rho_0 V k_B T} &= \chi_{AB}\bar{\phi}_A\bar{\phi}_B + \chi_{AC}\bar{\phi}_A\bar{\phi}_C + \chi_{BC}\bar{\phi}_B\bar{\phi}_C \\ &+\chi_{AI}\bar{\phi}_A\bar{\phi}_I + \chi_{BI}\bar{\phi}_B\bar{\phi}_I + \chi_{CI}\bar{\phi}_C\bar{\phi}_I \\ &+\frac{1}{fZ_0}\frac{1}{v_A}\bar{\phi}_A\ln\bar{\phi}_A + \frac{1}{Z_C}\frac{1}{v_C}\bar{\phi}_C\ln\bar{\phi}_C + \frac{1}{v_I}\bar{\phi}_I\ln\bar{\phi}_I. \end{aligned} \tag{3.1}$$

It should be noticed that the terms corresponding to the electrostatic interaction do not enter into the expression for the homogeneous free energy explicitly, since the system is electroneutral on average.

Using the incompressibility condition and the charge neutrality condition, we can write the homogeneous free energy in terms of $\phi_C$ alone. The other paramters are the Flory-Huggins paramters $\chi_{AB}, \chi_{AC}, \chi_{BC}, \chi_{AI}, \chi_{BI}, \chi_{CI}$, the volumes of different components $v_A, v_B, v_C, v_I$, the chain lengths $Z_0, Z_C$, the valence number $z_A, z_I$, the fraction of the A-block $f$, and the charge fraction $p_A$.

If for a given set of parameters, the free energy of the system is unstable with respect to a small fluctuation in composition, the system will tend to phase-separate. The homogeneous phase is then unstable. The boundary of the stable region of the homogeneous phase is the spinodal line, and is given by the condition

$$\frac{\partial^2 f_H}{\partial \phi_C^2} = 0. \tag{3.2}$$

In a $\phi - \chi$ plane, it is the boundary inside which the homogeneous phase is unstable, and the phase-separation occurs spontaneously in this region.

The critical point is determined by the following conditions,

$$\frac{\partial^2 f_H}{\partial \phi_C^2} = 0, \frac{\partial^3 f_H}{\partial \phi_C^3} = 0. \tag{3.3}$$

Below the critical point in the $\phi - \chi$ plane, the homogeneous phase is always stable.

In order to study the phase behavior of the homogeneous phase, we need to calculate the chemical potentials of the system as well. The chemical potential of the charged-neutral diblock copolymer is given by

$$\begin{aligned}
\frac{\mu_0}{k_B T} &= \frac{1}{k_B T}\frac{\partial F_H}{\partial n_0} \\
&= \frac{\partial f_H}{\partial n_0} V \rho_0 + f_H \rho_0 \frac{\partial V}{\partial n_0} \\
&= \frac{\partial f_H}{\partial \phi_A} Z_0 f v_A + \frac{\partial f_H}{\partial \phi_B} Z_0 (1-f) v_B - \frac{\partial f_H}{\partial \phi_I} \frac{Z_0 f p_A z_A}{z_I} v_I \\
&\quad + (Z_0 f v_A + Z_0 (1-f) v_B - \frac{Z_0 f p_A z_A}{z_I} v_I)[f_H - \sum_j \phi_j \frac{\partial f_H}{\partial \phi_j}].
\end{aligned} \tag{3.4}$$

The chemical potential of the $C$-homopolymer is

$$\begin{aligned}
\frac{\mu_C}{k_B T} &= \frac{1}{k_B T}\frac{\partial F_H}{\partial n_C} \\
&= \frac{\partial f_H}{\partial \phi_C} Z_C v_C + Z_C v_C [f_H - \sum_j \phi_j \frac{\partial f_H}{\partial \phi_j}].
\end{aligned} \tag{3.5}$$

If we denote the two coexistence phases by phase I and phase II, then the equilibrium concentrations are given by the solutions of the following equations,

$$\mu_0^{\mathrm{I}} = \mu_0^{\mathrm{II}}, \tag{3.6}$$

$$\mu_C^{\mathrm{I}} = \mu_C^{\mathrm{II}}, \tag{3.7}$$

$$\phi_A^{\mathrm{I}} + \phi_B^{\mathrm{I}} + \phi_C^{\mathrm{I}} + \phi_I^{\mathrm{I}} = 1, \tag{3.8}$$

$$\phi_A^{\mathrm{II}} + \phi_B^{\mathrm{II}} + \phi_C^{\mathrm{II}} + \phi_I^{\mathrm{II}} = 1. \tag{3.9}$$

There are eight unknown variables and four equations. Four more equations can be added using the the fact that A, B are connected and the charge neutrality condition has to be satisfied in each of the bulk phases,

$$(1-f)\phi_A^{\mathrm{I}} = f\phi_B^{\mathrm{I}}, \tag{3.10}$$

$$(1-f)\phi_A^{\mathrm{II}} = f\phi_B^{\mathrm{II}}, \tag{3.11}$$

$$\frac{1}{v_A} p_A z_A \phi_A^{\mathrm{I}} + \frac{1}{v_I} z_I \phi_I^{\mathrm{I}} = 0, \tag{3.12}$$

$$\frac{1}{v_A} p_A z_A \phi_A^{\mathrm{II}} + \frac{1}{v_I} z_I \phi_I^{\mathrm{II}} = 0. \tag{3.13}$$

The solution is now completely determined. For an appropriate set of parameters, the homogeneous phase is unstable and the system undergoes a macroscopic phase separation into one phase rich in charged polymers and one phase rich in neutral C-homopolymer. The boundary between the homogeneous phase and the phase-separated state is the phase coexistence curve, or the binodal.

In all the following applications, we assume for simplicity that the polymer monomers have the same bulk density as the reference density, therefore, $v_A = v_B = v_C = 1$. We also assume that the A and B monomers are the same except that A carries charge. Thus, the Flory interaction parameter between the A, B monomers $\chi_{AB} = 0$, and we use $\chi_{AC} = \chi_{BC} = \chi$.

## 3.1 Application to Charged Polymer Systems

For simplicity, we follow the same assumption of previous work on charged polymer systems that we can neglect the volume of the counterions, $v_I = 0$. Furthermore, we assume that the only interaction for the counterions is the Coulombic interaction, so that $\chi_{AI} = \chi_{BI} = \chi_{CI} = 0$. The valency of the charged monomer is always taken to be $z_A = 1$, and the valency of the counterions is taken to be $z_I = -1$.

First, we consider a system with $N_A = N_B = N_C/2 = 100$. This is a system composed of symmetric charged-neutral diblock copolymers, C homopolymers and counterions. Typical binodal and spinodal lines for three different charge fractions $p_A = 0, 0.05$ and $0.1$ are plotted in Fig. 3.1, illustrating the effect of charge fraction on the phase behavior.

As can be noticed from the phase diagram, for each charge fraction value, the spinodal line and the binodal line meet at a critical point. The region inside the binodal line is the phase separated state, and the remaining region is the homogeneous phase. The region inside the spinodal line is the unstable region of the homogeneous phase, where spontaneous phase separation occurs. The region between the binodal and spinodal line is the metastable region of the homogeneous phase.

The significance of the phase boundaries can be illustrated by examing the system with $p_A = 0.1$. A horizontal line corresponding to a certain value of $\chi$, for example $\chi = 0.055$, can be drawn. This line meets the binodal line at $\phi_C = \phi_1$,

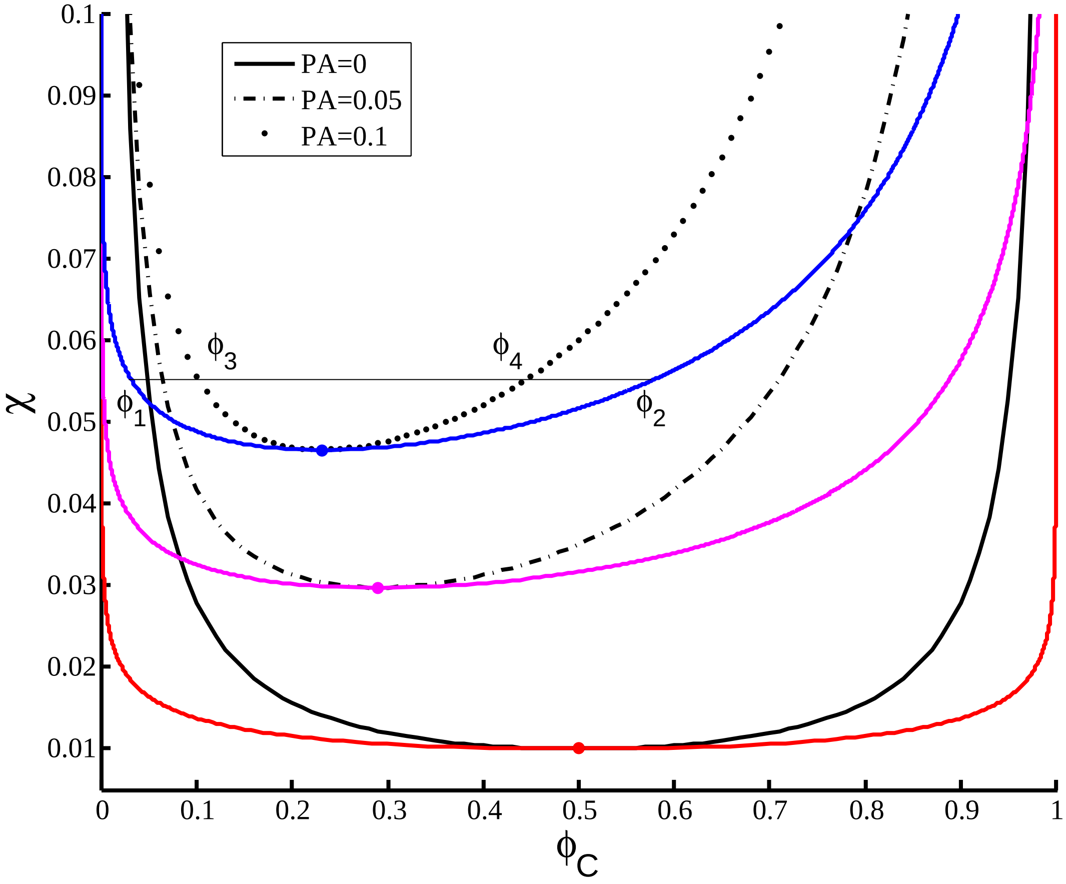

Figure 3.1: Binodal and spinodal lines for charged-neutral diblock copolymer/C-homopolymer systems, with $N_A = N_B = N_C/2 = 100$ and different charge fractions. The colored lines are the binodal lines, with the red color for $p_A = 0$, the purple color for $p_A = 0.05$, and the blue color for $p_A = 0.1$. The black curves are spinodal lines, with the solid line for $p_A = 0$, the dash-dot line for $p_A = 0.05$, and the dotted line for $p_A = 0.1$. The red big dot is the critical point for $p_A = 0$, the purple big dot is the critical point for $p_A = 0.05$, and the blue big dot is the critical point for $p_A = 0.1$.

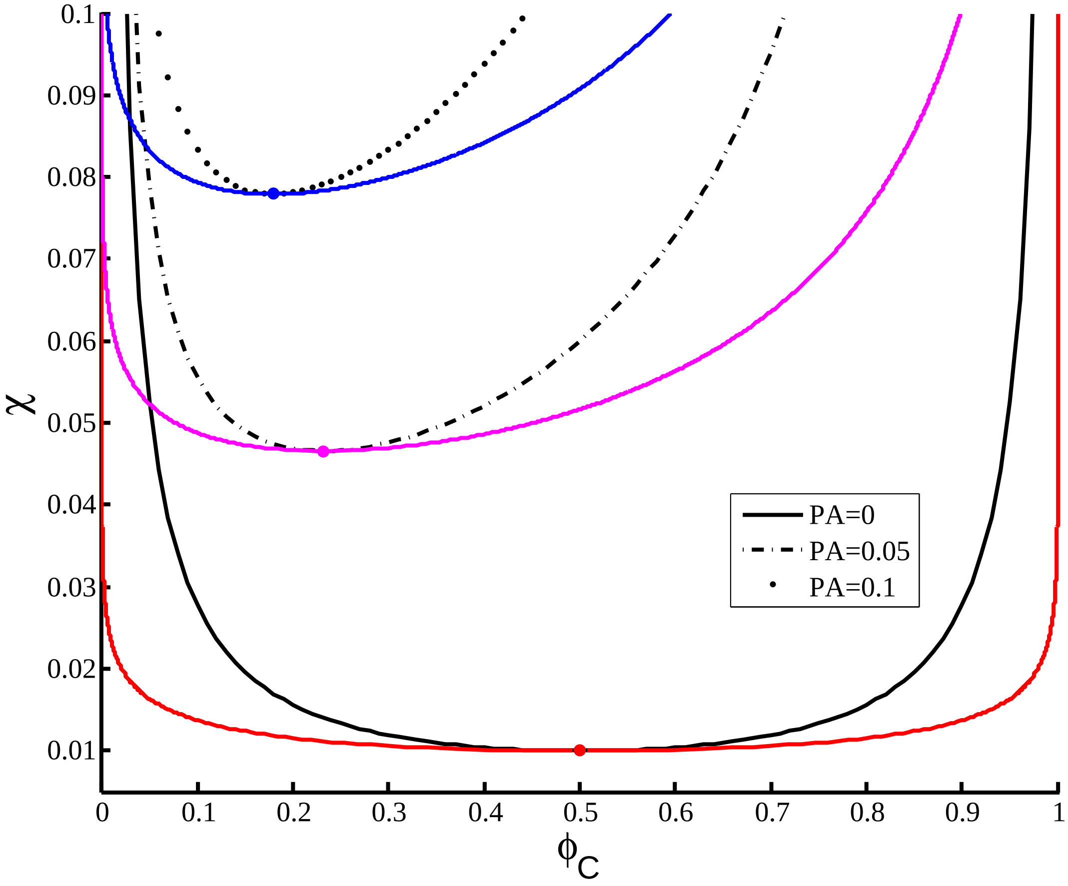

Figure 3.2: Binodal and spinodal lines for polyelectrolyte/C-homopolymer blends, with $N_A = N_C = 200$ and different charge fractions. The colored lines are the binodal lines, with the red color for $p_A = 0$, the purple color for $p_A = 0.05$, and the blue color for $p_A = 0.1$. The black curves are spinodal lines, with the solid line for $p_A = 0$, the dash-dot line for $p_A = 0.05$, and the dotted line for $p_A = 0.1$. The red big dot is the critical point for $p_A = 0$, the purple big dot is the critical point for $p_A = 0.05$, and the blue big dot is the critical point for $p_A = 0.1$.

and $\phi_C = \phi_2$. It also meets the spinodal line at $\phi_C = \phi_3$, and $\phi_C = \phi_4$. For an initial C-homopolymer concentration between $\phi_1$ and $\phi_2$, the system will phase separate into two phases, one with C-homopolymer concentration $\phi_1$, and the other with C-homopolymer concentration $\phi_2$.

As can be noticed from these phase boundaries, the region of the homogeneous phase increases as the charge fraction increases. This is because when the charge fraction of the chain increases, the number of counterions in the system increases as well. The entropic effect of the counteions is then increased, making the homogeneous phase more stable. The effect of the charges in the system is therefore to increase the miscibility of the system.

As a second example, we consider a system with $N_B = 0$, $N_A = N_C = 200$, corresponding to a polyelectrolyte/homopolymer blend. We examine the phase behavior at three different charge fractions as the previous system. The results are shown in Fig. 3.2. The general trend is that, as the charge fraction increases, the homogeneous phase region increases. This is again due to the entropic gain from the counterions.

The set of phase boundaries in Fig. 3.1 and in Fig. 3.2 can be compared. From the phase boundaries for $p_A = 0.1$ in Fig 3.1 to the phase boundaries for $p_A = 0.1$ in Fig. 3.2. the charged polymer in the system changes from half of the polymer chain charged to the whole polymer chain charged with the same charge fraction. By comparing these two plots, we can notice that the region of homogeneous phase increases as the whole chain becomes charged. This is because there are more counterions in the second system. The entropy effect of the counterions makes the homogeneous phase more favourable.

We also compare the phase boundaries for $p_A = 0.1$ in Fig. 3.1 with the phase boundaries for $p_A = 0.05$ in Fig. 3.2, these two systems contain the same number of counterions. The only difference is that in Fig. 3.1 the charged groups are carried by half of the charged polymer chain and in Fig. 3.2 the charged groups are carried by the whole chain of the charged polymer with half the charge fraction. We can see that these is no noticeable difference between these two sets of phase diagrams. This result illustrates that the system is insensitive to the charge distribution. We can further show that the stability and the phase diagram of the homogeneous phase of the system mainly depend on the total amount of charges on the charged polymer.

## 3.2 Application to Ionic Liquid Systems

As some ionic liquids have long enough alkyl chain on the cationic core [66], the chain-like architecture of these ionic liquids makes it possible to apply the charged polymer theory to investigate their phase behavior.

Generally speaking, ionic liquids are salts with low melting temperature, usually below 100 °C [67]. They are known to have good chemical and electro-chemical stability, high ionic conductivity, low flammability and negligible vapour pressure [68] [69]. They are most commonly composed of an asymmetric organic cation and an inorganic anion. Numerous possible ionic liquids can be obtained via chemical modifications by pairing selected cations and anions [70]. The sizes of the ions are usually mismatched and the molecules are usually asymmetric, making their crystalline forms weakly bounded and melting at low temperatures.

One of the most important properties of ionic liquid solvents is their ability to dissolve a wide range of inorganic, organic, and polymeric materials, such as cellulose [71]. For this reason, they are used as potential replacement for traditional solvents used in chemical processes. They also have useful application in making devices that depend on the transport of electrons for energy capture and storage due to their high conductivity, low volatility, and large liquidus [72].

In this section, we will apply the SCFT for charged polymer systems to the ionic liquid/homopolymer system to study the stability and phase diagram of the homogeneous phase. We can set the length of the charged polymer to a small value to represent the organic cation. Also, in the ionic liquid system, the volume of the anions is much larger than that of the counterions of the charged polymer system. Therefore, the volume of the anions should be taken into account in this case. We assume that the number of anions in the system is the same as the number of cation chains, $n_0 = n_I$. We also set the valency of the anions to be $z_I = -1$. In this case, the charge fraction of the cation chain is no longer a parameter, as it always equal to $1/fZ_0$. We set the degree of polymerization of the C-homopolymer to be 100, and let the cation to be symmetric diblock copolymer with half the chain charged, $f = 0.5$.

In the first application, we make the same assumption as in the charged polymer systems that the non-electrostatic interaction for the anions can be neglected, $\chi_{AI} = \chi_{CI} = \chi_{BI} = 0$. We set the degree of polymerization of the diblock copolymer to be 20. We then examine how the change of the size of the counterions can affect the system. The results are shown in Fig. 3.3. The binodal lines and spinodal lines at counterion size $v_I = 5, 10$, and 20 are given. The critical points for those systems have counterion size between 5 and 20 are all given as well. It can be observed that the homogeneous phase region becomes larger as the size of the anions increases. This indicates that, if we use the ionic liquid as a solvent for polymers, the larger the anion size, the better the solubility of the ionic liquid.

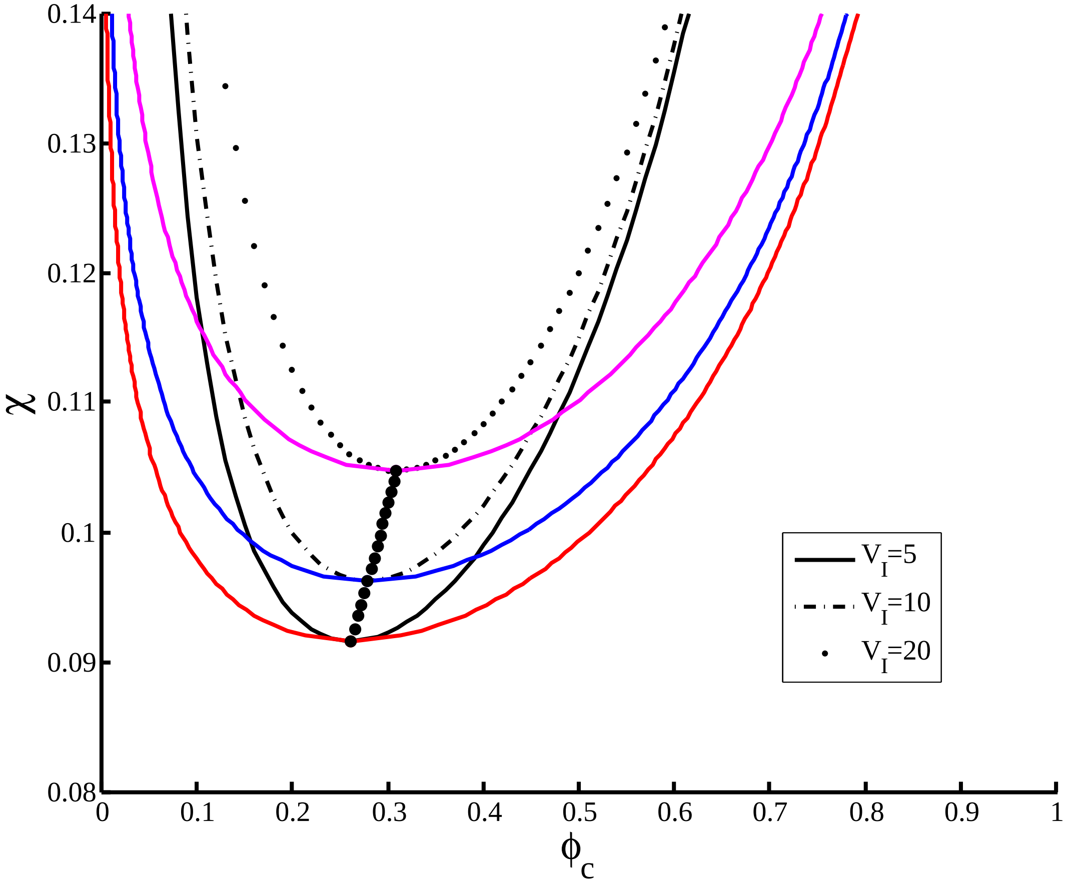

Figure 3.3: Binodal and spinodal lines for ionic liquid/C-homopolymer systems, with $N_A = N_B = 10, N_C = 100$ and different anion sizes. The colored lines are the binodal lines, with the red color for $v_I = 5$, the blue color for $v_I = 10$, and the purple color for $v_I = 20$. The black curves are spinodal lines, with the solid line for $v_I = 5$, the dash-dot line for $v_I = 10$, and the dotted line for $v_I = 20$. The big black dots are critical points drawn when $v_I$ changes from 5 to 20.

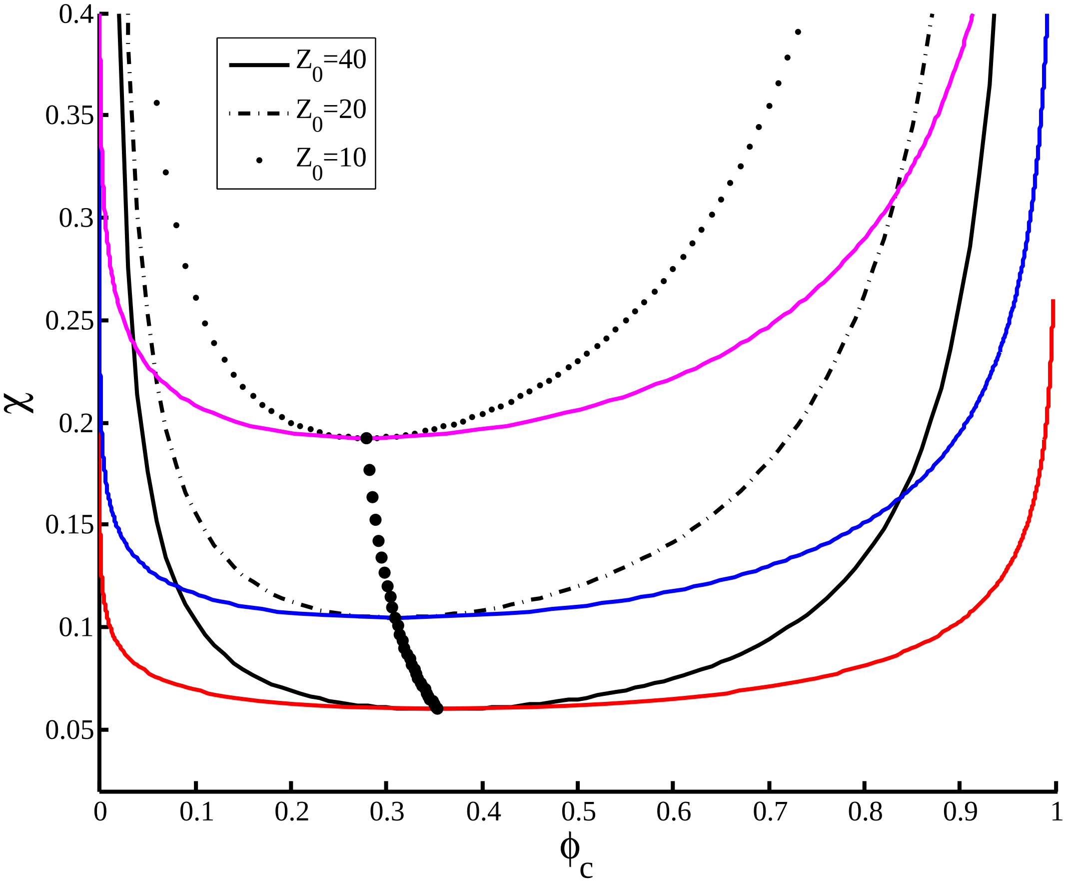

Figure 3.4: Binodal and spinodal lines for ionic liquid/C-homopolymer systems, with $N_C = 100$, the anion volume $v_I = 20$, and different cation chain lengths. The colored lines are the binodal lines, with the red color for $Z_0 = 40$, the blue color for $Z_0 = 20$, and the purple color for $Z_0 = 10$. The black curves are spinodal lines, with the solid line for $Z_0 = 40$, the dash-dot line for $Z_0 = 20$, and the dotted line for $Z_0 = 10$. The big black dots are critical points drawn when $Z_0$ changes from 10 to 40.

By setting $v_I$ to a fixed value 20, We also examine the effect of the length of the cation chain to the system. In this example, the C-homopolymer has a fixed length of 100. The results are shown in Fig. 3.4. The binodal lines and the spinodal lines at cation length 10, 20 and 40 are given. The critical points for those systems have cation length between 10 and 40 are all given as well. Fig. 3.4 illustrates that the region of the homogeneous phase increases rapidly as the chain length of the cation decreases. This is analogous to the neutral polymer systems. As the chain length increases, the repulsive interaction effect overcomes the entropic effect, the system undergoes phase separation.

Another application would be taking into account the non-electrostatic interaction of the anions with the C-homopolymer, which is represented by $\chi_{CI}$. As there is no phase separation between the anions and the cation chains, $\chi_{AI}$ and $\chi_{BI}$ can still set to be zero. We examine both attractive interaction and replusive interaction between the anions and the C-homopolymer. The spinodal lines and critical points for negative values of $\chi_{CI}$, $\chi_{CI} = -0.05$ are shown in Fig. 3.5. As illustrated in the figure, when the anions and the C-homopolymer have attractive interaction, by increasing the size of the anions, the homogeneous phase region becomes larger and it can also be noticed that it gets larger faster than in the system without the non-elctrostatic interaction between the anions and the C-homopolymer. By comparing Fig. 3.3 and Fig. 3.5, it can be seen that, for the same anion size, the homogenous phase region is larger in the system with attracive interaction between the anions and the C-homopolymer than in the system without this interaction. This can be understood as the attractive interaction between the anions and the C-homopolymer also stabilize the homogeneous phase.

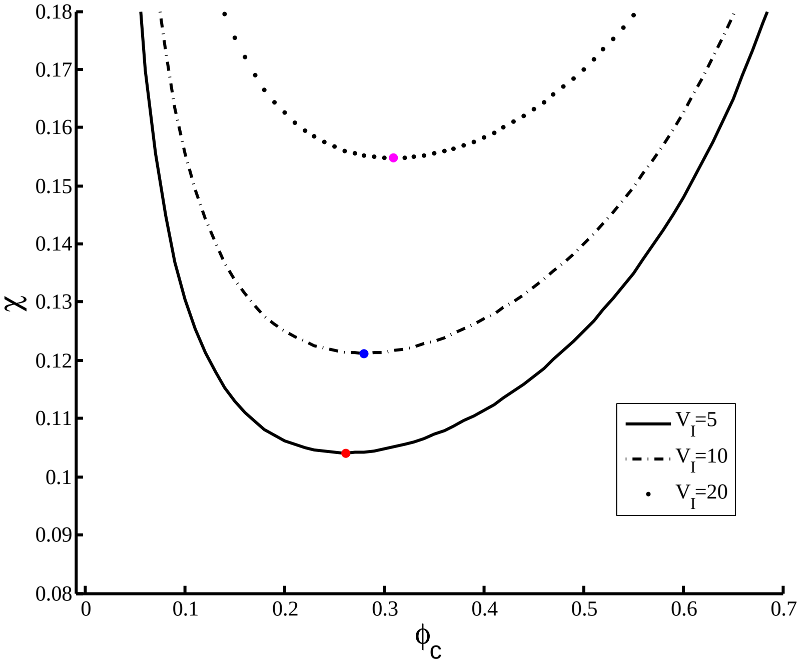

Figure 3.5: Spinodal lines and critical points for ionic liquid/C-homopolymer systems with different counterion volumes when $\chi_{CI} = -0.05$.

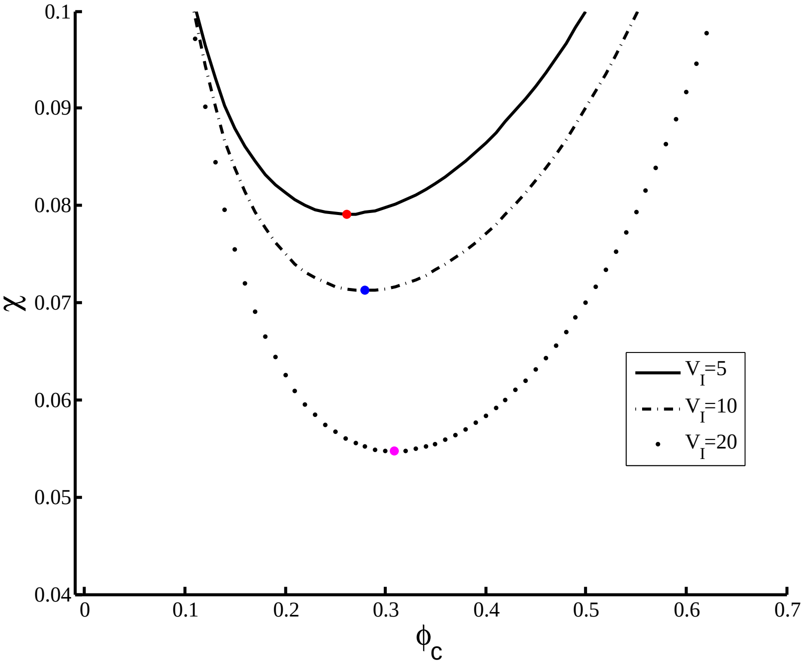

Figure 3.6: Spinodal lines and critical points for ionic liquid/C-homopolymer systems with different counterion volumes when $\chi_{CI} = 0.05$.

As a comparision , we consider the case when the anions and the C-homopolymer have replusive interaction, $\chi_{CI} = 0.05$, the spinodal lines and the critical points are shown in Fig. 3.6 for such ionic liquid system. The figure illustrates that the homogeneous phase region decreases as the size of the anions gets larger. By comparing Fig. 3.3 and Fig. 3.6, we observe that the homogeneous phase region gets smaller if the replusive interaction between the anions and the C-homopolymer is introduced in the system, as such system prefers phase separated state with less contact between the anions and the C-homopolymer.

To conclude, by calculating the homogeneous phase diagram, it is shown that ionic liquid solvents with larger anions have better solubility for polymers and the solubility is also increased by introducing attractive interaction between the anions and the polymer.

# Chapter 4

# Homogeneous Phases: Stability Analysis Using RPA

The self-consistent field theory of weakly charged polyelectrolyte systems developed in Chapter 2 is a coupled theory of the polymer mean-field theory and the electrostatic theory. It results in a large parameter space which is computationally expensive to explore. An approximation method which can describe the phase behavior approximately is therefore desirable. In this chapter, the random phase approximation (RPA) method will be used to investigate the stability of homogenous phases. For simplicity, we again assume that in the polyelectrolyte systems that will be studied in this chapter, the non-electrostatic interaction and the volume of the counterions is so small that it can be neglected.

The random phase approximation is an approximation method in which the free energy is expanded in a power series in the density fields [73]. It was first developed by Leibler [49] to study the microphase separation of neutral diblock copolymer systems, and has been extented to polyelectrolyte systems as well [50].

In this chapter, we apply the random phase approximation (RPA) to examine the stability limit of the homogeneous phase with respect to both macrophase and microphase separation.

Assuming that the variables are close to the homogenous phase ones, we can expand the free energy functional of the inhomogeneous system around the homogenous phase free energy,

$$\frac{F}{\rho_0 k_B T} = \frac{F_H}{\rho_0 k_B T} + \frac{\Delta F}{\rho_0 k_B T}. \tag{4.1}$$

An analysis of the second-order coefficient gives the spinodal line of the system.

For polyelectorlyte/homopolymer blends, the second-order free energy can be written in the simple form ( see Appendix C for details ),

$$\frac{\Delta F^{(2)}}{\rho_0 k_B T} = \frac{1}{2}\int \frac{d\mathbf{k}}{(2\pi)^2}\frac{\delta\tilde{\phi}_A(\mathbf{k})\delta\tilde{\phi}_A(-\mathbf{k})}{S_{AA}(\mathbf{k})}, \tag{4.2}$$

where the RPA scattering function $S_{AA}(\mathbf{k})$ is given by

$$\frac{1}{S_{AA}(\mathbf{k})} = \frac{1}{\bar{\phi}_A Z_A}[\frac{1}{g([R_g^A\mathbf{k}]^2)} + \frac{C_A}{[1+(\lambda\mathbf{k})^2]}] + \frac{1}{(1-\bar{\phi}_A)Z_C g([R_g^C\mathbf{k}]^2)} - 2\chi_{AC}, \tag{4.3}$$

where $C_A = p_A Z_A$ is the total number of elementary charges one polyelectrolyte chain, the screening parameter $\lambda$ and the Debye function $g(x)$ are defined in Appendix C.

It can be shown that, at very small $\mathbf{k}$, only the term related to the electrostatic interaction contributes, the above equation varies as $-\mathbf{k}^2$. At large $\mathbf{k}$, the above equation varies as $\mathbf{k}^2$, which corresponds to a macroscopic phase separation. This two asymptotic form together can exhibit a minimum at a finite wave number $q^0 \neq 0$.

The stability condition for the homogeneous phase depends on the sign of the above equation, which is the inverse of the scattering function. If $S_{AA}^{-1}(\mathbf{k}) > 0$, the contribution of any fluctuations to the free energy is always postive, the homogeneous phase is thus stable. If instead $S_{AA}^{-1}(\mathbf{k}) < 0$, the fluctuations reduce the free energy, so the homogeneous phase is unstable. Therefore, the stability condition for the homogeneous phase is

$$\min_{\mathbf{k}}\{\frac{1}{\bar{\phi}_A Z_A}[\frac{1}{g([R_g^A\mathbf{k}]^2)}+\frac{C_A}{[1+(\lambda\mathbf{k})^2]}]+\frac{1}{(1-\bar{\phi}_A)Z_C g([R_g^C\mathbf{k}]^2)}-2\chi_{AC}\}>0. \quad (4.4)$$

If the above equation has a minimum at some critical wave number $q_0 = 0$, the system goes through macrophase separation. On the other hand, if the minimum occurs at $q_0 > 0$, the system goes through microphase separation. The spinodal line is determined by the condition that $\min_{\mathbf{k}} S_{AA}^{-1}(\mathbf{k}) = 0$.

To illustrate the method of RPA, we apply it to two simple polyelectrolyte systems. In what follows, the polyelectrolytes are all charged homopolymers.

## 4.1 Polyelectrolyte/Homopolymer Blends

We first consider a system of polyelectrolyte/homopolymer blends with degree of polymerization $Z_A = Z_C = 1000$, and charge fraction $p_A = 0.01$. We define a paramter $\tau = 4\pi e^2/\epsilon k_B T b = l_B/b$, which is the dimensionless parameter associated with the electrostatic interactions. The larger the values of $\tau$, the lower the polarity of the system. When $\tau = 6$, typical plots of the inverse of the scattering function $S_{AA}^{-1}(\mathbf{k})$ are shown in Fig. 4.1 and Fig. 4.2. The thick lines are the inverse scattering function at different $\chi$. In each figure, we also use two thin blue lines to show the two source of contributions to the inverse scattering function represented by the thick blue line. It can be seen that the contribution from the the Debye function exhibits

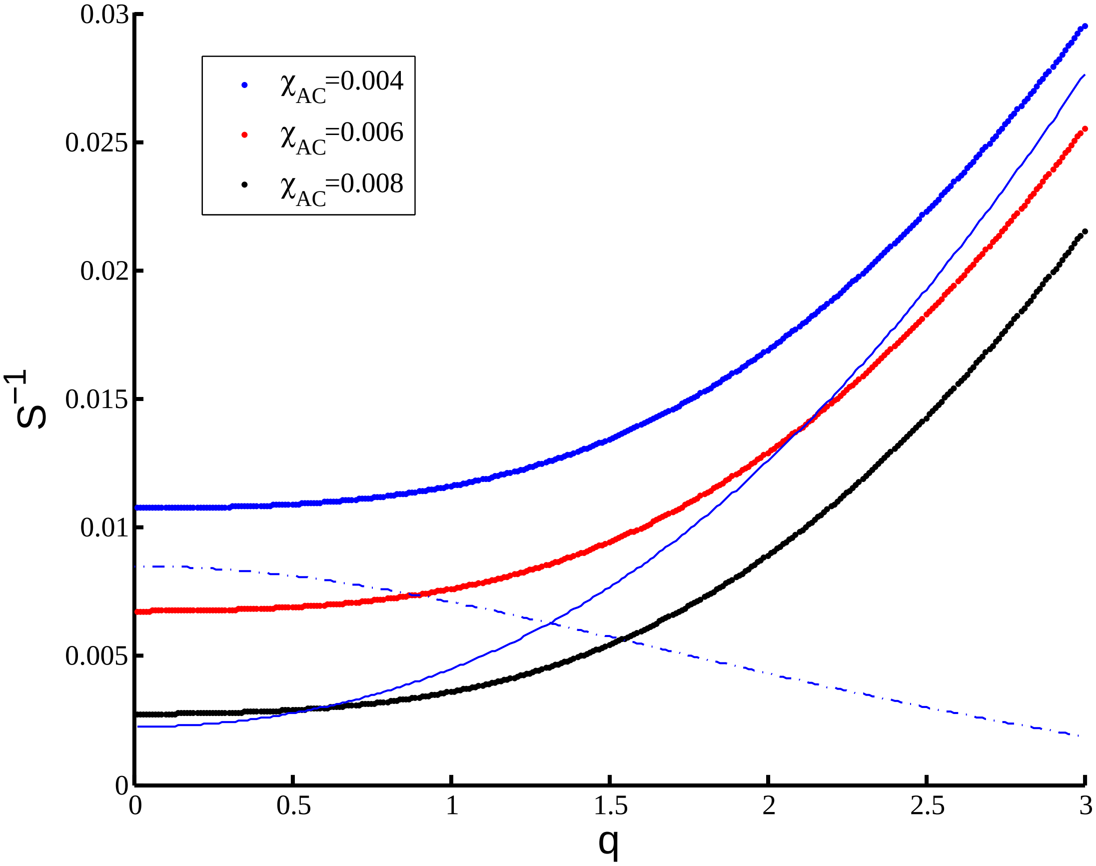

Figure 4.1: Plot showing the inverse of the scattering function (thick lines) as a function of the wave vector for A-polyelectrolyte/C-homopolymer blends at three different $\chi$ values when $\phi_A = 0.8$. The thick blue line is divided into two parts, with the thin blue dot line represents terms with Debye function, and the thin blue dash-dot line represents terms with electrostatic interaction.

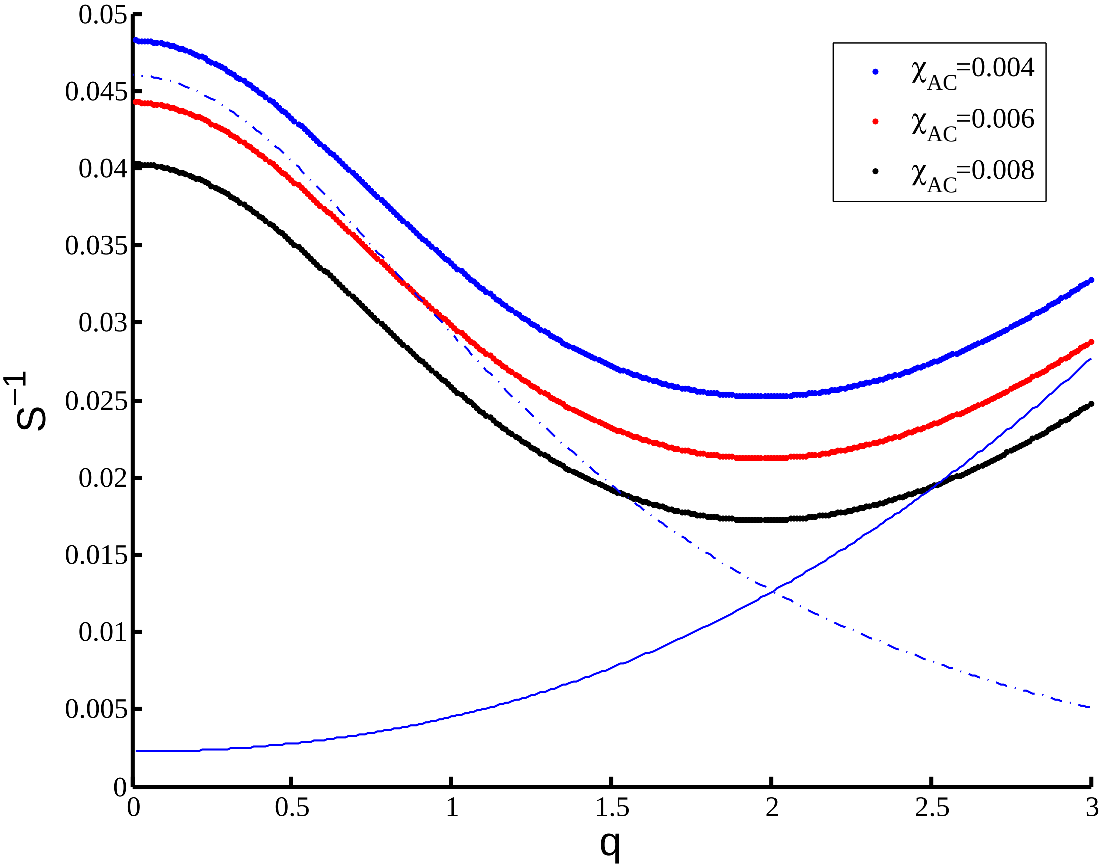

Figure 4.2: Plot showing the inverse of the scattering function (thick lines) as a function of the wave vector for A-polyelectrolyte/C-homopolymer blends at three different $\chi$ values when $\phi_A = 0.2$. The thick blue line is divided into two parts, with the thin blue dot line represents terms with Debye function, and the thin blue dash-dot line represents terms with electrostatic interaction.

a minimum at $q = 0$ and the contribution from the electrostatic interaction exhibits a maximum at $q = 0$.

In Fig. 4.1, The results are shown for this blend system with polyelectrolyte concentration $\phi_A = 0.8$, and different $\chi$ values. It is noticed that with this set of parameters, the inverse of the scattering function has the minimum at $q_0 = 0$. The minimum value approaches zero when $\chi$ increases. When $S_{AA}^{-1}(\mathbf{k})$ becomes negative, any small density fluctuations with $q_0 = 0$ decrease the free energy, leading to a growth of long wavelength fluctuations in the density field. This corresponds to a macrophase separation of the system.

In Fig. 4.2, The results are shown for this blend system with $\phi_A = 0.2$, and different $\chi$ values. other parameters are set as the same as used in Fig. 4.1. It is noticed that at this polyelectrolyte concentration, the resulting inverse of the scattering function has the minimum at $q_0 > 0$. As $\chi$ increases, the $S_{AA}^{-1}(\mathbf{k})$ changes from positive to negative. The Fourier mode with nonzero wave number $q_0$ becomes unstable, leading to the formation of ordered structure with length scale of $(q_0/2\pi)^{-1}$.

By comparing Fig. 4.1 and Fig. 4.2, it can be noticed that when the polyelectrolyte concentration is decreased, the electrostatic interaction contribution exhibits a much larger maximum at $q = 0$ and the Debye function contribution stays almost the same. A finite length scale can then be selected at small polyelectrolyte concentration, leading the system to form a periodic pattern.

In Fig. 4.3, we set the charge fraction to be $p_A = 0.01$ for this blend system and plot the critical value of $q_0$ as a function of the polyelectrolyte conentration $\phi_A$ at three different $\tau$ values, $\tau = 12, 6$ and 3. As can be noticed from the plot, as the $\phi_A$ value increases, the critical wavevector $q_0$ first increases from zero then decreases to

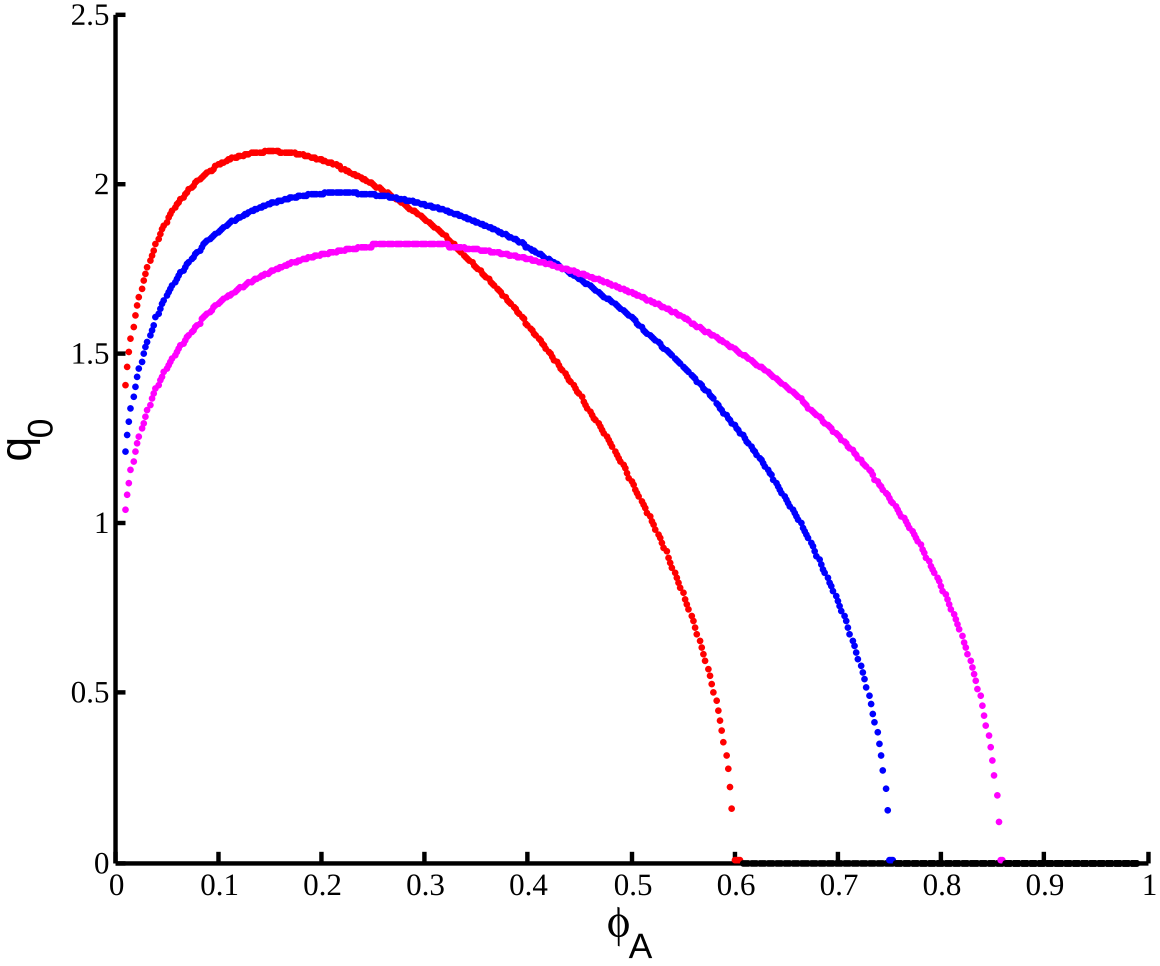

Figure 4.3: Plot showing the critical wave number $q_0$ as a function of the polyelectrolyte concentration $\phi_A$ for A-polyelectrolyte/C-homopolymer blends at different $\tau$ values. The red, blue and purple dotted curves are for non-zero values of $q_0$ when $\tau = 12$, 6 and 3, respectively. The $q_0$ values go to zero at large values of $\phi_A$ which is represented by the black dotted line.

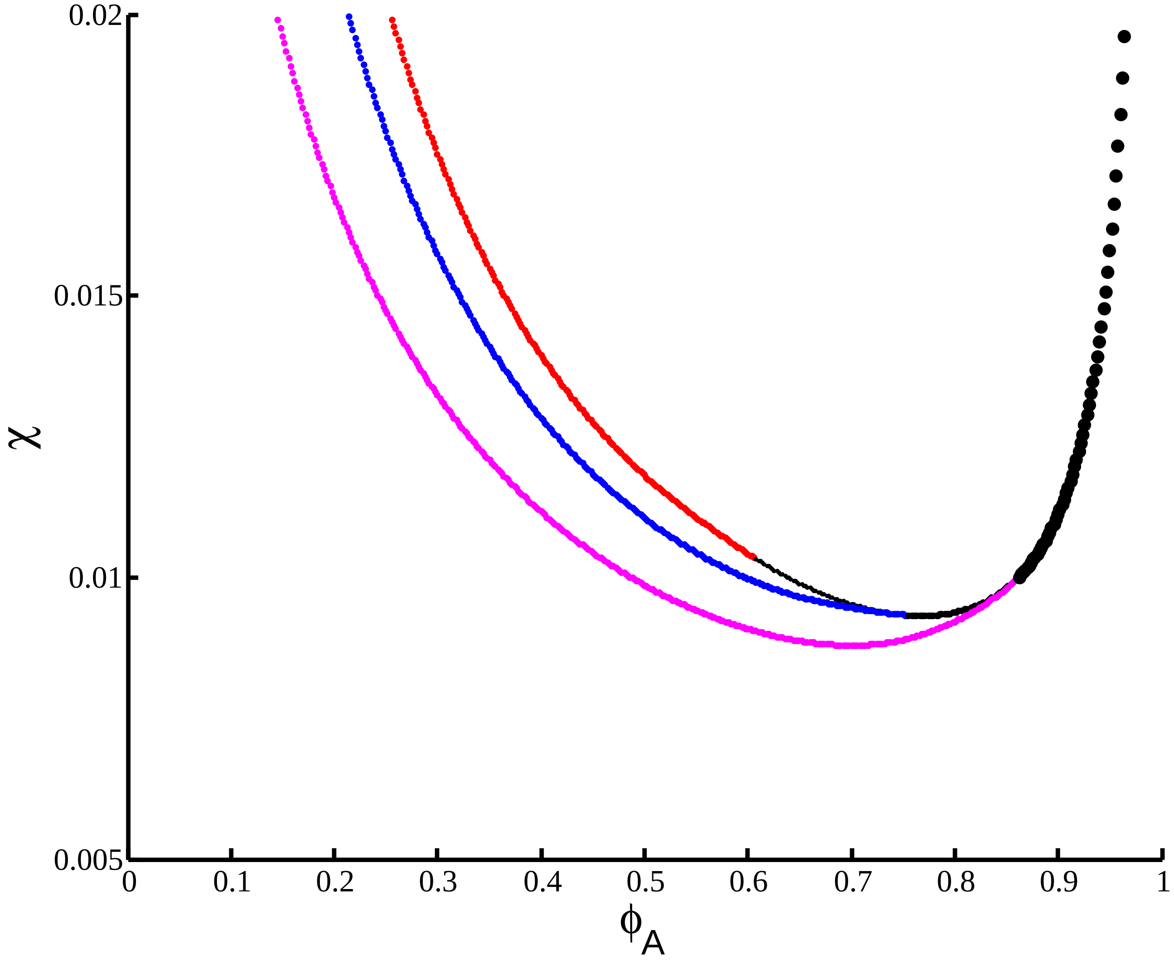

Figure 4.4: Spinodal lines for A-polyelectrolyte/C-homopolymer blends calculated at three different values of $\tau$. The small, midium, large size black dotted lines are for the macrophase separation boundaries at $\tau$ = 12, 6 and 3, respectively. The red, blue and purple curves are for microphase separation boundaries when $\tau$ = 12, 6 and 3, respectively.

zero and maintains the zero value at large $\phi_A$ values. This indicates that at small polyelectrolyte concentrations, the homogeneous phase is unstable with respect to the microphase separation when $\chi$ increases, and at large polyelectrolyte concentrations, the homogeneous phase is unstable with respect to the macrophase separation when $\chi$ increases. This can be explained from the the entropic point of view. At low polyelectrolyte concentrations, undergoing marcophase separation will significanlly reduce the space that counterions can occupy, leads to huge loss of entropy of the counterions. However, at large polyelectrolyte concentrations, the entropy decrease will be less pronounced, the macrophase separation can thus occur. Another feature that can be noticed from the plot is that the $\phi_A$ value at which $q_0$ becomes zero increases as the value of $\tau$ decreases. In what follows, we use $\phi_A^0$ to indicate this value.

The spinodals for the above system are shown in Fig. 4.4 for the same set of $\tau$ values as in Fig. 4.3. The colored curves denote the microphase separation transitions, while the black dotted lines are macrophase separation transitions. As can be noticed from the plot, the microphase separated region increases as the value of $\tau$ decreases. This is because as the value of $\tau$ decreases, the electrostatic interaction decreases as well, making the couterions less bounded to the polymer co-ion and gain more entropy. We can then conclude that the microphase separated structure can emerge mainly in medium with small $l_B$, or with large dielectric constant.

It is worthwhile to compare the above calculation with the work done by Nyrkova et al. [52]. Both the results exhibit the same feature that when $\tau$ decreases, the microphase separated region increases. The differences between the results are as follows, for the same value of $\tau$, the microphase separated region obtained in this work is larger than theirs. Their phase diagrams also show narrow macrophase separated region when polyelectrolyte concentrations are close to zero, which is not illustrated by our calculation.

It is also interesting to examine the effect of the charge fraction $p_A$ on the critical wave number $q_0$ as a function of polyelectrolyte concentration $\phi_A$. We consider four different values of $p_A$, $p_A = 0.005, 0.01, 0.015$ and $0.02$. The resulting plot is Fig. 4.5. As can be noticed from the plot, the wave vector $q_0$ which minimizes the inverse of structure function first increases with $\phi_A$ then decreases to zero and maintains the zero value at large $\phi_A$ values. Fig. 4.5 also illustrates that for the same $\phi_A$, the non-zero value of $q_0$ increases as the charge fraction increases. This indicates that the microphase separated structure will exhibit smaller period as the charge fraction increases. This can be understood as microphase separated structure with smaller period can have counterions occupy the space more homogeneously and gain larger entropy.

Another feature that can be noticed from Fig. 4.5 is that the values of $\phi_A^0$ are the same for the four different charge fraction values, which indicates that this $\phi_A^0$ value does not depend on $p_A$ but depends on the value of $\tau$ as can be seen from Fig. 4.3. By examining the inverse of the structure function, a general expression for this $\phi_A^0$ value can be obtained after long calculation,

$$\phi_A^0 = \frac{18}{18+\tau}. \tag{4.5}$$

In the above example with $\tau = 6$, the $q_0$ values all go to zero at $\phi_A = 0.75$ as shown in Fig. 4.5. The previous figure, Fig. 4.3, also illustrates that the $\phi_A^0$ value increases as the $\tau$ value decreases. It is worth noting that the above expression is

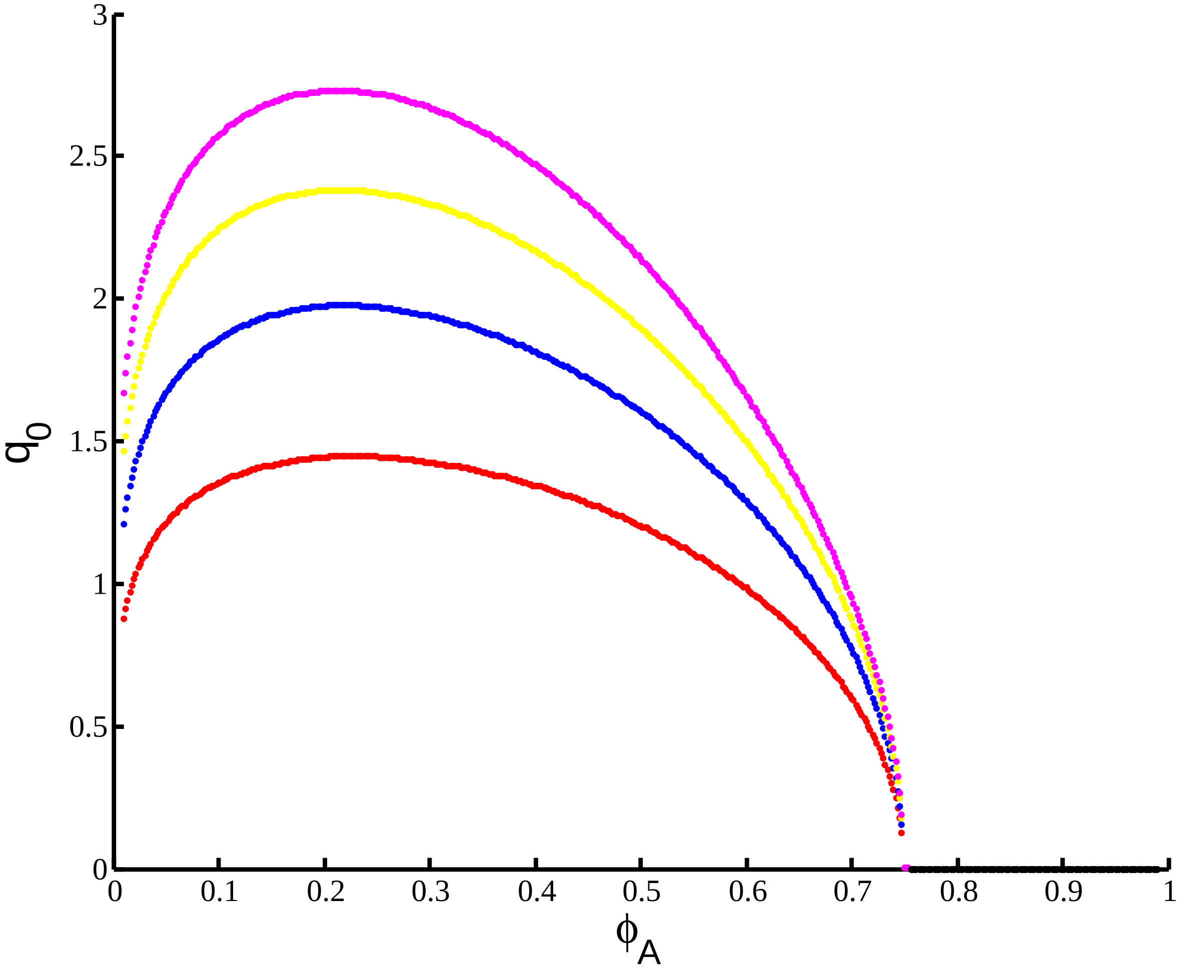

Figure 4.5: Plot showing the critical wave number $q_0$ as a function of the polyelectrolyte concentration $\phi_A$ for A-polyelectrolyte/C-homopolymer blends at different $p_A$ values. The red, blue, yellow and purple dotted curves are for non-zero values of $q_0$ when $p_A = 0.005, 0.01, 0.015$, and $0.02$, respectively. The $q_0$ values go to zero at large values of $\phi_A$, which is represented by the black dotted line.

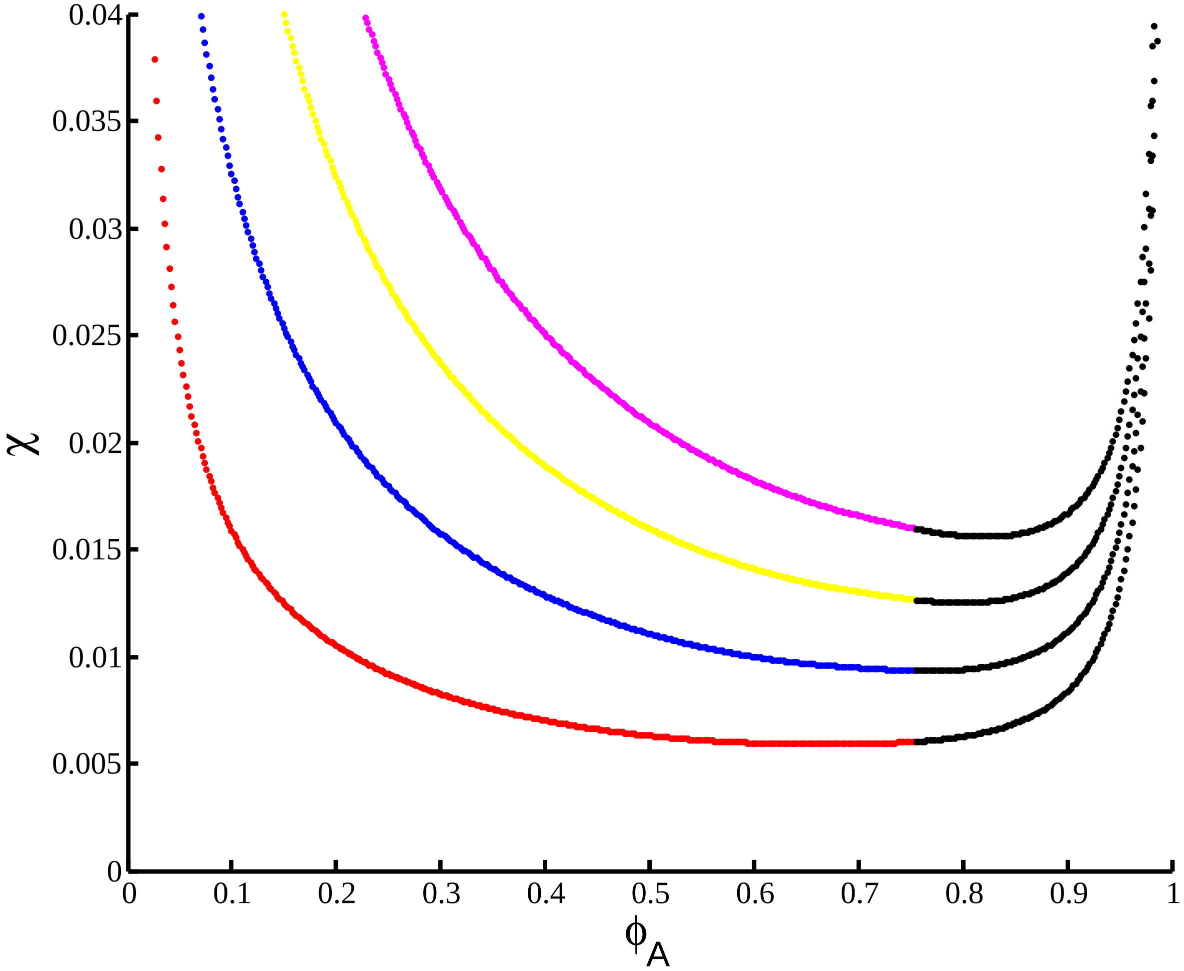

Figure 4.6: Spinodal lines for A-polyelectrolyte/C-homopolymer blends calculated at four different values of $p_A$, with $p_A = 0.005, 0.01, 0.015$ and $0.02$ from bottom to top, respectively. The colored lines represent microphase separation transitions and the black lines represent macrophase separation transitions.

obtained under the condition that the polyelectrolyte chain and homopolymer chain have the same length.

The corresponding spinodals for the above system are shown in Fig. 4.6 for the same set of $p_A$ values as in Fig. 4.5. The colored curves are the microphase separation transitions and the black dotted lines are the macrophase separation transitions. As can be noted from the plot, when the charge fraction increases, the homogeneous phase region increases as well. This can be understood from the entropic point of view. As the charge fraction increases, the number of counterions in the system increases as well. The entropic effect of the counterions thus increases, leading to a larger homogeneous phase region.

## 4.2 Polyelectrolytes in Poor Solvents

As a second example, we consider the mixture of weakly charged polyelectrolytes A and low molecular solvents S. This can be realized by setting the degree of polymerization of the neutral homopolymer to be $Z_C = 1$, and the Debye function to be $g([R_g^C \mathbf{k}]^2) = 1$. The RPA scattering function in this system is given by

$$\frac{1}{S_{AA}(\mathbf{k})} = \frac{1}{\bar{\phi}_A Z_A}[\frac{1}{g([R_g^A \mathbf{k}]^2)} + \frac{C_A}{[1+(\lambda \mathbf{k})^2]}] + \frac{1}{(1-\bar{\phi}_A)} - 2\chi_{AC}. \tag{4.6}$$

We set the degree of polymerization of the polyelectrolytes to be $Z_A = 1000$. Typical plots of the inverse of the scattering function $S_{AA}^{-1}(\mathbf{k})$ are shown in Fig. 4.7 and Fig. 4.8. In both plots, the charge fraction is set to be $p_A = 0.01$ and the dimensionless parameter $\tau$ is set to be $\tau = 30$. In Fig. 4.7, the results are shown for this solution system with polyelectrolyte concentration $\phi_A = 0.8$, and different $\chi$

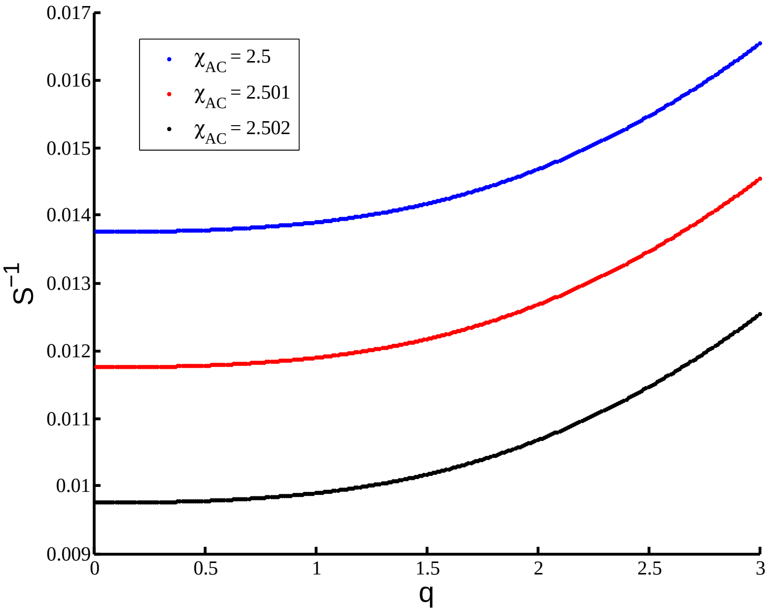

Figure 4.7: Plot showing the inverse of the scattering function as a function of the wave vector for polyelectrolyte solutions at three different $\chi$ values when polyelectrolyte conentration $\phi_A = 0.8$

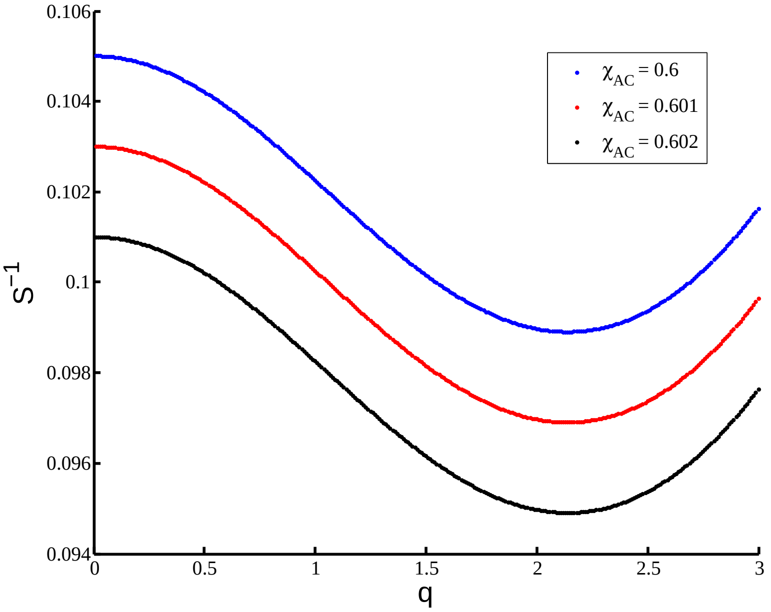

Figure 4.8: Plot showing the inverse of the scattering function as a function of the wave vector for polyelectrolyte solutions at three different $\chi$ values when polyelectrolyte concentration $\phi_A = 0.2$

values. It is noticed that with these parameter values, the inverse of the scattering function exhibits a minimum at $q_0 = 0$. The minimum value approaches zero when $\chi$ increases. When $S_{AA}^{-1}(\mathbf{k})$ becomes negative, any small density fluctuations with $q_0 = 0$ decrease the free energy. This corresponds to a macrophase separation of the system.

In Fig. 4.8, the results are shown for this solution system with polyelectrolyte concentration $\phi_A = 0.2$, and different $\chi$ values. Other parameters are set as the same as used in Fig. 4.7. Fig. 4.8 illustrates that the inverse of the scattering function exhibits a minimum at $q_0 > 0$. As $\chi$ increases, the $S_{AA}^{-1}(\mathbf{k})$ changes from positive to negative. The Fourier mode with nonzero wave number $q_0$ becomes unstable, leading to the formation of ordered structure with length scale of $(q_0/2\pi)^{-1}$.

In Fig. 4.9, we set the charge fraction to be $p_A = 0.01$ and plot the critical value $q_0$ as a function of the polyelectrolyte concentration $\phi_A$ at three different $\tau$ values, $\tau = 60, 50$, and 40. As can be noticed from the plot, as the $\phi_A$ value increases, the value of $q_0$ first increases from zero then decreases to zero and maintains the zero value at large $\phi_A$ values. This indicates that at small polyelectrolyte concentrations, the homogeneous phase is unstable with respect to the microphase separation when $\chi$ increases, and at large polyelectrolyte concentrations, the homogeneous phase is unstable with respect to the macrophase separation when $\chi$ increases. This is again due to the entropic reason. Although the system favors to phase separate at large $\chi$ to reduce the A-C contact, the macrophase separation is unstable at small polyelectrolyte concentrations as this will reduce the entropy of counterions significantly. Another feature that can be noticed from the plot is that the $\phi_A^0$ value at which $q_0$ becomes zero increases as the value of $\tau$ decreases.

The spinodals for the above system are shown in Fig. 4.10 for the same set

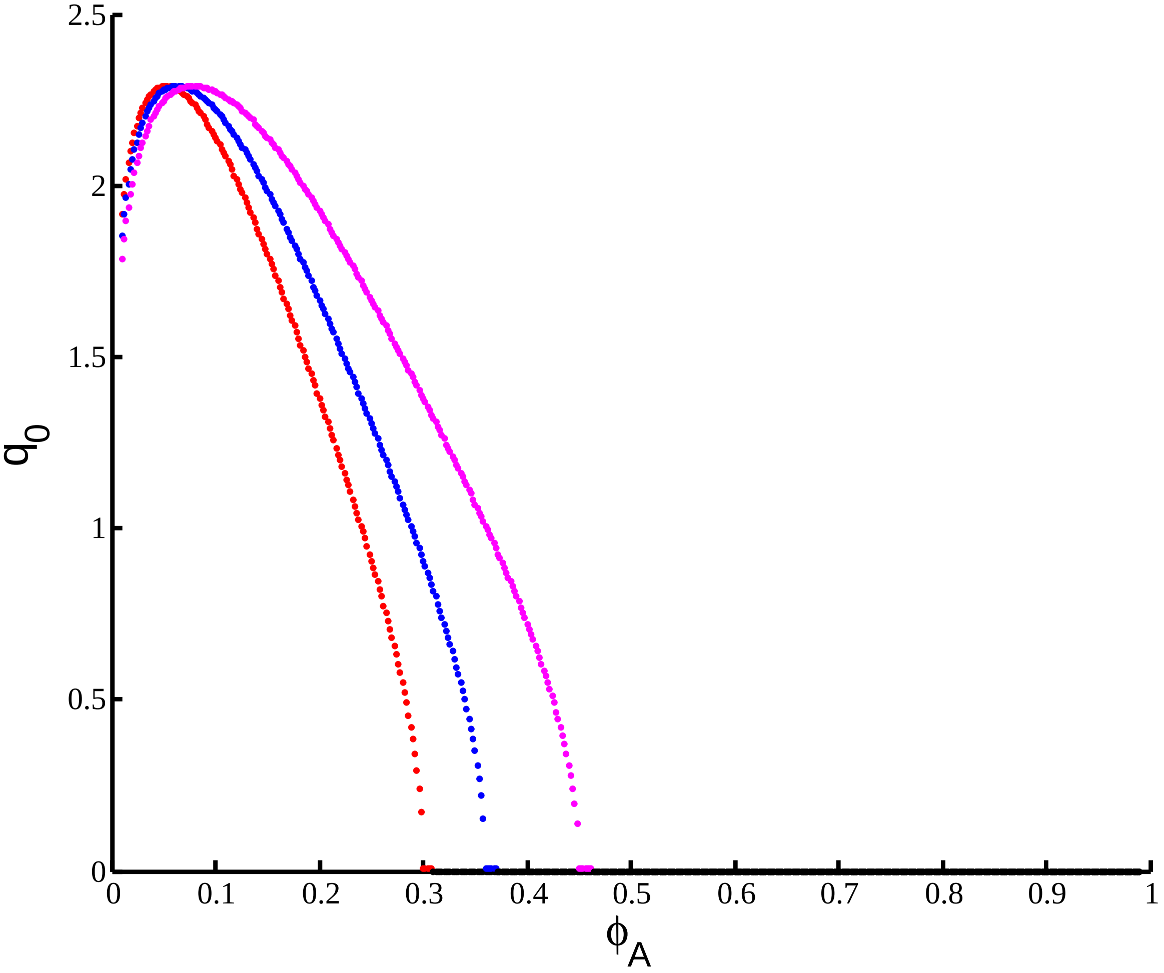

Figure 4.9: Plot showing the value of $q_0$ as a function of the polyelecltrolyte concentration $\phi_A$ for polyelectrolyte solutions at different $\tau$ values. The red, blue, and purple dotted curves are for non-zero values of $q_0$ when $\tau = 60, 50$, and 40, respectively. The values of $q_0$ go to zero at large values of $\phi_A$, which is represented by the black dotted line.

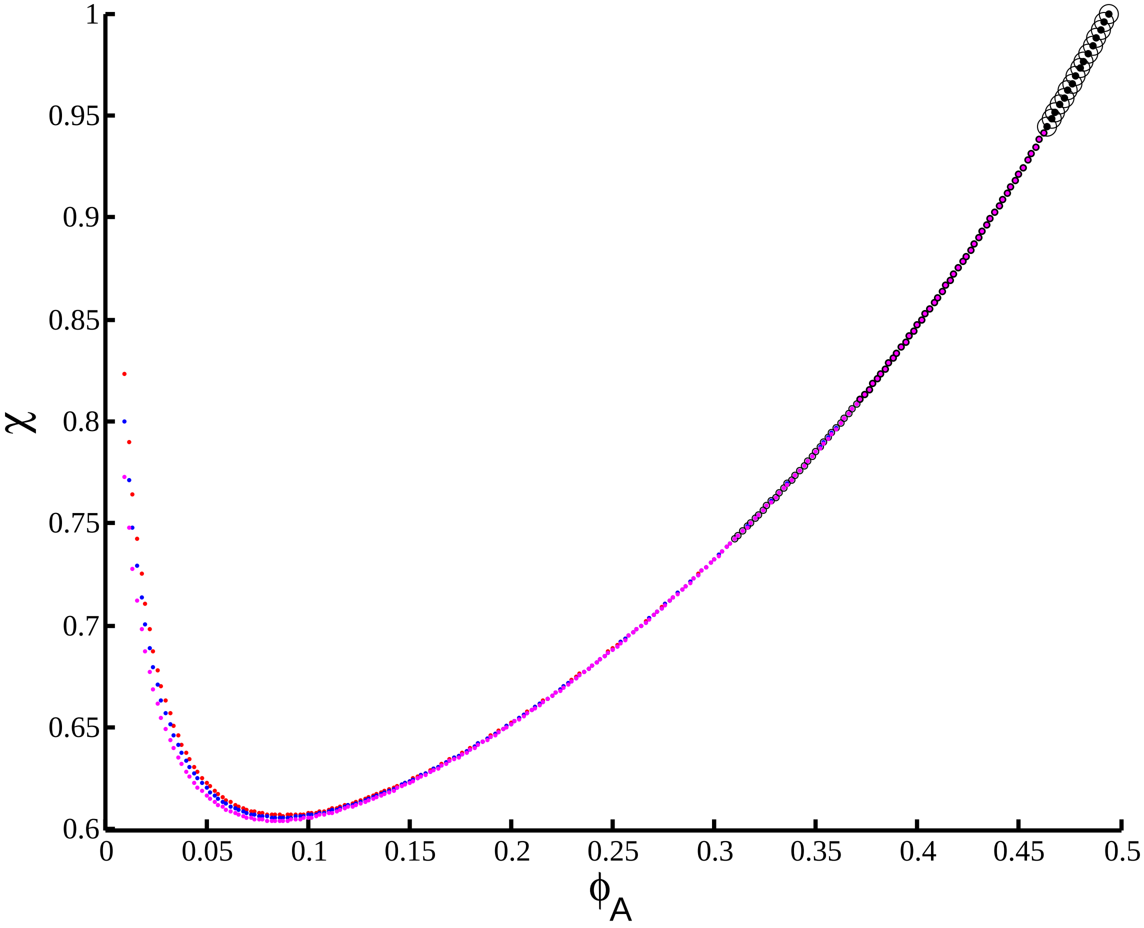

Figure 4.10: Spinodal lines for polyelectrolyte solutions calculated at three different values of $\tau$. The small black empty dotted line is for the macrophase separation transition at $\tau = 60$. The solid black dotted line is for the macrophase separation transition at $\tau = 50$. The large empty dotted line is for the macrophase separation transition at $\tau = 40$. The thin red, blue and purple lines (top to bottom) are microphase separation boundaries for $\tau = 60, 50$, and 40, respectively.

of $\tau$ values as in Fig. 4.9. The colored curves denote the microphase separation transitions, while the black lines are macrophase separation transitions. As can be noticed from the plot, the microphase separated region increases as the value of $\tau$ decreases. It indicates that smaller Bjerrum length of the system can stabilize the microphase separated state over the the macrophase separated state. This result is consistent with the work of Nykova et al. [52]. The difference is that the microphase separated region obtained in this work is much larger than theirs at the same value of $\tau$.

Fig. 4.10 also illustrates that the homogeneous phase regions are almost the same for these three different $\tau$ values. This is because in the solution system, the number of solvent molecules is much larger compared with the number of the counterions, thus the homogenous phase is mainly due to the entropy of the solvent molecules. Changing the parameter of the electrostatic interaction has neglectable effect on the homogenous phase region.

The effect of charge fraction $p_A$ on the value of $q_0$ as a function of $\phi_A$ is also interesting. We set $\tau = 40$ and consider four different values of $p_A$, $p_A = 0.005, 0.01, 0.015$, and 0.02. The results are shown in Fig. 4.11. As can be noticed from the plot, the critical wave vector $q_0$ which minimize the inverse of the structure function first increases with $\phi_A$ then decreases to zero and maintains the zero value at large $\phi_A$ values. At the same polyelectrolyte concentration, the non-zero value of $q_0$ increases as the charge fraction increases. This can be explained as systems with larger charge fractions prefer orderd structure with smaller period so that the counterions can occupy the system more homogeneously.

Fig. 4.11 also illustrates that the value of $\phi_A^0$ are the same for the four different

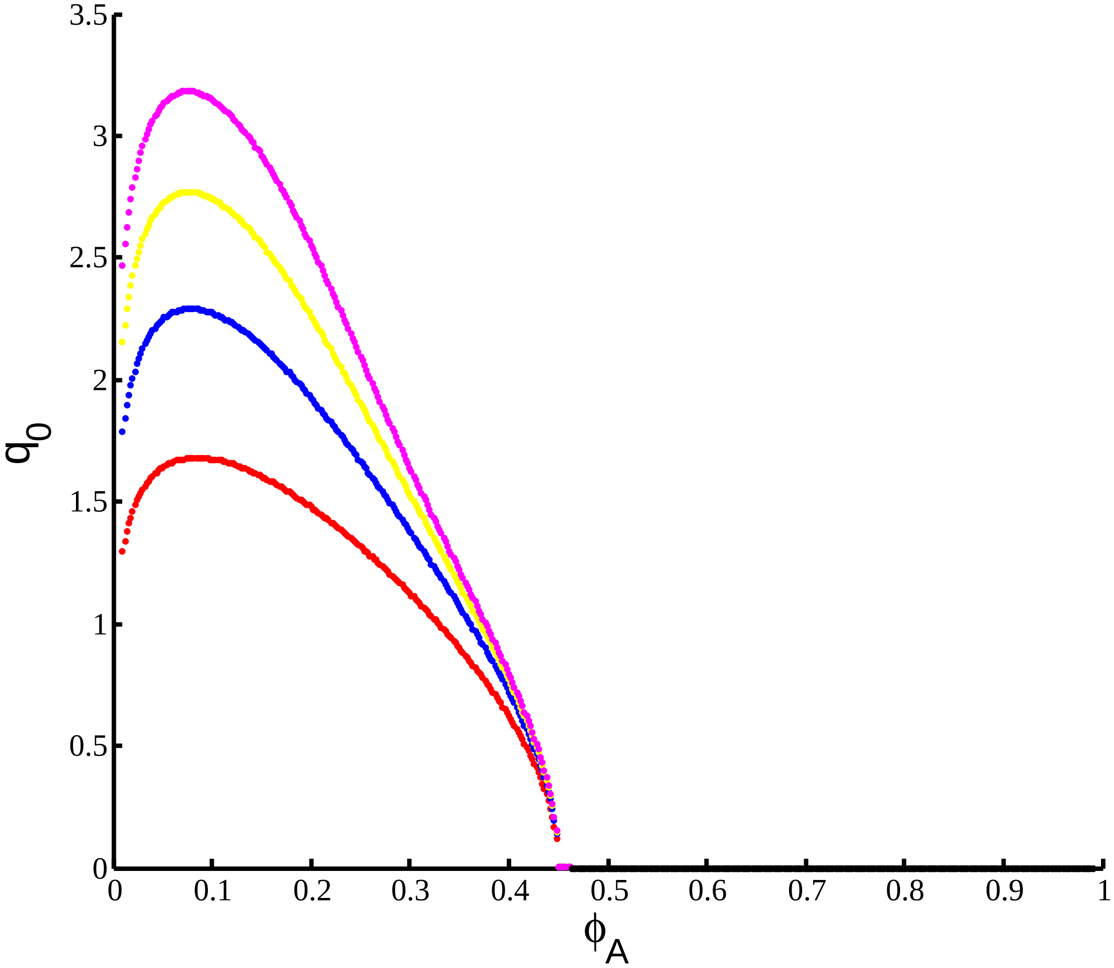

Figure 4.11: Plot showing the value of $q_0$ as a function of the polyelectrolyte concentration $\phi_A$ for polyelectrolyte solutions at different $p_A$ values. The red, blue, yellow and purple dotted curves are for non-zero values of $q_0$ when $p_A = 0.005, 0.01, 0.015,$ and 0.02, respectively. The $q_0$ values go to zero at large values of $\phi_A$, which is represented by the black dotted line.

charge fraction values, which indicates that this $\phi_A^0$ value does not depend on $p_A$ but depends on the value of $\tau$ as can be seen from Fig. 4.9. By examing the inverse of the structure function for this solvent system, a general expression for this $\phi_A^0$ value can be obtained,

$$\phi_A^0 = \frac{18}{\tau}. \tag{4.7}$$

In our example with $\tau = 40$, the $q_0$ values go to zero at $\phi_A = 0.45$ as shown in Fig. 4.11. It can also be noticed from Fig. 4.9 that the $\phi_A^0$ value increases as the $\tau$ value decreases. When $\tau \rightarrow 18$, $\phi_A^0 \rightarrow 1$, which indicates that the macrophase separation transition disappears. The system only exhibits microphase separation transition when $\tau \leqslant 18$. This is in contrast to the blend system where there is always macrophase separation transition at small $\tau$ values. This difference is due to the large entropy of the solvent molecules in the solution system. The macrophase separation transition is less prefered in the solution system than in the blend system where the translational entropy of the homopolymer is small. The result here is different from those of Nyrkova et al. [52]. Their calculation shows macrophase separated region for the solution system even when $\tau$ is as small as 1.

The corresponding spinodals for the above system are shown in Fig. 4.12 for the same set of $p_A$ values as in Fig. 4.11. The colored curves are the microphase separation transitions and the black lines are the macrophase separation transitions. As can be noticed form the plot, when the charge fraction increases, the homogeneous phase region increases as well. This is because as the charge fraction increases, the number of counterions in the system increases as well. The entropic effect of the counterions increases, leading to a larger homogeneous phase region.

By comparing the phase diagrams of the blend system and the solution system,

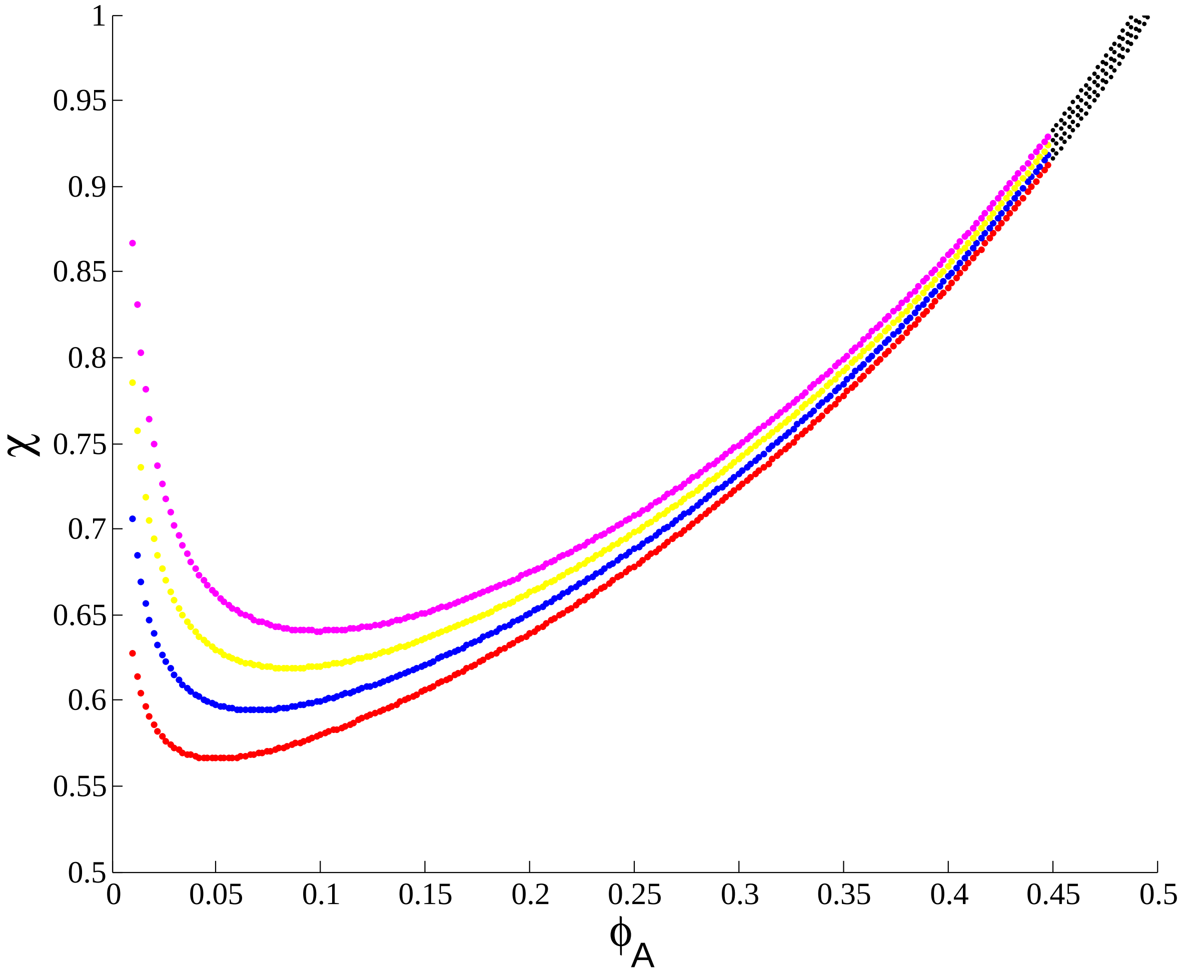

Figure 4.12: Spinodal lines for polyelectrolyte solutions calculated at $p_A = 0.005, 0.01, 0.015$ and $0.02$ from bottom to top, respectively. the colored lines represent microphase separation transitions and the black lines represent macrophase separation transitions

it can be seen that these two systems exhibit similar phase behavior. However, the influence of the charge fraction in the solution system is less pronounced than in the blend system. This is because in the solution system the entropy effect is mainly contributed by the solvent molecules. The number of counterions is much less than the number of solvent molecuels in this system and increase the number of counterions will only change the entropic effect slightly.

Another difference can be noticed from the the phase diagrams of the two systems is that, for the solution system, the $\chi$ value leads to phase separation is much larger than the blend system. This indicates that the solution system favours homogeneous phase more than the blend system. Only at very large $\chi$ values, the solution system undergoes phase separation. This is mainly due to the entropic effect of the solvent molecules. The entropy decreases more significantly in the solution system than in the blend system when the system transits from the homogeneous phase to phase separated state.

By comparing the phase diagram of the two systems, it can also be noticed that the value of $\tau$ required to get a macrophase separated state is much larger in the solution system than in the blend system. This indicates that only stable microphase separated state exhibits in the solution system when the Columnbic interaction is weak.

To conclude, random phase approximation has provided a convenient method to calculate the order-disorder transition for various parameter sets because of its mathmetical simplicity. The RPA phase diagrams presented in this chapter is qualitively correct and can be used as a guide for the full self-consistent field calculation. We are also able to predict the length scales of the ordered structures formed near the microphase transition line.

# Chapter 5

# Inhomogeneous Ordered Phases: Numerical SCFT Results

While the RPA calculation gives the instability boundaries of the homogeneous phases, details of the microphase structures can only be obtained by solving the full SCFT. Due to the nonlinear and non-local nature of the SCFT equations, the solutions are quite difficult to obtain. Analytic expression for the partition function and the chain progagators can be obtained by using Leibler's weak segregation theory [49] and Semenov's strong segregation theory [74]. Some discussions regarding these two theories applied in polyelectrolyte systems have been presented by Shi et al. [60]. Although these analytical methods are useful for giving some insights into the phase behavior of these system at extreme condidtions, it is desirable to use a more generalized method to investigate the phase behavior of the system under any segregation. Numerical methods such as real-space method and reciprocal-space method have proven to be powerful tools and capable of giving accurate predictions of the phase behavior of polymer systems.

Within the reciprocal-space method, the spatially varying functions are expanded using basis functions which can be either with specific symmetries or without specific symmetries. Most of the previous calculations assume the symmetry of the ordered phases and the basis functions can be constructed from the given symmetry. The first accurate numerical solutions of ordered phases for diblock copolymer melt were obtained by Matsen and Schick [75] using reciprocal-space method for simple structures. Later development on reciprocal-space method demonstrated that the basis functions can be expanded as generalized Fourier series and new complex structures can be identified [76].

The real-space method has the advantage of conceptually easily understandable, and is straightforward to implement. Technique such as finite difference method are available to solve the self-consistent equations. Numerical techniques have also been developed by Drolet and Fredrickson [77] and Bohbot-Raviv and Wang [78]. A combinatorial screening method which involves a direct implementation of SCFTT in real space in an adaptive arbitray cell has been proposed [77]. Later, a split-step method has also been propesed by Rasmussen et al [79] and the efficiency of the calculations was improved.

For the problem of polyelectrolyte systems, as we are only interested in demonstrating the formation of microphases, so we use the known structures. When the structures are known, it is simpler to use the reciprocal-space method.

In this section, we first discuss the general algorithm to solve the mean-field equations numerically, and then we apply the reciprocal-space method to the system of polyelectrolyte/homopolymer blends. The results are presented in the final subsection.

## 5.1 General Algorithm

In order to calculate the equilibrium structures for the polyelectrolyte system developed in Chapter 2, we have to solve for two sets of unknown fields: the density fields $\phi_j(\mathbf{r})$ and the potential fields $\omega_j(\mathbf{r}), \varphi(\mathbf{r})$. These two sets of fields are closely related and have to be solved self-consistently. The relation between these fields are shown in Fig. 5.1.

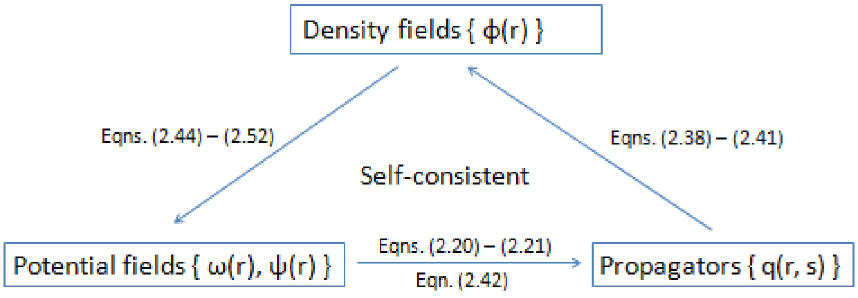

Figure 5.1: A schematic representation of the self-consistent field theory to illustrate the relation between the density fields, the potential fields and the propagators.

The potential fields can be evaluated from the density fields through eqns (2.44) - (2.52). The density fields can be calculated through eqns (2.38) - (2.41) using the propagators. The propagators are determined by solving the modified diffusion equations eqn (2.20) - eqn (2.21) for the polymer chains and eqn (2.42) for the counterions. These equations all depend on the potential fields.

The general procedure to solve this self-consistent problem is by an iteration method. Starting with an initial guess for the potential fields $\omega_j$, we solve for the propagators using eqn (2.20), (2.21) and (2.42). The density fields can then be calculated by solving eqn (2.38) - (2.41). Calculating the new potential fields using eqn (2.44) - (2.52). If the differences between the new and old potential fields are larger than a certain convergence criterion, we repeat these steps again using updated values of potential fields. The iteration stops once the differences between the new and old potential fields are less than the required precession. We can compute the free energy density from eqn (2.54) using the final obtained fields.

## 5.2 Reciprocal-Space Method

We use the polyelectrolytes as the reference and write $Z_A = N$, then the C-homopolymer has degree of polymerization $Z_C = \kappa_C N$. We treat the counterion as a polymer chain with arc length 1. Each polymer has an associated Kuhn length $b_\alpha = \sigma_\alpha b$, where $b$ is a reference Kuhn length and $\alpha = A, C, I$. We know that $\sigma_I = 0$ as counterion has no Kuhn length. We assume for simplicity that the valence number of polymer monomers to be $z_A = 1$, and the valence number of counterions to be $z_I = -1$. In the following expressions we will use the convention that all lengths are scaled by the Gaussian radius of gyration of the polyelectrolytes, $R_g = b\sqrt{N/6}$. The chain arc length is scaled by the degree of polymerization $N$. We redefine the fields by including the factor $N$, $N\omega_\alpha(\mathbf{r}) \to \omega_\alpha(\mathbf{r})$, $N\varphi(\mathbf{r}) \to \varphi(\mathbf{r})$, we also use the redefined

$\phi_I(\mathbf{r}) = \rho_I(\mathbf{r})/\rho_0$. The mean-field equations become

$$\phi_A(\mathbf{r}) = \frac{\bar{\phi}_A}{Q_A}\int_0^1 ds q_A(\mathbf{r},s)q_A(\mathbf{r},1-s), \tag{5.1}$$

$$\phi_C(\mathbf{r}) = \frac{\bar{\phi}_C}{\kappa_C Q_C}\int_0^{\kappa_C} ds q_C(\mathbf{r},s)q_C(\mathbf{r},\kappa_C-s), \tag{5.2}$$

$$\phi_I(\mathbf{r}) = \frac{\bar{\phi}_I}{Q_I} q_I(r,\frac{1}{N}), \tag{5.3}$$

$$\omega_A(\mathbf{r}) = \chi_{AC} N\phi_C(\mathbf{r}) + \eta(\mathbf{r}) + p_A\varphi(\mathbf{r}), \tag{5.4}$$

$$\omega_C(\mathbf{r}) = \chi_{AC} N\phi_A(\mathbf{r}) + \eta(\mathbf{r}), \tag{5.5}$$

$$\omega_I(\mathbf{r}) = v_I\eta(\mathbf{r}) - \varphi(\mathbf{r}), \tag{5.6}$$

$$\nabla^2\varphi(\mathbf{r}) = -\frac{N}{\kappa^2}[p_A\phi_A(\mathbf{r}) - \phi_I(\mathbf{r})], \tag{5.7}$$

$$1 = \phi_A(\mathbf{r}) + \phi_C(\mathbf{r}) + v_I\phi_I(\mathbf{r}). \tag{5.8}$$

where $Q_\alpha$ are single-chain partition functions,

$$Q_A = \frac{1}{V}\int d\mathbf{r} q_A(\mathbf{r},1), \tag{5.9}$$

$$Q_C = \frac{1}{V}\int d\mathbf{r} q_C(\mathbf{r},\kappa_C), \tag{5.10}$$

$$Q_I = \frac{1}{V}\int d\mathbf{r} q_I(\mathbf{r},\frac{1}{N}). \tag{5.11}$$

$$\tag{5.12}$$

The end-integrated propagators are solutions of the modified diffusion equations in the mean fields $\omega_\alpha(\mathbf{r})$,

$$\frac{\partial}{\partial s}q_\alpha(\mathbf{r},s) = \sigma_\alpha^2\nabla^2 q_\alpha(\mathbf{r},s) - \omega_\alpha(\mathbf{r})q_\alpha(\mathbf{r},s), \tag{5.13}$$

with the initial condition $q_\alpha(\mathbf{r}, 0) = 1$. The free energy density is given by

$$\begin{aligned}
\frac{NF}{\rho_0 k_B TV} &= (\bar{\phi}_A \mathrm{ln} \bar{\phi}_A + \frac{1}{\kappa_C} \bar{\phi}_C \mathrm{ln} \bar{\phi}_C + N \bar{\phi}_I \mathrm{ln} \bar{\phi}_I) \\
&+ \frac{1}{V} \int d\mathbf{r} \{ \chi_{AC} N \phi_A(\mathbf{r}) \phi_C(\mathbf{r}) + \sum_\alpha \omega_\alpha(\mathbf{r}) \phi_\alpha(\mathbf{r}) \} \\
&- \frac{1}{V} \int d\mathbf{r} \{ \phi_A(\mathbf{r}) \mathrm{ln} Q_A + \frac{1}{\kappa_C} \phi_C(\mathbf{r}) \mathrm{ln} Q_C + N \phi_I(\mathbf{r}) \mathrm{ln} Q_I \} \\
&+ \frac{1}{V} \int d\mathbf{r} \{ [p_A \phi_A(\mathbf{r}) - \phi_I(\mathbf{r})] \varphi(\mathbf{r}) - \frac{\kappa^2}{2N} |\nabla \varphi(\mathbf{r})|^2 \} \\
&+ \frac{1}{V} \int d\mathbf{r} \eta(\mathbf{r}) (\phi_A(\mathbf{r}) + \phi_C(\mathbf{r}) + v_I \phi_I(\mathbf{r}) - 1). \qquad (5.14)
\end{aligned}$$

The key aspect of the reciprocal space method is that the functions of interest within the self-consistent mean-field theory are all periodic functions. For an ordered phase, the reciprocal lattice vectors are completely specified by the symmetry of that structure. For a given ordered phase, the reciprocal lattice vectors $\mathbf{G}$ can be determined. These reciprocal lattice vectors are ordered according to their magnitudes $|\mathbf{G}|$. The plane waves $e^{i\mathbf{G}\cdot\mathbf{r}}$ corresponding to these reciprocal lattice vectors are used as basis functions. Any function $F(\mathbf{r})$ can be expressed using these basis functions,

$$F(\mathbf{r}) = \sum_{\mathbf{G}} F(\mathbf{G}) e^{i\mathbf{G}\cdot\mathbf{r}}. \qquad (5.15)$$

In Fourier space, the modified diffusion equations for the end-integrated propagators which were previously second order differential equation become first order,

$$\frac{\partial}{\partial t} q_\alpha(\mathbf{G}, t) = -\sum_{\mathbf{G}'} H_\alpha(\mathbf{G}, \mathbf{G}') q_\alpha(\mathbf{G}', t), \qquad (5.16)$$

where the Hamiltonians $H_\alpha(\mathbf{G},\mathbf{G}')$ are defined by

$$H_\alpha(\mathbf{G},\mathbf{G}') \equiv \sigma_\alpha^2 G^2 \delta_{\mathbf{G},\mathbf{G}'} + \omega_\alpha(\mathbf{G}-\mathbf{G}'). \tag{5.17}$$

Furthermore, for ordered strucrue, The basis functions can be grouped into stars. A set of new basis functions can be constructed,

$$f_n(\mathbf{r}) = \frac{1}{\sqrt{N_n}} \sum_{i\in n} S_i^n e^{i\mathbf{G}_i^n\cdot\mathbf{r}}. \tag{5.18}$$

where the wave vectors $\mathbf{G}_i^n$ are related by the point group operation within one star, and satisfy the relation $|\mathbf{G}_i^n|^2 = \lambda_n$. The factors $S_i^n$ assume the values ±1 determined by the symmetry of the structure and $N_n$ is the number of reciprocal lattice vectors within the $n$-th star.

A periodic function can then be expanded in terms of the new set of basis functions $f_n(\mathbf{r})$,

$$F(\mathbf{r}) = \sum_n F_n f_n(\mathbf{r}), \tag{5.19}$$

$$F_n = \frac{1}{V}\int d\mathbf{r} F(\mathbf{r}) f_n(\mathbf{r}). \tag{5.20}$$

The latter equation is the reverse transformation.

By expanding all the functions in terms of $f_n(\mathbf{r})$, the mean-field equations can be cast in terms of the expansion coefficients (see Appendix D for details). In particular, the chain-conformation Hamiltonians become symmetric matrices with matrix elements

$$H_{nm}^\alpha = \sigma_\alpha^2 \lambda_n \delta_{nm} + \sum_l \Gamma_{nml}\omega_l^\alpha, \tag{5.21}$$

where the coefficients $\Gamma_{nml}$ are defined by

$$\begin{aligned}\Gamma_{nml} &= \frac{1}{V}\int d\mathbf{r} f_n(\mathbf{r}) f_m(\mathbf{r}) f_l(\mathbf{r}) \\ &= \frac{1}{\sqrt{N_n N_m N_l}} \sum_{i\in n}\sum_{j\in m}\sum_{k\in l} S_i^n S_j^m S_k^l \delta_{\mathbf{G}_i^n+\mathbf{G}_j^m+\mathbf{G}_k^l,\mathbf{0}}. \end{aligned} \tag{5.22}$$

The eigenvalues and eigenfunctions of the matrices $H^\alpha_{nm}$ are solved from the equations

$$\sum_m H^\alpha_{nm}\psi^\alpha_{mi} = \varepsilon^\alpha_i \psi^\alpha_{ni}, \tag{5.23}$$

where $i$ labels the eigenvalues and eigenfunctions.

The single-chain partition functions are given by

$$Q_\alpha = \sum_i v^\alpha_i \psi^\alpha_{1i}\psi^\alpha_{1i}. \tag{5.24}$$

The density coefficients are written as

$$\phi^A_n = \frac{\bar{\phi}_A}{Q_A}\sum_{i,j} g^A_{ij} S^A_{n,ij}\psi^A_{1j}, \tag{5.25}$$

$$\phi^C_n = \frac{\bar{\phi}_C}{Q_C}\sum_{i,j} g^C_{ij} S^C_{n,ij}\psi^C_{1j}, \tag{5.26}$$

$$\phi^I_n = \frac{\bar{\phi}_I}{Q_I}\sum_{i} v^I_i \psi^I_{1i}\psi^I_{ni}. \tag{5.27}$$

where $v^\alpha_i, g^A_{ij}, g^C_{ij}, S^A_{n,ij}, S^C_{n,ij}$ are quantities constructed from the eigenvalues and eigenfunctions, and are given in Appendix D.

The coefficients of the fields are given by

$$\begin{aligned}
\varphi_n &= \frac{N}{\lambda_n \kappa^2}[p_A \phi_n^A - \phi_n^I], && (5.28)\\
\omega_n^A &= \chi_{AC} N \phi_n^C + p_A \varphi_n + \eta_n, && (5.29)\\
\omega_n^c &= \chi_{AC} N \phi_n^A + \eta_n, && (5.30)\\
\omega_n^I &= -\varphi_n + v_I \eta_n, && (5.31)\\
& && (5.32)
\end{aligned}$$

where the coefficients $\eta_n$ are to be adjusted so that the system satisfies the incompressibility condition

$$\phi_n^A + \phi_n^C + v_I \phi_n^I = \delta_{n,1}. \qquad (5.33)$$

The free energy density is

$$\begin{aligned}
f \;=\; & \sum_n \chi_{AC} N \phi_n^A \phi_n^C - \sum_n \sum_\alpha \omega_n^\alpha \phi_n^\alpha \\
& -\bar{\phi}_A \ln Q_A - \frac{\bar{\phi}_C}{\kappa_C} \ln Q_C - N\bar{\phi}_I \ln Q_I \\
& +\bar{\phi}_A \ln\bar{\phi}_A + \frac{\bar{\phi}_C}{\kappa_C} \ln\bar{\phi}_C + N\bar{\phi}_I \ln\bar{\phi}_I \\
& +\sum_n (p_A \phi_n^A - \phi_n^I)\varphi_n + \sum_n \frac{\kappa^2 \lambda_n}{2N} \varphi_n \varphi_n. \qquad (5.34)
\end{aligned}$$

The free energy density of the homogeneous phase is

$$f_H = \chi_{AC} N \bar{\phi}_A \bar{\phi}_C + \bar{\phi}_A \ln\bar{\phi}_A + \frac{\bar{\phi}_C}{\kappa_C} \ln\bar{\phi}_C + N\bar{\phi}_I \ln\bar{\phi}_I. \qquad (5.35)$$

At certain point of the phase diagram parameter space $(\chi_{AC}, \bar{\phi}_A, N, p_A, \kappa_C, \tau, v_I)$, the other parameters are $\kappa^2 = 6/\tau N$, $\bar{\phi}_C = 1 - \bar{\phi}_A - p_A v_I \bar{\phi}_A$, $\bar{\phi}_I = p_A \bar{\phi}_A$. For a given phase with a specified space group, we can determine the reciprocal lattice vector $G_i^n$, the coefficients $S_i^n$, and calculate the coefficients $\Gamma_{nml}$ and $\lambda_n$. We then choose a lattice periodicity $D$, and make an initial guess for the fields $\omega_n^\alpha$. The eigenvalue problem can be solved, $Q_\alpha$ and $\phi_n^\alpha$ can then be calculated. Next, we calculate the electrostatic potential $\varphi_n$, Lagrangian multiplier $\eta_n$, and the changes of the fields $\delta\omega_n^\alpha$. If these changes are larger than a certain convergence criterion, we calcualte the new $\omega_n^\alpha$, and using the new values to do the calculations again. The iteration continuous until the changes are smaller than the convergence criterion. The free energy density can be calculated when the iteration ends. The procedure is then repeated for a different lattice periodicity $D$, until the lowest free energy density is obtained. The phase diagram is obtained when we repeat the above procedure for all possible crystal symmetries. The equilibrium structure is the one gives the minimum free energy among all the candidates for the crystal symmetries.

Before we getting into detailed examples, it is worth noting that the accuracy of the reciprocal-space method depends on the number of basis functions used. The more basis function we choose, the higher the accuracy. However, it will take longer time to converge.

## 5.3 Results and Disscusion

Using the reciprocal-space method presented above, the self-consistent field theory developed in Chapter 2 will be investigated. Here, we focus on the classical phases: lamellae (LAM), cylinder on a hexagonal lattice (HEX), and sephere on a body-centered cubic lattice (BCC). We use 20 basis functions for the LAM structure, 30 basis functions for the HEX structure, and 40 basis functions for the BCC structure. We construct a two dimensional phase diagram with the abscissa being the polyelectrolyte volume fraction $\phi_A$ and the ordinate being the Flory-Huggins interaction parameter $\chi_{AC}$, which is scaled by the inverse of the degree of polymerization of the polyelectrolyte $N$. For each set of parameters $(\phi_A, \chi_{AC})$, we calculate the free energy for different morphologies. The phase diagram can be constructed by comparing of the free energies of different phases quantitatively. In the following calcuation, we assume for simplicity that the polyelectrolytes and the homopolymers have the same Kuhn length.

We first consider a system with $N = 1000$, and the charge fraction $p_A = 0.01$. The neutral C-homopolymers have the same length as the A-polyelectrolyte chains, which corresponds to $\kappa_C = 1$. We set the dimentionless parameter characterizing the electrostatic interaction to be $\tau = 3$. The phase diagram is shown in Fig 5.2. The RPA results are shown as well using the colored lines. As can be seen from the phase diagram, increase in $\chi_{AC}$ drives the system from the disordered phase into different ordered phases at small $\phi_A$ values. While at large $\phi_A$ values, the system is driven from the disordered phase into a 2-phase region, where the 2-phase region corresponds to the coexistence of lamellar and homogeneous phases, and is obtained by drawing the common tangent of the free energy curves.

As can be noticed from Fig. 5.2, the results from the SCFT and the RPA agree qualitatively. The phase behavior within the microphase separated region predicted by the RPA can be obtained by the SCFT. It shows large LAM phase region at intermediate $\phi_A$ values. The HEX phase regions and the BCC phase regions appear on both sides of the LAM phase region. However, the BCC and HEX phase to the

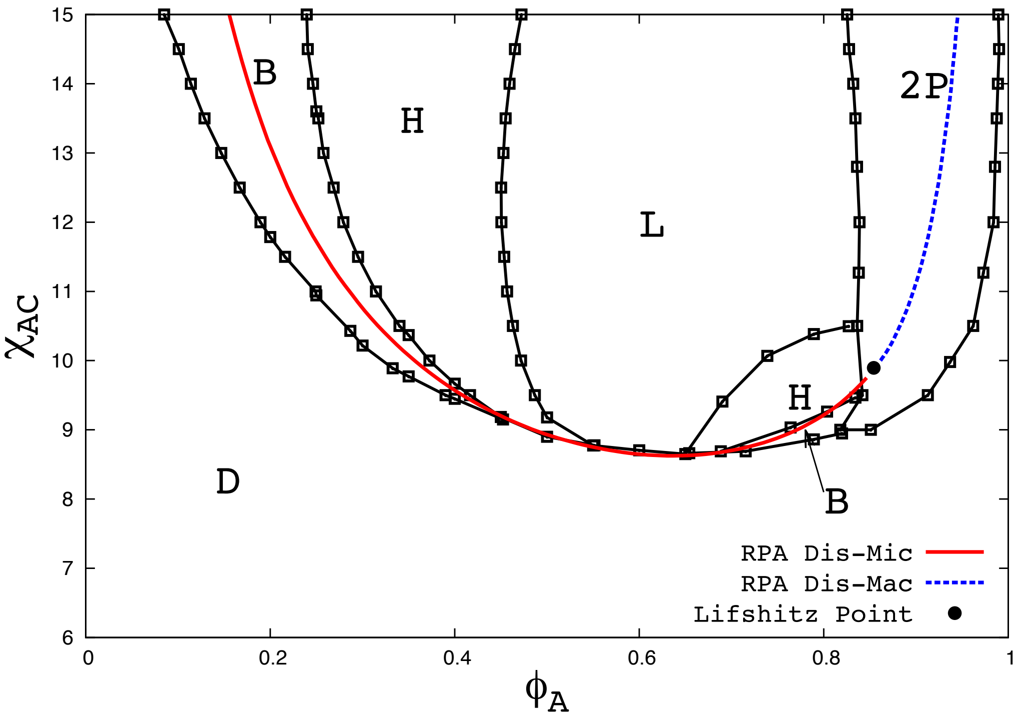

Figure 5.2: Phase diagram for polyelectrolyte/homopolymer blends with $N = 1000, \kappa_C = 1, \tau = 3$, and $p_A = 0.01$. The black lines in the figure denote the phase diagram constructed using the SCFT. The colored lines in the figure denote the phase diagram using the RPA. The symbols for phases are D (disordered/homogeneous), 2P (coexistence of two phases), L (lamellar), H (hexagonal/cylindrical), and B (body-centered cubic).

right of the LAM phase only appear at small region of $\chi_{AC}$ values above the critical point. At large $\chi_{AC}$ values, these phases vanish. We can thus predict that for a small region of $\phi_A$ values, when $\phi_A$ close to 0.75, by increasing the $\chi_{AC}$ values, we should observe, respectively, a homogeneous phase, a BCC phase, a HEX phase and a LAM phase.

The phase diagram can also be used to make qualitative argument when we fix $\chi_{AC}$ value. The phase diagram shows that, when the $\chi_{AC}$ value is in a certain small region above the critical point, by increasing the concentration of polyelectrolyte, the system will show phase transition of homogeneous $\rightarrow BCC_A \rightarrow HEX_A \rightarrow LAM \rightarrow HEX_C \rightarrow BCC_C \rightarrow$ 2-phase region $\rightarrow$ homogeneous, where the subscript A means an A-rich core in a C-rich matrix and vise versa for the subscript C. If the $\chi_{AC}$ value is fixed at another small region above the region we just discussed, the system will not go through the $BCC_C$ phase region when increase $\phi_A$, and at regions with $\chi_{AC}$ values even larger, the system will go directly from the LAM phase to the 2-phase region when increase $\phi_A$.

Fig. 5.3 compares the free energies of various phases as a function of $\chi_{AC}$ for a fixed $\phi_A = 0.5$. This figure illustrates that the free energy of all the phases converge to the free energy of homogenous phase at small $\chi_{AC}$ values. As $\chi_{AC}$ becomes larger, the LAM phase exhibits the lowest free energy. At even larger $\chi_{AC}$ values, the HEX phase exhibits the lowest free energy and becomes the stable state. It also shows that the macroscopically phase-separated state (into two homogeneous phases) never has the lowest free energy compared to the other states.

The period of the LAM phase and the HEX phase as a function of $\chi_{AC}$ are also illustrated in Fig. 5.4. It can be noticed that, for both phases, the period gets larger as

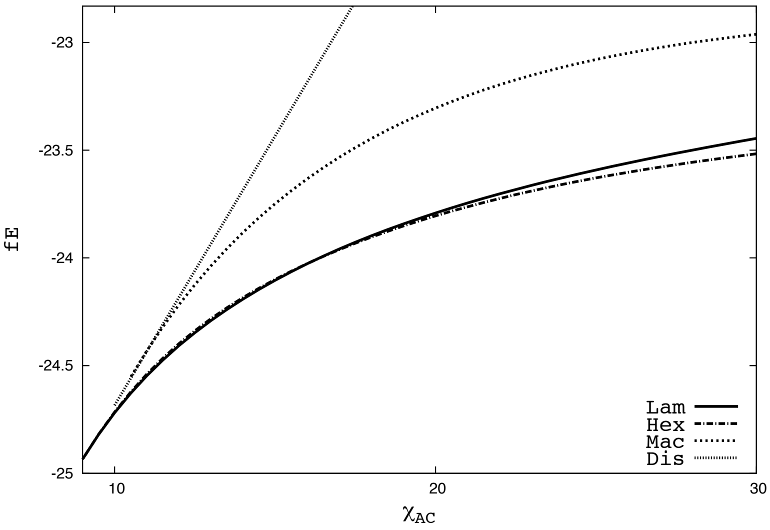

Figure 5.3: The free energy as a function of $\chi_{AC}$ for different phases when $\phi_A = 0.5$.

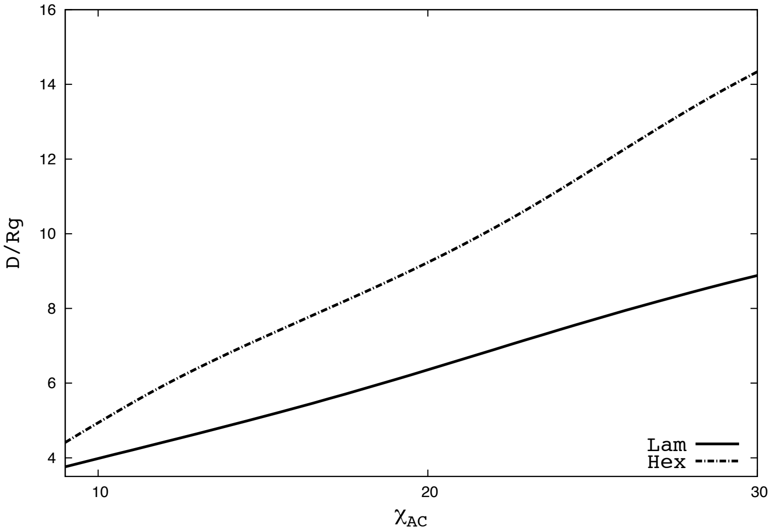

Figure 5.4: The period of lamellar and hexagonal phase as a function of $\chi_{AC}$ when $\phi_A = 0.5$

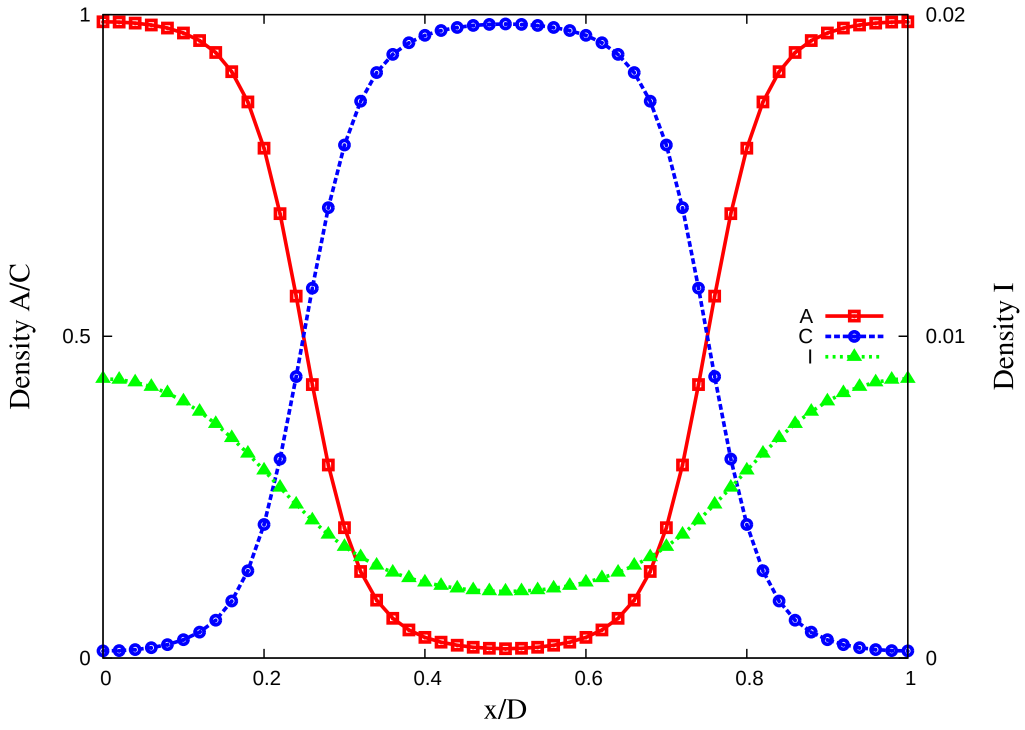

Figure 5.5: The density profiles for the three components in the blend system within one period when $\chi_{AC}N = 15$ and $\phi_A = 0.5$ . The red line is for the A-polyelectrolyte, the blue line is for the C-homopolymer and the green line is for the counterions.

the $\chi_{AC}$ value increases. This can be understood as the repulsive interaction between A-polyelectrolyte and C-homopolymer gets stronger, the system prefers a structure with longer period to reduce the contact between A and C.

To better understand the phase behavior of the system, density profiles for the three components the blend system are plotted for one period of the LAM phase for $\chi_{AC} = 15$ and $\phi_A = 0.5$. The results are shown in Fig. 5.5. The scale for the counterion density is 50 times the scale for the A-polyelectrolyte and C-homopolymer. It is shown that the the maximum and the minimum for the density of the counterions and the polyelectrolytes occur at the same place. This feature illustrates that, due to the Coulumbic interaction, the counterions always follow their co-ions of the polyelectrolytes. There is thus no phase separation between the polyelectrolytes and the counterions.

As a comparison, we also constructed phase diagrams for systems with $\kappa_C = 0.5$ and $\kappa_C = 1.5$. The other parameters are the same as in Fig. 5.2. The results are shown is Fig. 5.6 and Fig. 5.7, respectively. It can be noticed that, as the chain length of the homopolymer is reduced by half, the homogeneous phase becomes larger. When the chain length of the homopolymer is increased by half, the homogenous phase region reduces. These can be understood from the fact that the translational entropy of the C-homopolymer increases as the chain length decreases, making the homogeneous phase more favorable. In terms of the ordered phases, the effect of the change of C-homopolymer length is weak. The only noticeable difference is that the HEX phase and the BCC phase to the right of the LAM phase become larger as the homopolymer length decreases. This fact indicates again that the properties of the polyelectrolyte system is mainly depend on the entropy of the counterions and the

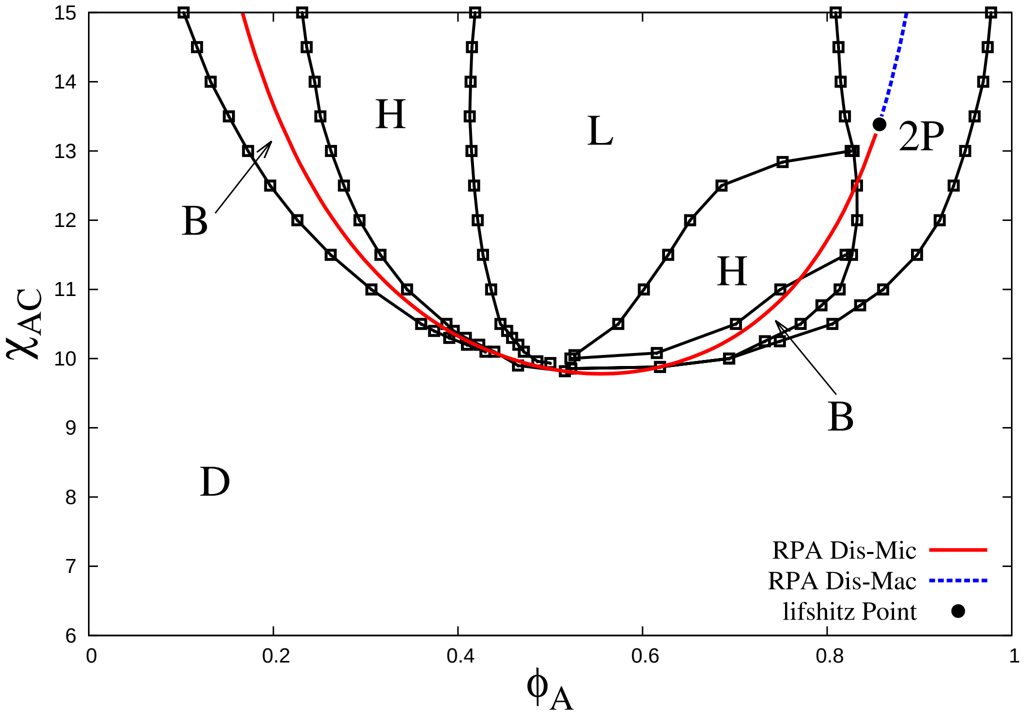

Figure 5.6: Phase diagram for polyelectrolyte/homopolymer blends with $N = 1000, \kappa_C = 0.5, \tau = 3$, and $P_A = 0.01$. The black lines in the figure denote the phase diagram constructed using the SCFT. The colored lines in the figure denote the phase diagram using the RPA. The symbols for phases are D (disordered/homogeneous), 2P (coexistence of two phases), L (lamellar), H (hexagonal/cylindrical), and B (body-centered cubic).

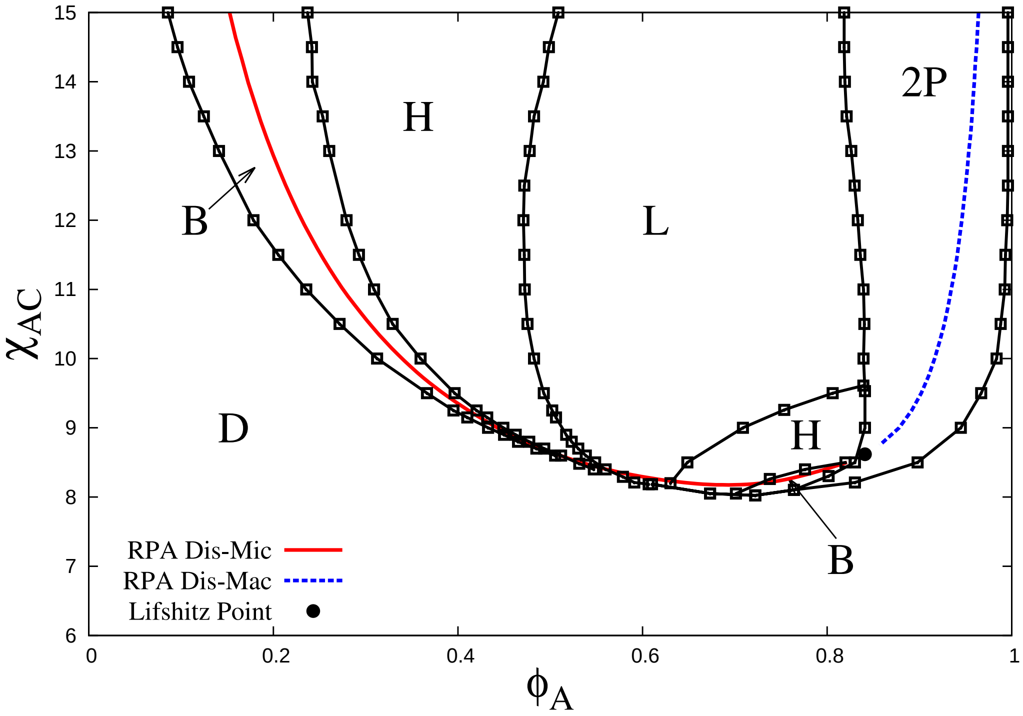

Figure 5.7: Phase diagram for polyelectrolyte/homopolymer blends with $N = 1000, \kappa_C = 1.5, \tau = 3$, and $P_A = 0.01$. The black lines in the figure denote the phase diagram constructed using the SCFT. The colored lines in the figure denote the phase diagram using the RPA. The symbols for phases are D (disordered/homogeneous), 2P (coexistence of two phases), L (lamellar), H (hexagonal/cylindrical), and B (body-centered cubic).

Coulombic interaction. The translational entropy of the chains themselves has rather small effect on the system.

It is also interesting to study the phase diagram in the $p_A - \phi_A$ plane with fixed Flory interaction parameter. We use $\chi_{AC} = 15$ and study the region of $p_A$ from 0.01 to 0.02. The calculated phase diagram is shown in Fig. 5.8. It can be seen that, the phase diagram in the $p_A - \phi_A$ plane is similar to the phase diagram in the $\chi_{AC} - \phi_A$ plane if it is flipped. This feature indicates that the effect of increasing the charge fraction is similar to the effect of decreasing the $\chi_{AC}$ value. They both stabilize the homogeneous phase over the order structures. Although the physical reason is different: increasing the charge fraction makes the entropy increase and decreasing the $\chi_{AC}$ reduces the contact interaction between A and C. It is worth noting that for the parameters we are choosing, there is no microphase separated state with $p_A$ larger than 0.02. This indicates that ordered structures can only occur in a small region of $p_A$ close to zero which might be diffcult to control experimentally.

To conclude, we constructed the phase diagrams for the polyelectrolyte/homopolymer system within the self-consistent field theory. The influence of the polyelectrolyte concentration, the homopolymer chain length, the interaction parameter and the charge fraction on the phase behavior have all been investigated.

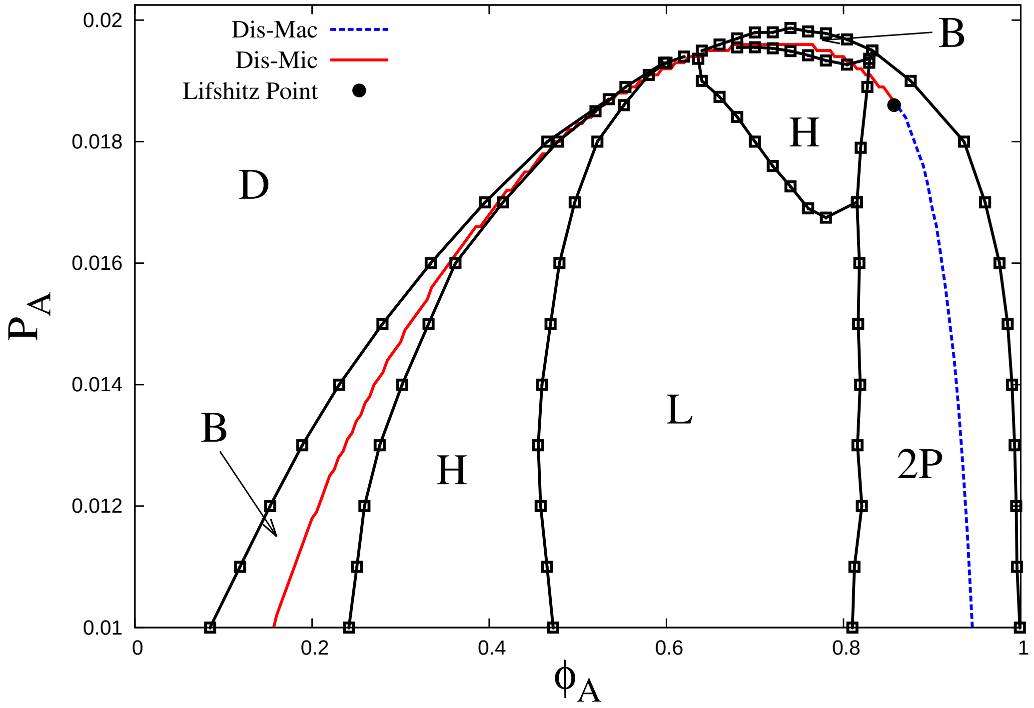

Figure 5.8: Phase diagram for polyelectrolyte/homopolymer blends with $N = 1000, \kappa_C = 1, \tau = 3$, and $\chi_{AC} = 15$. The black lines in the figure denote the phase diagram constructed using the SCFT. The colored lines in the figure denote the phase diagram using the RPA. The symbols for phases are D (disordered/homogeneous), 2P (coexistence of two phases), L (lamellar), H (hexagonal/cylindrical), and B (body-centered cubic).

# Chapter 6

# Summary

This thesis is devoted to the investigation of the phase behavior of polymeric systems containing weakly charged polyelectrolytes. In this chapter, we summarize the key results of this work and make some comments on the theoretical framework and the results.

## 6.1 Key Results

In this thesis, we have used the self-consistent filed theory to study the phase behavior of systems containing weakly charged polymers. We derived the set of mean-field equations for the charged-neutral diblock copolymer/homopolymer system. For a given set of input parameters, these equations can be solved to give the equilibrium concentrations of all the components and the conjugate fields. The free energy of the system can be computed using the calculated concentrations and fields to analyze the phase behavior of the system.

We investigated the homogeneous phase behavior of the charged polymer/homopolymer system and the ionic liquid/homopolymer system. In the former case, we found that the charged polymer with larger charge fraction has larger miscibility with the homopolymer and the charge distribution on the chain has no pronounced effect on the miscibility of the system. In the second case, we obtained the results that polymers can be dissolved better in ionic liquid solvent with larger anions and the attractive interaction between the anions and the polymer also increases the solubility of the ionic liquid.

The RPA method has also applied to investigate the stabilitlity limit of the homogeneous phase with respect to both micro- and macro-phase separation for the polyelectrolyte/homopolymer blends and the polyeletrolyte solutions. Both systems exhibit microphase transitions at low polyelectrolyte concentration and macrophase transitions at high polyelectrolyte concentration. The effect of larger dielectric constant is to stabilize the microphase separated state over the macrophase separated state for both systems. The effect of larger charge fraction is to stabilize the homogeneous phase over phase-separated state and this effect is less pronounced in the solution system than in the blend system.

The reciprocal-space method has been applied to solve the self-consistent field equations for fast convergence and high accuracy. Full phase diagrams are presented for polyelectrolyte/homopolymer blends showing microphase separated states of lamellae, hexagonal and BCC, as well as a 2-phase region. The effects of the homopolymer chain length, the interaction parameter, the polyelectrolyte concentration and the charge fraction on the system have all been investigated. In particular, the results reveal that increasing the interaction parameter and increasing the charge fraction have opposite effects on the system.

## 6.2 Comments

Several comments can be made on the present work:

1.The present work is based on some essential assumptions, (a) It has been assumed that the charges on the polymers are smeared so that they can be described Gaussian chains. Therefore, the theory presented here can be applied only to weakly charged polyelectrolytes; (b) We also assumed that the dielectric constant of the system is a constant, which is a weak assumption for strongly inhomogeneous systems; (c) The two-body interaction is short ranged and can be characterized by the Flory-Huggins interaction parameter; (d) The hard-core repulsive interactions can be reflected by the incompressibility constraint.

2. The shortcoming of the present work connected with the mean-field character of our calculation. The mean-field approximation is poor near the critical point where the fluctuations are strong and should be taken into account.

3. The present work is the first time full phase diagrams of polyelectrolyte/homopolymer blends are obtained within the self-consistent field theory framework. Other than the lamellar structure obtained by previous studies, we also found microphase separated structures of hexgonal and BCC, as well as a 2-phase region of coexistence of lamellar and homogeneous phase. It is straightforward to apply the reciprocal-space method to polyelectrolyte solutions to get the full phase diagram.

4. The theoretical framework developed in the present work can be used to study the phase behavior of other weakly charged polyelectrolyte systems by setting appropriate parameters and boundary conditions. Examples include the adsorption of polyelectrolytes at oppositely charged surfaces, polyelectrolyte solution between charged surfaces, and grafted polyelectrolytes.

5. Observation of microdomains in charged polymer systems is an active topic of experimental research. The phase diagrams obtained in the present work can be viewed as a starting point to understand the complex phase behaviors of charged polymer system, and can also guide possible future experiments.

# Appendix A

# Electrostatic energy

In a charged system, if we let the inhomogeneous charge density be $\hat{\rho}_e(\mathbf{r})$, the electrostatic interaction between the charged components can be written as

$$U_e = \frac{1}{2}\int d\mathbf{r}\hat{\rho}_e(\mathbf{r})v(\mathbf{r}-\mathbf{r}')\hat{\rho}_e(\mathbf{r}'), \tag{A.1}$$

where

$$v(\mathbf{r}) = l_B/\mathbf{r}. \tag{A.2}$$

$l_B \ = e^2/\epsilon k_B T$ is the Bjerrum length at which a thermal energy is comparable to the elctrostatic interaction between two unit charges. It is equal to about $7\mathring{A}$ at room temperature for dielectric constant of water.

The above form of electrostatic energy can be transformed by introducing the electrostatic field $\psi(\mathbf{r})$,

$$\begin{aligned}
& \exp[-\frac{1}{2}\int d\mathbf{r}\hat{\rho}_e(\mathbf{r})v(\mathbf{r}-\mathbf{r}')\hat{\rho}_e(\mathbf{r}')] \\
= \; & C\int D\psi(\mathbf{r})\exp[-\frac{1}{2}\int d\mathbf{r}d\mathbf{r}'\psi(\mathbf{r})v^{-1}(\mathbf{r}-\mathbf{r}')\psi(\mathbf{r}') + i\int d\mathbf{r}\hat{\rho}_e(\mathbf{r})\psi(\mathbf{r})] \\
= \; & C\int D\psi(\mathbf{r})\exp[-\frac{1}{2}\int d\mathbf{r}d\mathbf{r}'\psi(\mathbf{r})\frac{\epsilon}{4\pi}\nabla\cdot\nabla\delta(\mathbf{r}-\mathbf{r}')\psi(\mathbf{r}') + i\int d\mathbf{r}\hat{\rho}_e(\mathbf{r})\psi(\mathbf{r})].
\end{aligned}$$

If we consider $I = \int d\mathbf{r}d\mathbf{r}'\psi(\mathbf{r})\nabla\cdot\nabla\delta(\mathbf{r}-\mathbf{r}')\psi(\mathbf{r}')$, we can get

$$I = \int d\mathbf{r}d\mathbf{r}'\psi(\mathbf{r})\nabla\cdot\{\nabla[\delta(\mathbf{r}-\mathbf{r}')\psi(\mathbf{r}')] - \nabla\psi(\mathbf{r}')\delta(\mathbf{r}-\mathbf{r}')\}. \tag{A.3}$$

The first term on the right side of the above equation vanishes, as $\mathbf{r}' \to \infty$, $\psi(\mathbf{r}') \to 0$. So

$$\begin{aligned}
I &= -\int d\mathbf{r}d\mathbf{r}'\psi(\mathbf{r})\nabla\cdot\{\nabla\psi(\mathbf{r}')\delta(\mathbf{r}-\mathbf{r}')\} \\
&= -\int d\mathbf{r}d\mathbf{r}'\psi(\mathbf{r})\nabla\psi(\mathbf{r}')\nabla\delta(\mathbf{r}-\mathbf{r}') \\
&= \int d\mathbf{r}d\mathbf{r}'\psi(\mathbf{r})\nabla\psi(\mathbf{r}')\delta(\mathbf{r}-\mathbf{r}') \\
&= \int d\mathbf{r}\psi(\mathbf{r})\nabla\psi(\mathbf{r}) \\
&= \int d\mathbf{r}\{\nabla\cdot[\psi(\mathbf{r})\cdot\nabla\psi(\mathbf{r})] - |\nabla\psi(\mathbf{r})|^2\}. \qquad (A.4)
\end{aligned}$$

The first term vanishes, so $I = -\int d\mathbf{r}|\nabla\psi(\mathbf{r})|^2$. We have

$$\begin{aligned}
& \exp[-\frac{1}{2}\int d\mathbf{r}\hat{\rho}_e(\mathbf{r})v(\mathbf{r}-\mathbf{r}')\hat{\rho}_e(\mathbf{r}')] \\
= \; & C\int D\psi(\mathbf{r})\exp[-\int d\mathbf{r}\frac{\epsilon}{8\pi}|\nabla\psi(\mathbf{r})|^2 + \int d\mathbf{r}\hat{\rho}_e(\mathbf{r})\psi(\mathbf{r})]. \qquad (A.5)
\end{aligned}$$

We can see that the electrostatic energy of the system can be wrritten as

$$U_e(\{\hat{\rho}_e\}, \{\psi\}) = \int d\mathbf{r}[\hat{\rho}_e(\mathbf{r})\psi(\mathbf{r}) - \frac{\epsilon}{8\pi}|\nabla\psi(\mathbf{r})|^2]. \tag{A.6}$$

# Appendix B

# Partition function as a functional integral

The partition function of the system can be written in terms of a functional integral over all the chain conformations and counterion positions,

$$\begin{aligned}\mathcal{Z} &= \prod_k \left(\frac{\zeta_k^{n_k}}{n_k!}\right) \int \prod_\beta \left[\prod_{i=1}^{n_\beta} \left(D\mathbf{R}_i^\beta(t) P_\beta(\{\mathbf{R}_i^\beta(t)\})\right)\right] \int \prod_{i=1}^{n_I} d\mathbf{r}_i^I \int D\psi(\mathbf{r}) \\ & \prod_{i=1}^{n_0} \left[\sum_{\{c_{i,A}(t)\}} P(\{c_{i,A}(t)\})\right] \exp\left[-\frac{E(\{\hat{\rho}\},\{\psi\})}{k_B T}\right] \prod_{\mathbf{r}} \delta\left[\sum_j \hat{\phi}_j(\mathbf{r}) - 1\right]. \end{aligned} \tag{B.7}$$

To proceed, we insert the indentity

$$1 = \int \prod_j \{D\rho_j \prod_r \delta[\rho_j(\mathbf{r}) - \hat{\rho}_j(\mathbf{r})]\} D\rho_e \prod_r \delta[\rho_e(\mathbf{r}) - \hat{\rho}_e(\mathbf{r})] \tag{B.8}$$

into the partition function to get

$$\begin{aligned}\mathcal{Z} &= \prod_k (\frac{\zeta_k^{n_k}}{n_k!}) \int \prod_j \{D\rho_j\} D\rho_e \int D\psi \prod_{\mathbf{r}} \delta[\sum_j \phi_j(\mathbf{r}) - 1] \exp[-\frac{E(\{\rho\},\{\psi\})}{k_B T}] \\ &\int \prod_{i=1}^{n_0} [\sum_{\{c_{i,A}(t)\}} P(\{c_{i,A}(t)\})(D\mathbf{R}_i^0(t) P_0(\{\mathbf{R}_i^0(t)\}))] \int \prod_{i=1}^{n_C} [(D\mathbf{R}_i^C(t) P_C(\{\mathbf{R}_i^C(t)\}))] \\ &\int \prod_{i=1}^{n_I} d\mathbf{r}_i^I \prod_j \{\prod_r \delta[\rho_j(\mathbf{r}) - \hat{\rho}_j(\mathbf{r})]\} \prod_r \delta[\rho_e(\mathbf{r}) - \hat{\rho}_e(\mathbf{r})].\end{aligned} \tag{B.9}$$

We now introduce a set of fields $\omega_j(\mathbf{r})$ so that

$$\prod_{\mathbf{r}} \delta[\rho_j(\mathbf{r}) - \hat{\rho}_j(\mathbf{r})] = \int D\omega_j \exp\{\int d\mathbf{r} \omega_j(\mathbf{r})[\rho_j(\mathbf{r}) - \hat{\rho}_j(\mathbf{r})]\}. \tag{B.10}$$

In terms of the field $\omega_j(\mathbf{r})$, we have

$$\begin{aligned}\mathcal{Z} &= \prod_k (\frac{\zeta_k e}{n_k})^{n_k} \int \prod_j \{D\rho_j D\omega_j\} D\rho_e D\omega_e \int D\psi \prod_{\mathbf{r}} \delta[\sum_j \phi_j(\mathbf{r}) - 1] \\ &\exp[-\frac{E(\{\rho\},\{\psi\})}{k_B T} + \int d\mathbf{r} \{\sum_j \omega_j(\mathbf{r})\rho_j(\mathbf{r}) + \omega_e(\mathbf{r})\rho_e(\mathbf{r})\}] \\ &\int \prod_{i=1}^{n_0} [\sum_{\{c_{i,A}(t)\}} P(\{c_{i,A}(t)\})(D\mathbf{R}_i^0(t) P_0(\{\mathbf{R}_i^0(t)\})] \\ &\exp\{-\int d\mathbf{r}[\omega_A(\mathbf{r})\hat{\rho}_A(\mathbf{r}) + \omega_B(\mathbf{r})\hat{\rho}_B(\mathbf{r}) + \omega_e(\mathbf{r})\hat{\rho}_{A,e}(\mathbf{r})]\} \\ &\int \prod_{i=1}^{n_C} [(D\mathbf{R}_i^C(t) P_C(\{\mathbf{R}_i^C(t)\})] \exp\{-\int d\mathbf{r} \omega_C(\mathbf{r})\hat{\rho}_C(\mathbf{r})\} \\ &\int \prod_{i=1}^{n_I} d\mathbf{r}_i^I \exp\{-\int d\mathbf{r}[\omega_I(\mathbf{r})\hat{\rho}_I(\mathbf{r}) + \omega_e(\mathbf{r})\hat{\rho}_{I,e}(\mathbf{r})]\},\end{aligned} \tag{B.11}$$

where we have used the Stirling's approximation for $n_k!$,

$$n_k! \approx (\frac{n_k}{e})^{n_k}. \tag{B.12}$$

Assuming $c_{i,A}(t) = c_A(t)$, We can now use the definition of the densities to obtain

$$\begin{aligned}
&\int \prod_{i=1}^{n_0} [\sum_{\{c_{i,A}(t)\}} P(\{c_{i,A}(t)\})(D\mathbf{R}_i^0(t) P_0(\{\mathbf{R}_i^0(t)\})] \\
&\exp\{-\int d\mathbf{r}[\omega_A(\mathbf{r})\hat{\rho}_A(\mathbf{r}) + \omega_B(\mathbf{r})\hat{\rho}_B(\mathbf{r}) + \omega_e(\mathbf{r})\hat{\rho}_{A,e}(\mathbf{r})]\} \\
= &\int \prod_{i=1}^{n_0} [\sum_{\{c_{i,A}(t)\}} P(\{c_{i,A}(t)\})(D\mathbf{R}_i^0(t) P_0(\{\mathbf{R}_i^0(t)\})] \\
&\exp\{-\sum_{i=1}^{n_0} \int_0^{fZ_0} dt[\omega_A(\mathbf{R}_i^0(t)) + Z_A e C_{i,A}(t)\omega_e(\mathbf{R}_i^0(t))] - \sum_{i=1}^{n_0} \int_{fZ_0}^{Z_0} dt\omega_B(\mathbf{R}_i^0(t))\} \\
= &(\int \sum_{c_A(t)} P(\{c_A(t)\}) D\mathbf{R}^0(t) P_0(\{\mathbf{R}^0(t)\}) \\
&\exp\{-\int_0^{fZ_0} dt[\omega_A(\mathbf{R}^0(t)) + z_A e c_A(t)\omega_e(\mathbf{R}^0(t))] - \int_{fZ_0}^{Z_0} dt\omega_B(\mathbf{R}^0(t))\})^{n_0} \\
= &Q_0^{n_0},
\end{aligned} \tag{B.13}$$

where the functions $Q_0$ is defined for one chain by

$$\begin{aligned}
Q_0 \equiv &\int D\mathbf{R}^0(t) P_0(\{\mathbf{R}^0(t)\}) \sum_{c_A(t)} P(\{c_A(t)\}) \\
&\exp\{-\int_0^{fZ_0} dt[\omega_A(\mathbf{R}^0(t)) + z_A e c_A(t)\omega_e(\mathbf{R}^0(t))] - \int_{fZ_0}^{Z_0} dt\omega_B(\mathbf{R}^0(t))\} \\
= &\int D\mathbf{R}^0(t) P_0(\{\mathbf{R}^0(t)\}) \exp\{-\int_0^{fZ_0} dt\omega_A^{eff}(\mathbf{R}^0(t), t) - \int_{fZ_0}^{Z_0} dt\omega_B(\mathbf{R}^0(t))\},
\end{aligned} \tag{B.14}$$

which is the single $AB$-diblock chain partition function, where the effective external field $\omega_A^{eff}(\mathbf{r},t)$ is defined by

$$\omega_A^{eff}(\mathbf{r},t) = -\ln(\sum_{\{c_A(t)\}} p(c_A(t),t)\exp\{-[\omega_A(\mathbf{r}) + z_A e c_A(t)\omega_e(\mathbf{r})]\}) \tag{B.15}$$

.

For the $C$-homopolymer, we have

$$\begin{aligned} & \int \prod_{i=1}^{n_C} [(D\mathbf{R}_i^C(t) P_C(\{\mathbf{R}_i^C(t)\})]\exp\{-\int d\mathbf{r}\omega_C(\mathbf{r})\hat{\rho}_C(\mathbf{r})\} \\ = & \int \prod_{i=1}^{n_C} [(D\mathbf{R}_i^C(t) P_C(\{\mathbf{R}_i^C(t)\})]\exp[-\sum_{i=1}^{n_C}\int_0^{Z_C} dt\omega_C(\mathbf{R}^C(t))] \\ = & (\int D\mathbf{R}_i^C(t) P_C(\{\mathbf{R}_i^C(t)\})\exp[-\int_0^{Z_C} dt\omega_C(\mathbf{R}^C(t))])^{n_C} \\ = & Q_C^{n_C}, \end{aligned} \tag{B.16}$$

where the function $Q_C$ is the single $C$-polymer partition function.

For the counterions, we have

$$\begin{aligned} & \int \prod_{i=1}^{n_I} d\mathbf{r}_i^I \exp\{-\int d\mathbf{r}[\omega_I(\mathbf{r})\hat{\rho}_I(\mathbf{r})) + z_I e\omega_e(\mathbf{r})\hat{\rho}_I(\mathbf{r})]\} \\ = & \int \prod_{i=1}^{n_I} d\mathbf{r}_i^I \exp\{-\sum_{i=1}^{n_I}[\omega_I(\mathbf{r}_i^I) + z_I e\omega_e(\mathbf{r}_i^I)]\} \\ = & Q_I^{n_I}, \end{aligned} \tag{B.17}$$

where the single particle partition function $Q_I$ is defined by

$$\begin{aligned} Q_I &\equiv \int d\mathbf{r}\exp\{-[\omega_I(\mathbf{r}) + z_I e\omega_e(\mathbf{r})]\} \\ &= \int d\mathbf{r}\exp\{-\omega_I^{eff}(\mathbf{r})\}, \end{aligned} \tag{B.18}$$

where the effective ionic fields $\omega_I^{eff}(\mathbf{r})$ is defined by

$$\omega_I^{eff}(\mathbf{r}) = \omega_I(\mathbf{r}) + z_I e\omega_e(\mathbf{r}). \tag{B.19}$$

In terms of these factors $Q_k$, the partition function of the system is

$$\begin{aligned} \mathcal{Z} &= \int \prod_j \{D\rho_j D\omega_j\} \int D\rho_e D\omega_e \int D\psi \prod_{\mathbf{r}} \delta[\sum_j \phi_j(\mathbf{r}) - 1] \prod_k (\frac{\zeta_k e Q_k}{n_k})^{n_k} \\ &\quad \exp[-\frac{E(\{\rho\},\{\psi\})}{k_B T} + \int d\mathbf{r}\{\sum_j \omega_j(\mathbf{r})\rho_j(\mathbf{r}) + \omega_e(\mathbf{r})\rho_e(\mathbf{r})\}]. \end{aligned} \tag{B.20}$$

Therefore, the partition function of the system can be written in the form of a functional integral,

$$\mathcal{Z} = \int \prod_j \{D\rho_j D\omega_j\} \int D\rho_e D\omega_e \int D\psi \prod_{\mathbf{r}} \delta[\sum_j \phi_j(\mathbf{r}) - 1]\exp[-\frac{F(\{\rho\},\{\omega\},\{\psi\})}{k_B T}], \tag{B.21}$$

where the free energy functional $F(\{\rho\},\{\omega\},\{\psi\})$ is given by

$$\begin{aligned} \frac{F(\{\rho\},\{\omega\},\{\psi\})}{k_B T} &= \frac{W(\{\rho_P\})}{k_B T} + \frac{U_e(\{\rho_e\},\{\psi\})}{k_B T} - \sum_k n_k \ln(\frac{\zeta_k e Q_k}{n_k}) \\ &\quad - \int d\mathbf{r}\{\sum_j \omega_j(\mathbf{r})\rho_j(\mathbf{r}) + \omega_e(\mathbf{r})\rho_e(\mathbf{r})\}. \end{aligned} \tag{B.22}$$

Next, we simplify the form of the interaction potential $W(\{\rho\})$ by introducing the symmetric form of the potential,

$$U_{j,j'}(\mathbf{r}) = W_{j,j'}(\mathbf{r}) - \frac{1}{2\rho_{0j}\rho_{0j'}}[W_{jj}(\mathbf{r})\rho_{0j}^2 + W_{j'j'}(\mathbf{r})\rho_{0j'}^2]. \tag{B.23}$$

Using the incompressbility condition $\sum_j \rho_j(\mathbf{r})/\rho_{0j} = 1$ and the fact that $U_{jj}(\mathbf{r}) = 0$, we can write

$$\begin{aligned} W(\{\rho\}) \;=\; & \frac{1}{2}(W_{AA}\rho_{0A}n_0 fZ_0 + W_{BB}\rho_{0B}n_0(Z_0 - fZ_0) + W_{CC}\rho_{0C}n_C Z_C + W_{II}\rho_{0I}n_I) \\ & + \int d\mathbf{r}d\mathbf{r}' U_{AB}(\mathbf{r}-\mathbf{r}')\rho_A(\mathbf{r})\rho_B(\mathbf{r}') + \int d\mathbf{r}d\mathbf{r}' U_{AI}(\mathbf{r}-\mathbf{r}')\rho_A(\mathbf{r})\rho_I(\mathbf{r}') \\ & + \int d\mathbf{r}d\mathbf{r}' U_{AC}(\mathbf{r}-\mathbf{r}')\rho_A(\mathbf{r})\rho_C(\mathbf{r}') + \int d\mathbf{r}d\mathbf{r}' U_{BI}(\mathbf{r}-\mathbf{r}')\rho_B(\mathbf{r})\rho_I(\mathbf{r}') \\ & + \int d\mathbf{r}d\mathbf{r}' U_{BC}(\mathbf{r}-\mathbf{r}')\rho_B(\mathbf{r})\rho_C(\mathbf{r}') + \int d\mathbf{r}d\mathbf{r}' U_{CI}(\mathbf{r}-\mathbf{r}')\rho_C(\mathbf{r})\rho_I(\mathbf{r}'), \end{aligned} \tag{B.24}$$

where the constant $W_{jj}$ is the integral of the potential

$$W_{jj} = \int d\mathbf{r} W_{jj}(\mathbf{r}). \tag{B.25}$$

We assume that the interaction has the form

$$U_{jj'}(\mathbf{r}) = U_{jj'}\delta(\mathbf{r}). \tag{B.26}$$

Then we can have the simple form for the interaction potential

$$\begin{aligned} W(\{\rho\}) &= \frac{1}{2}(W_{AA}\rho_{0A}n_0 f Z_0 + W_{BB}\rho_{0B}n_0(Z_0 - fZ_0) + W_{CC}\rho_{0C}n_C Z_C + W_{II}\rho_{0I}n_I) \\ &+U_{AB}\int d\mathbf{r}\rho_A(\mathbf{r})\rho_B(\mathbf{r}) + U_{AI}\int d\mathbf{r}\rho_A(\mathbf{r})\rho_I(\mathbf{r}) \\ &+U_{AC}\int d\mathbf{r}\rho_A(\mathbf{r})\rho_C(\mathbf{r}) + U_{BI}\int d\mathbf{r}\rho_B(\mathbf{r})\rho_I(\mathbf{r}) \\ &+U_{BC}\int d\mathbf{r}\rho_B(\mathbf{r})\rho_C(\mathbf{r}) + U_{CI}\int d\mathbf{r}\rho_C(\mathbf{r})\rho_I(\mathbf{r}). \end{aligned} \tag{B.27}$$

As we are working in an ensemble in which the volume $V$, the number of particles $n_j$, and the temperature $T$ are fixed, the average densities $\bar{\rho}_j$ are constants. For the polymers, we have

$$\bar{\rho}_A = \frac{1}{V}\int d\mathbf{r}\rho_A(\mathbf{r}) = \frac{n_0 f Z_0}{V},$$
$$\bar{\rho}_B = \frac{1}{V}\int d\mathbf{r}\rho_B(\mathbf{r}) = \frac{n_0(1-f)Z_0}{V},$$
$$\bar{\rho}_C = \frac{1}{V}\int d\mathbf{r}\rho_C(\mathbf{r}) = \frac{n_C Z_C}{V},$$

and for the anions, we have

$$\bar{\rho}_I = \frac{1}{V}\int d\mathbf{r}\rho_I(\mathbf{r}) = \frac{n_I}{V}.$$

The interaction parameters $U_{jj'}$ are usually given in the form of Flory-Huggins parameters defined by

$$k_B T\chi_{jj'} \equiv U_{jj'}\frac{\rho_{0j}\rho_{0j'}}{\rho_0}. \tag{B.28}$$

Using the above expressions, and working with the volume fractions of the monomers and the ions instead of the densities, the free energy functional can now be cast in the form

$$\begin{aligned}
\frac{F}{\rho_0 k_B T} \quad = \quad & \int d\mathbf{r}\{\sum_j \mu_{0j}\phi_j(\mathbf{r}) + \chi_{AB}\phi_A(\mathbf{r})\phi_B(\mathbf{r}) + \chi_{AI}\phi_A(\mathbf{r})\phi_I(\mathbf{r}) + \chi_{AC}\phi_A(\mathbf{r})\phi_C(\mathbf{r}) \\
& + \chi_{BI}\phi_B(\mathbf{r})\phi_I(\mathbf{r}) + \chi_{BC}\phi_B(\mathbf{r})\phi_C(\mathbf{r}) + \chi_{CI}\phi_C(\mathbf{r})\phi_I(\mathbf{r})\} \\
& - \int d\mathbf{r}\{\sum_j \frac{\rho_{0j}}{\rho_0}\omega_j(\mathbf{r})\phi_j(\mathbf{r}) + \omega_e(\mathbf{r})\phi_e(\mathbf{r})\} \\
& + \int d\mathbf{r}\{\phi_e(\mathbf{r})\varphi(\mathbf{r}) - \frac{\kappa^2}{2}|\nabla\varphi(\mathbf{r})|^2\} \\
& - V\frac{\rho_{0A}}{\rho_0}\frac{\bar{\phi}_A}{fZ_0}\ln(\frac{Q_0}{\bar{\phi}_A}) - V\frac{\rho_{0C}}{\rho_0}\frac{\bar{\phi}_C}{Z_C}\ln(\frac{Q_C}{\bar{\phi}_C}) - V\frac{\rho_{0I}}{\rho_0}\frac{\bar{\phi}_I}{1}\ln(\frac{Q_I}{\bar{\phi}_I}). \qquad \text{(B.29)}
\end{aligned}$$

# Appendix C

# Random phase approximation

We consider a system contains positively charged polymer A, neutral homopolymer C and counterions, and we assume that $z_A = 1, z_I = -1$ and $v_A = v_C = 1$. For convenience, we redefine the ionic volume fractions by using the reference density $\rho_0$ as $\phi_I(\mathbf{r}) = \rho_I(\mathbf{r})/\rho_0$. The free energy of the system then has the form

$$\begin{aligned}
\frac{F}{\rho_0 k_B T} &= V(\frac{1}{Z_A}\bar{\phi}_A \ln\bar{\phi}_A + \frac{1}{Z_c}\bar{\phi}_C \ln\bar{\phi}_C + \bar{\phi}_I \ln\bar{\phi}_I) \\
&+ \int d\mathbf{r} \chi_{AC}\phi_A(\mathbf{r})\phi_C(\mathbf{r}) \\
&- \int d\mathbf{r}\{\sum_j \omega_j(\mathbf{r})\phi_j(\mathbf{r}) + \frac{1}{Z_A}\phi_A(\mathbf{r})\ln Q_A + \frac{1}{Z_C}\phi_C(\mathbf{r})\ln Q_C + \phi_I(\mathbf{r})\ln Q_I\} \\
&+ \int d\mathbf{r}\{[p_A\phi_A(\mathbf{r}) - \phi_I(\mathbf{r})]\varphi(\mathbf{r}) - \frac{\kappa^2}{2}|\nabla\varphi(\mathbf{r})|^2\}, \qquad \text{(C.30)}
\end{aligned}$$

where $j = A, C, I$. We assume that the concentrations and the fields have the form

$$\begin{aligned}
\phi_j &= \bar{\phi}_j + \delta\phi_j(\mathbf{r}), \\
\omega_j &= \bar{\omega}_j + \delta\omega_j(\mathbf{r}), \\
\varphi &= \bar{\varphi} + \delta\varphi(\mathbf{r}). \qquad \text{(C.31)}
\end{aligned}$$

The expansion of single particle partition function is simple

$$\begin{aligned}
Q_I &= \frac{1}{V}\int d\mathbf{r}\exp[-\omega_I(\mathbf{r})] \\
&= \exp[-\bar{\omega_I}]\frac{1}{V}\int d\mathbf{r}\exp[-\delta\omega_I(\mathbf{r})] \\
&\approx \exp[-\bar{\omega_I}]\frac{1}{V}\int d\mathbf{r}\{1 - \delta\omega_I(\mathbf{r}) + \frac{1}{2}[\delta\omega_I(\mathbf{r})]^2 + \cdots\} \\
&= \bar{Q_I}\{1 - \frac{1}{V}\int d\mathbf{r}\delta\omega_I(\mathbf{r}) + \frac{1}{2V}\int d\mathbf{r}[\delta\omega_I(\mathbf{r})]^2 + \cdots\}, \qquad \text{(C.32)}
\end{aligned}$$

where $\bar{Q_I} = \exp[-\bar{\omega_I}]$ is the homogeneous single particle partition function.

Next, we need to expand the single chain partition function in terms of $\delta\omega_\alpha(\mathbf{r})$, $\alpha = A, C$. This can be obtained by solving the modified diffusion equation for the propagators perturbatively. The perturbation solution for $q(\mathbf{r}, t)$ can be obtained following the work of Shi et al. [80]. The single chain partition function $Q_\alpha$ can be obtained as

$$\begin{aligned}
Q_\alpha &= e^{-\bar{\omega}_\alpha Z_\alpha} - \frac{1}{V}\int d\mathbf{r}d\mathbf{r}'\int dt' G_\alpha(\mathbf{r}-\mathbf{r}', Z_\alpha - t')e^{-\bar{\omega}_\alpha t'}\delta\omega_\alpha(\mathbf{r}') \\
&+ \frac{1}{V}\int d\mathbf{r}d\mathbf{r}'d\mathbf{r}''\int dt'dt'' G_\alpha(\mathbf{r}-\mathbf{r}', Z_\alpha - t')G_\alpha(\mathbf{r}'-\mathbf{r}'', t'-t'')e^{-\bar{\omega}_\alpha t''}\delta\omega_\alpha(\mathbf{r}')\delta\omega_\alpha(\mathbf{r}'') \\
&+ \cdots, \qquad \text{(C.33)}
\end{aligned}$$

where the Green function is the solution of the modified diffusion equation.

For the homogenous phase, it is convenient to work in the Forurier space

$$\delta\omega_j(\mathbf{r}) = \int \frac{d\mathbf{k}}{(2\pi)^3} e^{i\mathbf{k}\cdot\mathbf{r}} \delta\tilde{\omega}_j(\mathbf{k}). \tag{C.34}$$

The single particle partition function for the counterions can be written in Fourier space as

$$Q_I = \bar{Q}_I\{1 - \frac{1}{V}\delta\tilde{\omega}_I(0) + \frac{1}{2V}\int \frac{d\mathbf{k}}{(2\pi)^3}\delta\tilde{\omega}_I(\mathbf{k})\delta\tilde{\omega}_I(-\mathbf{k}) + \cdots\}. \tag{C.35}$$

The single chain partition function can be written as

$$Q_\alpha = \bar{Q}_\alpha\{1 - \frac{1}{V}Z_\alpha\delta\tilde{\omega}_\alpha(\mathbf{0}) + \frac{1}{2V}\int \frac{d\mathbf{k}}{(2\pi)^3} Z_\alpha^2 g([R_g^\alpha k]^2)\delta\tilde{\omega}_\alpha(\mathbf{k})\delta\tilde{\omega}_\alpha(-\mathbf{k}) + \cdots\}, \tag{C.36}$$

where $\bar{Q}_\alpha$ is the partition function for the homogeneous phase, $R_g^\alpha \equiv b_\alpha^2 Z_\alpha/6$ is the radius of gyration of the polymer chains, and the Debye function $g(x)$ is defined by

$$g(x) = 2\frac{(x - 1 + e^{-x})}{x^2}. \tag{C.37}$$

These expressions can be used to obtain

$$\begin{aligned} V\bar{\phi}_I \ln Q_I &= -V\bar{\omega}_I\bar{\phi}_I - \bar{\phi}_I\delta\tilde{\omega}_I(0) + \frac{1}{2}\int \frac{d\mathbf{k}}{(2\pi)^3}\bar{\phi}_I\delta\tilde{\omega}_I(-\mathbf{k})\delta\tilde{\omega}_I(-\mathbf{k}) + \cdots, \\ V\frac{\bar{\phi}_\alpha}{Z_\alpha}\ln Q_\alpha &= -V\bar{\omega}_\alpha\bar{\phi}_\alpha - \bar{\phi}_\alpha\delta\tilde{\omega}_\alpha(0) + \frac{1}{2}\int \frac{d\mathbf{k}}{(2\pi)^3}\bar{\phi}_\alpha Z_\alpha g([R_g^\alpha k]^2)\delta\tilde{\omega}_\alpha(\mathbf{k})\delta\tilde{\omega}_\alpha(-\mathbf{k}) + \cdots. \end{aligned}$$

Inserting these expressions in the free energy functional. we obtain

$$\frac{F}{\rho_0 k_B T} = \frac{F_H}{\rho_0 k_B T} + \frac{\Delta F}{\rho_0 k_B T}, \tag{C.38}$$

where $F_H$ is the free energy of the homogeneous phase

$$\frac{F_H}{\rho_0 V k_B T} = \chi_{AC}\bar{\phi}_A\bar{\phi}_C + \frac{1}{Z_A}\bar{\phi}_A \ln\bar{\phi}_A + \frac{1}{Z_c}\bar{\phi}_C \ln\bar{\phi}_C + \bar{\phi}_I \ln\bar{\phi}_I. \tag{C.39}$$

The free energy due to the fluctuations $\Delta F$ has the form

$$\Delta F = \Delta F^{(1)} + \Delta F^{(2)} + \cdots , \tag{C.40}$$

where the first order free energy vanishes, $\Delta F^{(1)} = 0$, and the second-order free energy is given by

$$\begin{aligned} \frac{\Delta F^{(2)}}{\rho_0 k_B T} \quad = \quad & \int \frac{d\mathbf{k}}{(2\pi)^3} \{ \chi_{AC} \delta\tilde{\phi}_A(\mathbf{k}) \delta\tilde{\phi}_C(-\mathbf{k}) - \sum_j \delta\tilde{\omega}_j \delta\tilde{\phi}_j(-\mathbf{k}) \\ & -\frac{1}{2}\bar{\phi}_A Z_A g([R_g^A k]^2) \delta\tilde{\omega}_A(\mathbf{k}) \delta\tilde{\omega}_A(-\mathbf{k}) \\ & -\frac{1}{2}\bar{\phi}_C Z_C g([R_g^C k]^2) \delta\tilde{\omega}_C(\mathbf{k}) \delta\tilde{\omega}_C(-\mathbf{k}) \\ & -\frac{1}{2}\bar{\phi}_I \delta\tilde{\omega}_I(\mathbf{k}) \delta\tilde{\omega}_I(-\mathbf{k}) \\ & +\delta\phi_e(\mathbf{k}) \delta\tilde{\varphi}(-\mathbf{k}) - \frac{\kappa^2 \mathbf{k}^2}{2} \delta\tilde{\varphi}(\mathbf{k}) \delta\tilde{\varphi}(-\mathbf{k}) \}, \end{aligned} \tag{C.41}$$

where $\delta\tilde{\phi}_e(\mathbf{k})$ is the charge density defined by

$$\delta\tilde{\phi}_e(\mathbf{k}) = p_A \delta\tilde{\phi}_A(\mathbf{k}) - \delta\tilde{\phi}_I(\mathbf{k}). \tag{C.42}$$

For many cases, it is conveneient to express the free energy functional in terms of the polymer concentrations only. This can be achieved by invoking the random phase approximation, which is obtained by setting the variational derivatives of the free energy with respect to the $\omega_\alpha$'s to zero,

$$\begin{aligned} \frac{\delta \Delta F^{(2)}}{\delta \omega_\alpha} &= 0, && \text{(C.43)} \\ \frac{\delta \Delta F^{(2)}}{\delta \varphi} &= 0. && \text{(C.44)} \end{aligned}$$

We can obtain

$$\begin{aligned} \delta\omega_A(\mathbf{k}) &= - \frac{\delta\tilde{\phi}_A(\mathbf{k})}{\bar{\phi}_A Z_A g([R_g^A \mathbf{k}]^2)}, \\ \delta\omega_C(\mathbf{k}) &= - \frac{\delta\tilde{\phi}_C(\mathbf{k})}{\bar{\phi}_C Z_C g([R_g^C \mathbf{k}]^2)}, \\ \delta\tilde{\omega}_I(\mathbf{k}) &= -\frac{\delta\tilde{\phi}_I(\mathbf{k})}{\bar{\phi}_I}, \\ \delta\tilde{\varphi}(\mathbf{k}) &= \frac{1}{\kappa^2 \mathbf{k}^2}\delta\tilde{\phi}_e(\mathbf{k}). && \text{(C.45)} \end{aligned}$$

Inserting these expressions into the free energy, we get

$$\begin{aligned} \frac{\Delta F^{(2)}}{\rho_0 k_B T} &= \int \frac{d\mathbf{k}}{(2\pi)^3}\{\chi_{AC}\delta\tilde{\phi}_A(\mathbf{k})\delta\tilde{\phi}_C(-\mathbf{k}) + \frac{\delta\tilde{\phi}_A(\mathbf{k})\delta\tilde{\phi}_A(-\mathbf{k})}{2\bar{\phi}_A Z_A g([R_g^A \mathbf{k}]^2)} \\ &\quad + \frac{\delta\tilde{\phi}_C(\mathbf{k})\delta\tilde{\phi}_C(-\mathbf{k})}{2\bar{\phi}_C Z_C g([R_g^C \mathbf{k}]^2)} + \frac{\delta\tilde{\phi}_I(\mathbf{k})\delta\tilde{\phi}_I(-\mathbf{k})}{2\bar{\phi}_I} \\ &\quad + \frac{\delta\tilde{\phi}_e(\mathbf{k})\delta\tilde{\phi}_e(-\mathbf{k})}{2(\kappa\mathbf{k}))^2}\}. && \text{(C.46)} \end{aligned}$$

In order to obtain $\Delta F$ in terms of the molecular densities, we can perform the functional integral over the counterion density. Because the integrals are Gaussian, we can eliminate the ionic densities by minimizing the free energy with respect to $\delta\tilde{\phi}_I(\mathbf{k})$, leading to the relation

$$\delta\tilde{\phi}_I(\mathbf{k}) = \frac{\bar{\phi}_I}{(\kappa\mathbf{k})^2}\delta\tilde{\phi}_e(\mathbf{k}). \tag{C.47}$$

Inserting this relation into the definition of the charge density, we can obtain a self-consistent equation for $\delta\tilde{\phi}_e(\mathbf{k})$, which can be solved to give

$$\begin{aligned}\delta\tilde{\phi}_e(\mathbf{k}) &= \frac{1}{1+\bar{\phi}_I/(\kappa\mathbf{k})^2} p_A \delta\tilde{\phi}_A(\mathbf{k}) \\ &= \frac{1}{1+\bar{\phi}_I/(\kappa\mathbf{k})^2}\delta\tilde{\phi}_{p,e}(\mathbf{k}),\end{aligned} \tag{C.48}$$

where $\delta\tilde{\phi}_{p,e}(\mathbf{k})$ is the charge density due to the charges on the polymers.

Putting the expression for the charge densities into the free energy, we get

$$\begin{aligned}\frac{\Delta F^{(2)}}{\rho_0 k_B T} &= \int \frac{d\mathbf{k}}{(2\pi)^3}\{\chi_{AC}\delta\tilde{\phi}_A(\mathbf{k})\delta\tilde{\phi}_C(-\mathbf{k}) + \frac{\delta\tilde{\phi}_A(\mathbf{k})\delta\tilde{\phi}_A(-\mathbf{k})}{2\bar{\phi}_A Z_A g([R_g^A\mathbf{k}]^2)} \\ &\quad + \frac{\delta\tilde{\phi}_C(\mathbf{k})\delta\tilde{\phi}_C(-\mathbf{k})}{2\bar{\phi}_C Z_C g([R_g^C\mathbf{k}]^2)} + \frac{\delta\tilde{\phi}_{p,e}(\mathbf{k})\delta\tilde{\phi}_{p,e}(-\mathbf{k})}{2[(\kappa\mathbf{k}))^2+\bar{\phi}_I]}\}.\end{aligned} \tag{C.49}$$

We can define a Debye-Huckel screening parameter $\lambda$ by the relation

$$\lambda^{-2} = \frac{\bar{\phi}_I}{\kappa^2} = \frac{4\pi e^2}{\epsilon k_B T}\rho_I. \tag{C.50}$$

The free energy can now be written in the simple form

$$\begin{aligned}\frac{\Delta F^{(2)}}{\rho_0 k_B T} &= \int \frac{d\mathbf{k}}{(2\pi)^3}\{\chi_{AC}\delta\tilde{\phi}_A(\mathbf{k})\delta\tilde{\phi}_C(-\mathbf{k}) + \frac{\delta\tilde{\phi}_A(\mathbf{k})\delta\tilde{\phi}_A(-\mathbf{k})}{2\bar{\phi}_A Z_A g([R_g^A\mathbf{k}]^2)} \\ &\quad + \frac{\delta\tilde{\phi}_C(\mathbf{k})\delta\tilde{\phi}_C(-\mathbf{k})}{2\bar{\phi}_C Z_C g([R_g^C\mathbf{k}]^2)} + \frac{1}{2\bar{\phi}_I}\frac{\delta\tilde{\phi}_{p,e}(\mathbf{k})\delta\tilde{\phi}_{p,e}(-\mathbf{k})}{[1+(\lambda\mathbf{k})^2]}\}, \end{aligned} \tag{C.51}$$

where the last term show that the ions is the screening of the long range Coulomb interactions.

Furthmore, by using the assumption that the volumes of the counterions can be neglected, we have $\delta\tilde{\phi}_A(\mathbf{k}) + \delta\tilde{\phi}_C(\mathbf{k}) = 0$. The second-order free energy can then be written in the simple form

$$\frac{\Delta F^{(2)}}{\rho_0 k_B T} = \frac{1}{2}\int \frac{d\mathbf{k}}{(2\pi)^2}\frac{\delta\tilde{\phi}_A(\mathbf{k})\delta\tilde{\phi}_A(-\mathbf{k})}{S_{AA}(\mathbf{k})}, \tag{C.52}$$

where the RPA scattering function $S_{AA}(\mathbf{k})$ is given by

$$\frac{1}{S_{AA}(\mathbf{k})} = \frac{1}{\bar{\phi}_A Z_A}[\frac{1}{g([R_g^A\mathbf{k}]^2)} + \frac{C_A}{[1+(\lambda\mathbf{k})^2]}] + \frac{1}{(1-\bar{\phi}_A)Z_C g([R_g^C\mathbf{k}]^2)} - 2\chi_{AC}, \tag{C.53}$$

where $C_A = p_A Z_A$ is the total number of elementary charges one polymer chain carries.

# Appendix D

# Reciprocal-space method

For an ordered phase, the reciprocal lattice vectors are completely specified by the symmetry of that structure. For a given ordered phase, the reciprocal lattice vectors $\mathbf{G}$ can be determined. These reciprocal lattice vectors are ordered according to their magnitudes $|\mathbf{G}|$. The plane waves $e^{i\mathbf{G}\cdot\mathbf{r}}$ corresponding to these reciprocal lattice vectors are used as basis functions. Any function $F(\mathbf{r})$ can be expressed using these basis functions,

$$F(\mathbf{r}) = \sum_{\mathbf{G}} F(\mathbf{G}) e^{i\mathbf{G}\cdot\mathbf{r}}, \tag{D.54}$$

$$F(\mathbf{G}) = \frac{1}{V} \sum_{\mathbf{G}} F(\mathbf{r}) e^{-i\mathbf{G}\cdot\mathbf{r}}. \tag{D.55}$$

The latter equation is the reverse transformation.

These basis functions satisfy the orthogonal condition,

$$\int d\mathbf{r} e^{-i\mathbf{G}'\cdot\mathbf{r}} e^{i\mathbf{G}\cdot\mathbf{r}} = V \delta_{\mathbf{G},\mathbf{G}'}. \tag{D.56}$$

The densities and the fields can be expanded in the form

$$\phi_\alpha(\mathbf{r}) = \sum_{\mathbf{G}} \phi_\alpha(\mathbf{G}) e^{i\mathbf{G}\cdot\mathbf{r}}, \tag{D.57}$$

$$\omega_\alpha(\mathbf{r}) = \sum_{\mathbf{G}} \omega_\alpha(\mathbf{G}) e^{i\mathbf{G}\cdot\mathbf{r}}, \tag{D.58}$$

$$\varphi(\mathbf{r}) = \sum_{\mathbf{G}} \varphi(\mathbf{G}) e^{i\mathbf{G}\cdot\mathbf{r}}. \tag{D.59}$$

$$\tag{D.60}$$

The ordered structure is then completely specified by the Fourier components $\phi_\alpha(\mathbf{G})$ and $\omega_\alpha(\mathbf{G})$. In terms of these Fourier components, the mean-field equations in Fourier space become

$$\phi_A(\mathbf{G}) = \frac{\bar{\phi}_A}{Q_A} \sum_{\mathbf{G}'} \int_0^1 dt\, q_A(\mathbf{G}', t) q_A(\mathbf{G}-\mathbf{G}', 1-t), \tag{D.61}$$

$$\phi_C(\mathbf{G}) = \frac{\bar{\phi}_C}{\kappa_C Q_C} \sum_{\mathbf{G}'} \int_0^{\kappa_C} dt\, q_C(\mathbf{G}', t) q_C(\mathbf{G}-\mathbf{G}', \kappa_C - t), \tag{D.62}$$

$$\phi_I(\mathbf{G}) = \frac{\bar{\phi}_I}{Q_I} \sum_{\mathbf{G}'} q_I(\mathbf{G}', \frac{1}{N}), \tag{D.63}$$

$$G^2 \varphi(\mathbf{G}) = \frac{N}{\kappa^2} [p_A \phi_A(\mathbf{G}) - \phi_I(\mathbf{G})], \tag{D.64}$$

$$\omega_A(\mathbf{G}) = \chi_{AC} \phi_C(\mathbf{G}) + p_A \varphi(\mathbf{G}) + \eta(\mathbf{G}), \tag{D.65}$$

$$\omega_C(\mathbf{G}) = \chi_{AC} \phi_A(\mathbf{G}) + \eta(\mathbf{G}), \tag{D.66}$$

$$\omega_I(\mathbf{G}) = v_I \eta(\mathbf{G}) + \varphi(\mathbf{G}), \tag{D.67}$$

$$\delta_{\mathbf{G},\mathbf{0}} = \phi_A(\mathbf{G}) + \phi_C(\mathbf{G}) + v_I \phi_I(\mathbf{G}). \tag{D.68}$$

The single chain partition functions $Q_\alpha$ are given by

$$\begin{aligned} Q_A &= q_A(\mathbf{G}=\mathbf{0},1), && \text{(D.69)} \\ Q_C &= q_C(\mathbf{G}=\mathbf{0},\kappa_C), && \text{(D.70)} \\ Q_I &= q_I(\mathbf{G}=\mathbf{0},\frac{1}{N}). && \text{(D.71)} \end{aligned}$$

In Fourier space, the modified diffusion equations for the end-integrated propagators which were previously second order differential equation become first order,

$$\frac{\partial}{\partial t} q_\alpha(\mathbf{G},t) = -\sum_{\mathbf{G}'} H_\alpha(\mathbf{G},\mathbf{G}') q_\alpha(\mathbf{G}',t), \tag{D.72}$$

where the Hamiltonians $H_\alpha(\mathbf{G},\mathbf{G}')$ are defined by

$$H_\alpha(\mathbf{G},\mathbf{G}') \equiv \sigma_\alpha^2 G^2 \delta_{\mathbf{G},\mathbf{G}'} + \omega_\alpha(\mathbf{G}-\mathbf{G}'). \tag{D.73}$$

The initial conditions for the propagators in Fourier space are

$$q_A(\mathbf{G},0) = q_C(\mathbf{G},0) = q_I(\mathbf{G},0) = \delta_{\mathbf{G},\mathbf{0}}. \tag{D.74}$$

The solution of the modified diffusion equation can be obtained by making an analogy with the Schrödinger equation in quantum mechanics. In order to do this, we construct the eigenvalues and eigenfunctions of the Hamiltonian, $H_\alpha(\mathbf{G},\mathbf{G}')$

$$\sum_{\mathbf{G}'} H_\alpha(\mathbf{G},\mathbf{G}') \psi_n^\alpha(\mathbf{G}') = \varepsilon_n^\alpha \psi_n^\alpha(\mathbf{G}'). \tag{D.75}$$

Due to the Hermitian nature of the hamiltonian matrix, all the eigenvalues are real and the eigenfunctions form a complete orthonormal set,

$$\sum_{\mathbf{G}} \psi_n^{\alpha *}(\mathbf{G})\psi_m^{\alpha}(\mathbf{G}) = \delta_{nm}, \tag{D.76}$$

$$\sum_{n} \psi_n^{\alpha *}(\mathbf{G})\psi_n^{\alpha}(\mathbf{G}') = \delta_{\mathbf{G},\mathbf{G}'}. \tag{D.77}$$

Therefore the propagators can be expanded in terms of the eigenfunctions, leading to solutions

$$q_\alpha(\mathbf{G}, t) = \sum_n e^{-\varepsilon_n^\alpha t} q_n^\alpha(0)\psi_n^\alpha(\mathbf{G}), \tag{D.78}$$

where the coefficients $q_n^\alpha(0)$ are determined by the appropriate initial conditions

$$q_n^\alpha(0) = \psi_n^{\alpha *}(\mathbf{0}). \tag{D.79}$$

Solving the eigenvalue problem is a very time-consuming task as it requires $O(M^3)$ operations for a $M \times M$ matrix. For an orderd structure, this calculation can be simplified by exploiting the symmetry of the structure under investigation. As we know, for ordered structure, the Fourier coefficients are not independed, They are related by the point group symmetry. The basis functions can be grouped into starts. A set of new basis functions can be constructed,

$$f_n(\mathbf{r}) = \frac{1}{\sqrt{N_n}} \sum_{i \in n} S_i^n e^{i\mathbf{G}_i^n \cdot \mathbf{r}}, \tag{D.80}$$

where the wave vectors $\mathbf{G}_i^n$ are related by the point group operation within one star, and satisfy the relation $|\mathbf{G}_i^n|^2 = \lambda_n$. The factors $S_i^n$ assume the values $\pm 1$ determined by the symmetry of the structure and $N_n$ is the number of reciprocal lattice vectors within the $n$-th star.

A periodic function $F(\mathbf{r})$ can then be expanded in terms of the new set of basis functions $f_n(\mathbf{r})$,

$$\begin{aligned} F(\mathbf{r}) &= \sum_n F_n f_n(\mathbf{r}), && \text{(D.81)} \\ F_n &= \frac{1}{V}\int d\mathbf{r} F(\mathbf{r}) f_n(\mathbf{r}). && \text{(D.82)} \end{aligned}$$

The latter equation is the reverse transformation.

The basis functions satisfy the orthogonal condition

$$\int d\mathbf{r} f_n(\mathbf{r}) f_m(\mathbf{r}) = V\delta_{nm}, \tag{D.83}$$

and they are also eigenfunctions of Laplacian operator

$$\nabla^2 f_n(\mathbf{r}) = -\lambda_n f_n(\mathbf{r}). \tag{D.84}$$

Expanding all periodic functions in terms of $f_n(\mathbf{r})$, the mean-field equations can be cast in terms of these coefficients, just as the Fourier representation described above. In particular, the chain-conformation Hamiltonians become symmetric matrices with matrix elements

$$H^{\alpha}_{nm} = \sigma^2_{\alpha}\lambda_n\delta_{nm} + \sum_l \Gamma_{nml}\omega^{\alpha}_l, \tag{D.85}$$

where the coefficients $\Gamma_{nml}$ are defined by

$$\begin{aligned} \Gamma_{nml} &= \frac{1}{V}\int d\mathbf{r} f_n(\mathbf{r}) f_m(\mathbf{r}) f_l(\mathbf{r}) \\ &= \frac{1}{\sqrt{N_n N_m N_l}} \sum_{i\in n}\sum_{j\in m}\sum_{k\in l} S^n_i S^m_j S^l_k \delta_{\mathbf{G}^n_i+\mathbf{G}^m_j+\mathbf{G}^l_k,\mathbf{0}}. && \text{(D.86)} \end{aligned}$$

The eigenvalues and eigenfunctions of the matrices $H^{\alpha}_{nm}$ are solved from the equations

$$\sum_m H^{\alpha}_{nm}\psi^{\alpha}_{mi} = \varepsilon^{\alpha}_i \psi^{\alpha}_{ni}, \tag{D.87}$$

where $i$ labels the eigenvalues and eigenfunctions. The eigenfunctions form a complete orthonormal set,

$$\begin{aligned} \sum_n \psi^{\alpha}_{ni}\psi^{\alpha}_{nj} &= \delta_{ij}, && \text{(D.88)} \\ \sum_i \psi^{\alpha}_{ni}\psi^{\alpha}_{mi} &= \delta_{nm}. && \text{(D.89)} \end{aligned}$$

The end-integrated propagators can be written as

$$q^{\alpha}_n(t) = \sum_i e^{-\varepsilon^{\alpha}_i t}\psi^{\alpha}_{1i}\psi^{\alpha}_{ni}. \tag{D.90}$$

The single-chain partition function and density coefficients can be expressed in the following form

$$\begin{aligned} Q_{\alpha} &= q^{\alpha}_1(\kappa_{\alpha}) = \sum_i e^{-\varepsilon^{\alpha}_i \kappa_{\alpha}}\psi^{\alpha}_{1i}\psi^{\alpha}_{1i}, && \text{(D.91)} \\ \phi^A_n &= \frac{\bar{\phi}_A}{Q_A}\int_0^1 ds \sum_{m,l}\Gamma_{nml} q^A_m(s) q^A_l(1-s), && \text{(D.92)} \\ \phi^C_n &= \frac{\bar{\phi}_C}{\kappa_C Q_C}\int_0^{\kappa_C} ds \sum_{m,l}\Gamma_{nml} q^C_m(s) q^C_l(\kappa_C - s), && \text{(D.93)} \\ \phi^I_n &= \frac{\bar{\phi}_I}{Q_I}\sum_i e^{-\varepsilon^I_i \frac{1}{N}}\psi^I_{1i}\psi^I_{1i}. && \text{(D.94)} \end{aligned}$$

Quantities using the eigenvalues and eigenfunctions of $H^{\alpha}_{nm}$ can be construced to simplify the mean-field equations,

$$v_i^A = e^{-\varepsilon_i^A}, \qquad v_i^C = e^{-\varepsilon_i^C \kappa_C}, \qquad v_i^I = e^{-\varepsilon_i^I \frac{1}{N}}, \tag{D.95}$$

$$S_{n,ij}^A = \sum_{m,l} \Gamma_{nml} \psi_{mi}^A \psi_{lj}^A, \qquad S_{n,ij}^C = \sum_{m,l} \Gamma_{nml} \psi_{mi}^C \psi_{lj}^C, \tag{D.96}$$

$$g_{ij}^A = \frac{\psi_{1i}^A (v_i^A - v_j^A)}{(\varepsilon_j^A - \varepsilon_i^A)}, \qquad g_{ij}^C = \frac{\psi_{1i}^C (v_i^C - v_j^C)}{(\varepsilon_j^C - \varepsilon_i^C)\kappa_C}. \tag{D.97}$$

Using these quantities, the single-chain partition functions can be written as

$$Q_\alpha = \sum_i v_i^\alpha \psi_{1i}^\alpha \psi_{1i}^\alpha. \tag{D.98}$$

The density coefficients are given by

$$\phi_n^A = \frac{\bar{\phi}_A}{Q_A} \sum_{i,j} g_{ij}^A S_{n,ij}^A \psi_{1j}^A, \tag{D.99}$$

$$\phi_n^C = \frac{\bar{\phi}_C}{Q_C} \sum_{i,j} g_{ij}^C S_{n,ij}^C \psi_{1j}^C, \tag{D.100}$$

$$\phi_n^I = \frac{\bar{\phi}_I}{Q_I} \sum_i v_i^I \psi_{1i}^I \psi_{ni}^I. \tag{D.101}$$

The coefficients of the fields are

$$\varphi_n = \frac{N}{\lambda_n \kappa^2} [p_A \phi_n^A - \phi_n^I], \tag{D.102}$$

$$\omega_n^A = \chi_{AC} N \phi_n^C + p_A \varphi_n + \eta_n, \tag{D.103}$$

$$\omega_n^c = \chi_{AC} N \phi_n^A + \eta_n, \tag{D.104}$$

$$\omega_n^I = -\varphi_n + v_I \eta_n, \tag{D.105}$$

where the coefficients $\eta_n$ are to be adjusted so that the system satisfies the incompressibility condition

$$\phi_n^A + \phi_n^C + v_I \phi_n^I = \delta_{n,1}. \tag{D.106}$$

# Bibliography

[1] P. G. de Gennes. *Scaling Concepts in Polymer Physics.* Cornell Univ. Press, New York, USA, 1979.

[2] R. A. L. Jones. *Soft Condensed Matter.* Oxford Univ. Press Inc., New York, USA, 2002.

[3] M. Doi. *Introduction to Polymer Physics.* Oxford Univ. Press Inc., New York, USA, 1996.

[4] R. R. Netz and D. Andelman. *Phys. Rep.*, 380:1, 2003.

[5] D. Andelman. *Proceedings of the Nato ASI & SUSSP on Soft condensed matter physics in molecular and cell biology"*, page 97, 2006.

[6] A. Veis. *Biological Polyelectrolytes.* Marcel Dekker, New York, USA, 1970.

[7] A. Rembaum. *Polyelectrolytes and Their Applications.* D. Reidel Pub. Co., Boston, USA, 1975.

[8] S. E. Kudaibergenov. *Adv. Polym. Sci.*, 144:115, 1999.

[9] A. V. Dobrynin, R. H. Colby, and M. Rubinstein. *J. Polym. Sci. B: Polym. Phys.*, 42:3513, 2004.

[10] A. Katchalsky and I. R. Miller. *J. Polym. Sci.*, 13:57, 1954.

[11] T. Soddemann, H. Schiessel, and A. Blumen. *Phys. Rev. E*, 57:2081, 1998.

[12] F. Oosawa. *Polyelectrolytes.* Marcel Dekker, New York, USA, 1971.

[13] M. Hara. *Polyelectrolytes.* Marcel Dekker, New York, USA, 1993.

[14] J. L. Barrat and J. F. Joanny. *Adv. Chem. Phys.*, 94:1, 1996.

[15] A. Y. Grosberg and A. R. Khohklov. *Giant Molecules: Here, There, and Everywhere.* World Scientific, New Jersey, USA, 2011.

[16] A. V. Dobrynin and M. Rubinstein. *Prog. Polym. Sci.*, 30:1049, 2005.

[17] M. Muthukumar. *Polymer Translocation.* CRC Press, Boca Raton, USA, 2001.

[18] C. Tanford. *Physical Chemistry of Macromolecules.* Wiley, New York, USA, 1961.

[19] M. G. Brereton and T. A. Viglis. *Macromolecules*, 23:2044, 1990.

[20] V. Yu. Borue and I. Ya. Erukhimovich. *Macromolecules*, 23:3625, 1990.

[21] I. A. Nyrkova, M. Doi, and A. R. Khokhlov. *Polym. Prepr.*, 34:926, 1993.

[22] P. B. Warren. *J. Phys. II*, 7:343, 1997.

[23] P. G. de Gennes, P. Pincus, and R. M. Velasco. *E. J. Phys.*, 37:1461, 1976.

[24] A. R. Khokhlov. *J. Phys. A*, 13:979, 1980.

[25] A. R. Khokhlov and K. A. Khachaturian. *Polymer*, 23:1742, 1982.

[26] A. V. Lyulin, B. Dunweg, O. V. Borisov, and A. A. Darinskii. *Macromolecules*, 32:3264, 1999.

[27] M. J. Lee, M. M. Grenn, F. Mikes, and H. Morawetz. *Macromolecules*, 35:4216, 2002.

[28] Q. Liao, A. V. Dobrynin, and M. Rubinstein. *Macromolecules*, 36:3386, 2003.

[29] A. V. Dobrynin, M. Rubinstein, and S. P. Obuhkov. *Macromolecules*, 29:2974, 1996.

[30] A. V. Dobrynin and M. Rubinstein. *Macromolecules*, 32:915, 1999.

[31] A. V. Dobrynin and M. Rubinstein. *Macromolecules*, 34:1964, 2001.

[32] H. Limbach and C. Holm. *Comput. Phys. Commun.*, 147:321, 2002.

[33] H. Limbach and C. Holm. *J. Phys. Chem. B*, 107:8041, 2003.

[34] J. F. Joanny and L. Leibler. *J. Phys.*, 51:545, 1990.

[35] S. Forster and M. Schmidt. *Adv. Polym. Sci.*, 120:51, 1995.

[36] P. J. Flory. *Principles of Polymer Chemistry.* Cornell Univ. Press, New York, USA, 1953.

[37] M. W. Matsen and F. S. Bates. *Macromolecules*, 29:1091, 1996.

[38] M. Shibayama, T. Tanaka, and C. C. Han. *J. Chem. Phys.*, 97:6829, 1992.

[39] V. Y. Borue and I. Y. Erukhimovich. *Sov. Phys. Dokl*, 31:146, 1986.

[40] V. Y. Borue and I. Y. Erukhimovich. *Macromolecules*, 21:3240, 1988.

[41] V. V. Vasilevskaya, S. G. Strodubtsev, and A. R. Khokhlov. *Vysokomolec. Soed.*, 29B:930, 1992.

[42] I. A. Nyrkova and A. R. Khokhlov. *Vysokomolec. Soed.*, 31B:575, 1989.

[43] I. A. Nyrkova, A. R. Khokhlov, and Y. Y. Kramarenko. *Polym. Sci. USSR*, 32:852, 1990.

[44] A. R. Khokhlov and I. A. Nyrkova. *Macromolecules*, 25:1493, 1992.

[45] Y. Rabin and J. F. Marko. *Macromolecules*, 24:2134, 1991.

[46] M. Benmouna and T. A. Vilgis. *Macromolecules*, 24:3866, 1991.

[47] M. Benmouna and Y. Bouayed. *Macromolecules*, 25:5318, 1992.

[48] A. V. Dobrynin and I. Y. Erukhimovich. *Sov. Phys.-JETP*, 72:751, 1991.

[49] L. Leibler. *Macromolecules*, 13:1602, 1980.

[50] E. E. Dormidontova, I. Y. Erukhimovich, and A. R. Khokhlov. *Macromol. Theory Simul.*, 3:661, 1994.

[51] A. V. Gritsevich. *Polym. Sci. Ser. A*, 50:58, 2008.

[52] A. Nyrkova I, A. R. Khokhlov, and M. Doi. *Macromolecules*, 27:4220, 1994.

[53] S. F. Edwards. *Proc. Phys. Soc.*, 85:613, 1965.

[54] E. Helfandi. *J. Chem. Phys.*, 62:999, 1975.

[55] E. Helfandi. *Macromolecules*, 8:552, 1975.

[56] K. M. Hong and J. Noolandi. *Macromolecules*, 14:727, 1981.

[57] J. Noolandi and K. M. Hong. *Macromolecules*, 15:482, 1982.

[58] K. R. Shull and E. J. Kramer. *Macromolecules*, 23:4769, 1990.

[59] K. R. Shull. *Macromolecules*, 26:2346, 1993.

[60] A.-C. Shi and J. Noolandi. *Macromol. Theroy Simul.*, 8:214, 1999.

[61] Q. Wang, T. Taniguchi, and G. H. Fredrickson. *J.Chem. Phys.*, 108:6733, 2004.

[62] R. Kumar and M. Muthukumar. Microphase separation in polyelectrolyteic diblock copolymer melt: weak segaration limit. *arXiv:0805.2968*, 2008.

[63] S. Yang, A. Vishnyakov, and A. V. Neimark. *J.Chem. Phys.*, 134:054104, 2011.

[64] G. H. Fredrickson. *The Equilibrium Theory of Inhomogeneous Polymers*. Clarendon press, Oxford, UK, 2006.

[65] E. Raphael and J. F. Joanny. *Europhys. Lett.*, 13:623, 2011.

[66] W. Jiang, Y. T. Wang, T. Y. Yan, and G. A. Voth. *J. Phys. Chem. C*, 112:1132, 2008.

[67] E. W. Castner Jr and J. F. Wishart. *J. Chem. Phys*, 132:120901, 2008.

[68] H. O. Hamaguchi and R. Ozawa. *Adv. Chem. Phys.*, 131:85, 2005.

[69] M. N. Kobrak. *Adv. Chem. Phys.*, 139:85, 2008.

[70] N. V. Plechkova and K. R. Seddon. *Chem. Soc. Rev.*, 37:123, 2008.

[71] T. Welton. *Chem. Rev.*, 99:2071, 1999.

[72] J. N. Barisci. *Electrochemistry commun.*, 6:22, 2004.

[73] T. Kawakatsu. *Statistical Physics of Polymers: An Introduction.* Springer, Berlin, Germany, 2004.

[74] A. N. Semenov. *Sov. Phys. JETP*, 61:733, 1985.

[75] M. W. Matsen and M. Schick. *Phys. Rev. Lett*, 72:2660, 1994.

[76] Z. J. Guo, G. J. Zhang, F. Qiu, H. D. Zhang, Y. L. Yang, and A.-C. Shi. *Phys. Rev. Lett*, 101:028301, 2008.

[77] F. Drolet and G. H. Fredrickson. *Phys. Rev. Lett*, 83:4317, 1999.

[78] Y. Bohbot-Raviv and Z. G. Wang. *Phys. Rev. Lett*, 85:3428, 2000.

[79] K. Rasmussen and G. Kalosakas. *J. Polym. Sci., Part B: Polym. Phys.*, 40:1777, 2002.

[80] A.-C. Shi, J. Noolandi, and R. C. Desai. *Macromolecules*, 29:6487, 1996.